AEDC-TR-68-265

LABORATORY VERIFICATION STUDIES OF ROTATIONAL AND VIBRATIONAL TEMPERATURE MEASUREMENTS BY THE ELECTRON BEAM TECHNIQUE

William D. Williams

ARO, Inc.

February 1969

VON KÁRMÁN GAS DYNAMICS FACILITY
ARNOLD ENGINEERING DEVELOPMENT CENTER
AIR FORCE SYSTEMS COMMAND
ARNOLD AIR FORCE STATION, TENNESSEE

NOTICES

When U. S. Government drawings specifications, or other data are used for any purpose other than a definitely related Government procurement operation, the Government thereby incurs no responsibility nor any obligation whatsoever, and the fact that the Government may have formulated, furnished, or in any way supplied the said drawings, specifications, or other data, is not to be regarded by implication or otherwise, or in any manner licensing the holder or any other person or corporation, or conveying any rights or permission to manufacture, use, or sell any patented invention that may in any way be related thereto.

Qualified users may obtain copies of this report from the Defense Documentation Center.

References to named commercial products in this report are not to be considered in any sense as an endorsement of the product by the United States Air Force or the Government.

LABORATORY VERIFICATION STUDIES OF ROTATIONAL AND VIBRATIONAL TEMPERATURE MEASUREMENTS BY THE ELECTRON BEAM TECHNIQUE

William D. Williams
ARO, Inc.

FOREWORD

The work reported herein was sponsored by the Arnold Engineering Development Center (AEDC), Air Force Systems Command (AFSC), Arnold Air Force Station Tennessee, under Program Element 63101F, Project A014.

The results of research presented were obtained by ARO, Inc. (a subsidiary of Sverdrup & Parcel and Associates, Inc.), contract operator of AEDC, AFSC, under Contract F40600-69-C-0001. The work was conducted under ARO Project Nos. VJ3821 and 3921 from January 1, 1968 to September 1968. This material was presented to the University of Tennessee as a thesis in partial fulfillment of the requirements for the degree of Master of Science. The manuscript was submitted for publication on October 25, 1968.

Sincere thanks are due Dr. J.W.L. Lewis of ARO, Inc., who directed this work and who worked closely with me, Mr. A.D. Killian for his invaluable technical skill, and Mr. B. L. Sandford for his aid with the computer calculations.

This technical report has been reviewed and is approved.

Vincent A. Rocco
2nd Lieutenant, USAF
Research Division
Directorate of Plans
and Technology

Edward R. Feicht
Colonel, USAF
Director of Plans
and Technology

ABSTRACT

Although under study for several years by many investigators the electron beam technique remains a somewhat controversial diagnostic method for high velocity gas flows. In order to verify the physical parameters and limits of this technique precise laboratory experiments have been conducted. By injecting an electron beam into an experimental chamber containing slowly flowing nitrogen and spectroscopically examining the resulting spontaneous light emission the analysis of this technique is accomplished.

Measurements of the rotational and vibrational temperatures of nitrogen have been made over the temperature range 78° - 300°K and at pressures of 0.001-1.00 Torr using a 10 KV electron beam with currents of 0.06-4.5 milliamperes. The measurements were made photoelectrically, and signal amplification and averaging were accomplished with a lock-in amplifier.

The results of the rotational temperature measurements display a dependence of rotational temperatures on gas density and beam current. Rotational temperature was also found to vary with the number of spectral lines used and with the vibrational band as well.

Vibrational band intensities of the N_2^+ $[1^-]$ system were measured by electronic integration of the rotational structure, and a pressure dependence of various band intensity ratios was observed.

TABLE OF CONTENTS

LIST OF TABLES

LIST OF FIGURES

FIGURE PAGE

FIGURE PAGE

FIGURE PAGE

FIGURE PAGE

NOMENCLATURE

A_b	Electron beam cross sectional area
$A_{m,v',K'}^{\ell;v_2'',K_2''}$	Einstein's spontaneous transition probability for emission between states m, v',K' and ℓ, v_2'', K_2'' multiplied by the number of molecules in state m, v', K' ($N_{v',K'}^{m}$)
a	Thermal diffusivity
$B_{v_1''}$	Rotational constant corresponding to the v_1'' vibrational level
c	Speed of light
c_1	A constant in the rotational line intensity equations, defined in Equation 30
c_2	A constant in the rotational line intensity equations, defined in Equation 31
c_p	Specific heat at constant pressure
E_K	Energy eigenvalue for a general K rotational level
$E_{K_1''}$	Energy eigenvalue for the K_1'' rotational level
E_v	Energy eigenvalue for a general v vibrational level
$E_{v_1''}$	Energy eigenvalue of the v_1'' vibrational level
$E_{v,K}$	Interaction energy eigenvalue for the general v and K levels
$E_{v_1'',K_1''}$	Interaction energy eigenvalue of the v_1'' and K_1'' levels
$-e$	Electronic charge
$(G)_o$	A function of rotational quantum number and rotational temperature
$G(v_1'')$	Term value for the v_1'' vibrational level

g_K	Rotational level degeneracy
H	Ratio of heat source strength per unit volume and unit time to thermal conductivity
h	Planck's constant
$\hbar$	Planck's constant divided by 2π
I_p	Intensity of radiation of a P branch line
I_R	Intensity of radiation of an R branch line
I_{RTv}	Intensity ratio of vibrational bands
$I_{v'v_2''}$	Intensity of radiation from the v' to v_2'' transition
$I_{v',K'}^{v_2'',K_2''}$	Intensity of radiation from the v', K' to v_2'', K_2'' transition
i_b	Beam current
J	Rotational quantum number - includes electron spin
j_b	Beam current density
K	Rotational quantum number - excludes electron spin, K = 0, 1, 2, 3 .....); thermal conductivity
K_1''	Refers to rotational level of N_2 $X^1\sum$ state
K'	Refers to rotational level of N_2^+ $B^2\sum$ state
K_2''	Refers to rotational level of N_2^+ $X^2\sum$ state
k	Boltzmann constant
ℓ	Refers to N_2^+ $x^2\sum$ state
m	Refers to N_2^+ $B^2\sum$ state
N_T	Nitrogen molecule number density
N_2^+ $[1^-]$	First negative system of nitrogen
N_2 $[2^+]$	Second positive system of nitrogen

$N_2^+ B^2\sum$	Upper electronic state of nitrogen ion
$N_2^+ X^2\sum$	Ground state of nitrogen ion
$N_2 X^1\sum$	Ground state of nitrogen molecule
$N_{v,K}$	Number of molecules in the general K rotational level of the general v vibrational level of an electronic state
$N_{v_1'',K_1''}$	Number of molecules in the K_1'' rotational level of the v_1'' vibrational level of the $N_2 X^1\sum$ state
$N_{v',K'}$	Number of molecules in the K' rotational level of the v' vibrational level of the $N_2^+ B^2\sum$ state
n	Refers to $N_2 X^1\sum$ state; ratio of chamber radius to beam radius
P_c	Chamber pressure
P_p	Relative rotational transition probability for the P branch
P_R	Relative rotational transition probability for the R branch
$p(v',v_1'')$	Vibrational strength factor of the v_1'' to v' transition
$p(v',v_2'')$	Vibrational strength factor of the v' to v_2'' transition
$(p.f.)_+$	Partition function
$\dot{q}$	Heat source strength per unit volume and unit time
$q(v',v_1'')$	Franck-Condon factor for the v_1'' to v' transition
$q(v',v_2'')$	Franck-Condon factor for the v' to v_2'' transition
R	Individual gas constant
$R_e(r)$	Functional form of the electronic transition moment
r	Beam radius
$S^{K'}_{K_1''}$	Rotational line strength
s	Number of data points or spectral scans

T	Temperature
T_R	Rotational temperature
T_v	Vibrational temperature
T_w	Chamber wall temperature
$\frac{\overline{T_R}}{T_w}$	Weighted average of T_R/T_w
t	Time; total
v	Vibrational quantum number, $v = 0, 1, 2, 3, \ldots$
v_1''	Refers to vibrational level of N_2 $X^1\sum$ state
v_2''	Refers to vibrational level of N_2^+ $X^2\sum$ state
v'	Refers to vibrational level of N_2^+ $B^2\sum$ state
(v', v_2'')	Vibrational band designation
$W_{v,K}$	Energy of vibration and rotation of the v,K state
$\frac{W}{\rho J_b}$	Energy dissipation function of the electron beam in air
y_i	Ratio of measured rotational temperature to chamber wall temperature for the ith spectral scan
ζ	Number of transitions per second into the m,v',K' state due to electron beam excitation
λ_R, λ_P	Wavelength of an R branch and a P branch line, respectively
$\lambda_{v',K'}^{v_2'',K_2''}$	Wavelength of the v',K' to v_2'',K_2'' emission
λ_{ab}	Vibrational band wavelength due to transition from level a to level b
ρ	Gas density

σ_i Ratio of standard deviation of measured rotational temperature for the ith spectral scan to the chamber wall temperature

$\overline{\sigma}$ Standard deviation of an average

$\sigma_{\Delta K = \pm 2,0}$ Collision cross section for rotational excitation by slow electrons

$\sigma_{n \to m}$ Total inelastic cross section for the N_2 $X^1\sum \rightarrow N_2^+ B^2\sum$ transition

ϕ Angle in cylindrical coordinates

ψ Quantum mechanical wave function

ω_m, ω_n Electronic degeneracy of state m and n, respectively

CHAPTER I
INTRODUCTION

A method for directly measuring nitrogen rotational and vibrational temperatures in wind tunnel flows is the electron beam technique (the EBT) pioneered by Dr. E. P. Muntz (1,2,3,4).[1] This technique involves the ionization and excitation of nitrogen molecules with a beam of moderately energetic electrons (10-100 KEV). The resulting spontaneous emission in the spectral region 3500-5000 Å is predominantly that of the first negative system of nitrogen ($N_2^+ [1^-]$). The intensity distribution of the system's vibrational bands can be related to an effective vibrational temperature of nitrogen, and the rotational fine structure of this system's vibrational bands has an intensity distribution that can be related to an effective rotational temperature of nitrogen. At low gas densities the beam is well-defined; therefore, observation of emission at different positions along the beam allows "point" temperature measurements. Experimental determinations of vibrational and rotational temperatures in nitrogen wind tunnel flows then should permit more accurate knowledge of the effect of non-equilibrium on flow properties. Furthermore, in many cases the rotational temperature should be the same as the translational temperature of the test gas.

---

[1]Numbers in parentheses refer to similarly numbered references in the bibliography.

Analyses by Muntz (1) and Petrie (5) proposed the excitation process to be directly from the neutral ground state molecules (N_2 $X^1\sum$) to the excited states of the molecular ion (N_2^+ $B^2\sum$) by inelastic collisions with high energy electrons (see Figure 1). These analyses discounted other paths of excitation to N_2^+ $B^2\sum$ such as cascade population, double excitation, and secondary excitation of ground state ions. The possibility of emission excited by secondaries with energies in excess of 18.7 ev (the energy difference between N_2 $X^1\sum$ and N_2^+ $B^2\sum$) was not theoretically discounted, but it was not explicitly included in the theory.

The observed emission corresponds to the electronic transition N_2^+ $B^2\sum \rightarrow N_2^+$ $X^2\sum$ (the ground state of the molecular ion) with the average lifetime of the excited ions on the order of 10^{-8} seconds. Muntz (1) also showed that for number densities on the order of $10^{16}/cm^3$ at room temperature the excited gas particle should experience little interference due to gas kinetic collisions during the process of excitation and emission. Therefore, a theoretical prediction was made of the emission intensities as a function of temperature in the rotational and vibrational bands of N_2^+ [1-]. For clarification these equations developed by Muntz are reviewed in the next section.

The controversy over this technique has arisen due to an apparent disagreement between measured rotational temperatures and the actual temperature of low temperature nitrogen, to an apparent dependence of measured rotational temperature upon number of spectral lines, to an apparent density dependence of measured rotational and vibrational

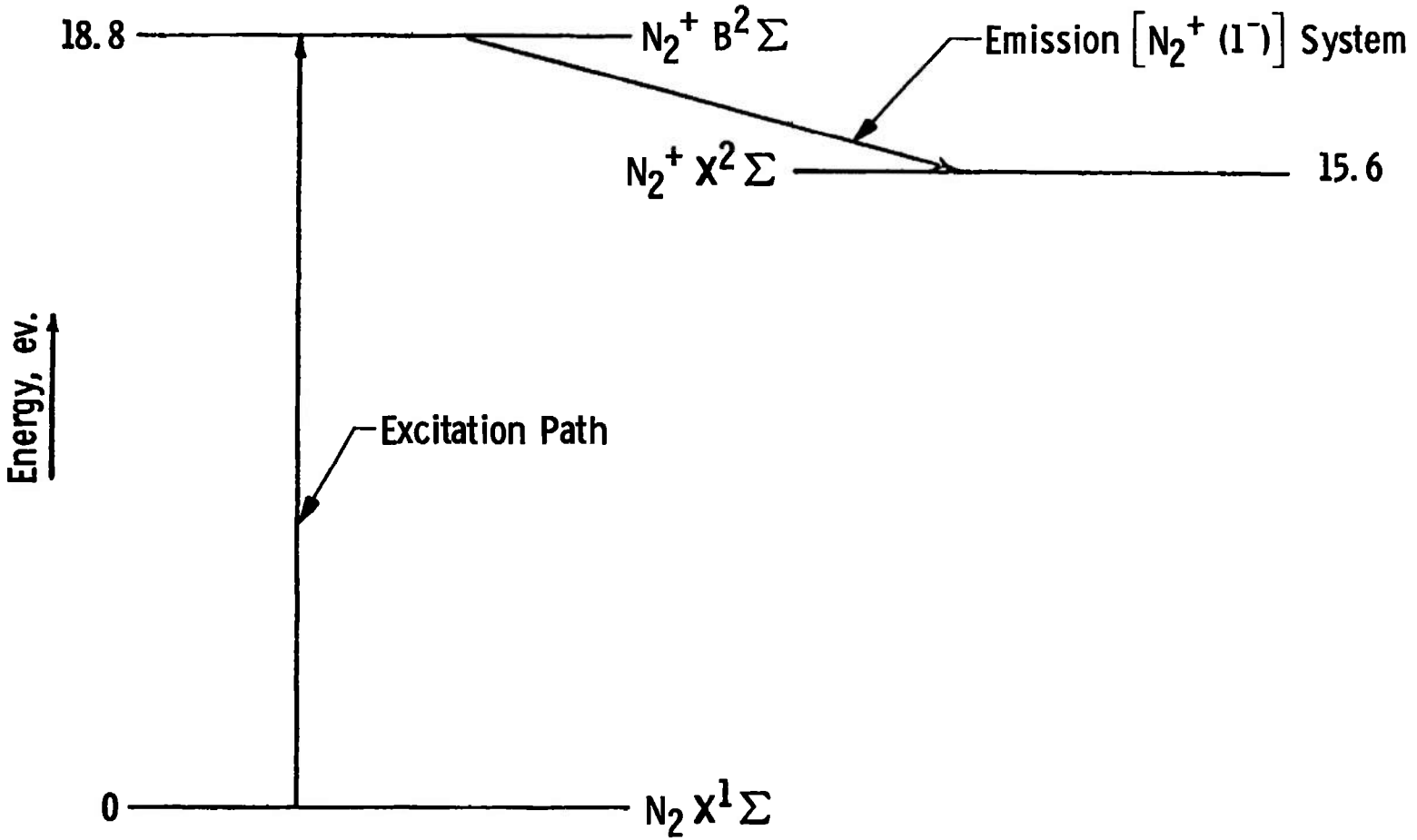

Fig. 1 Simplified, General Excitation-Emission Diagram

AEDC-TR-68-265

temperatures, and to the possibility of a localized beam heating effect.

Therefore, in an effort to precisely determine the physical parameters, limits, and foibles of the electron beam technique a laboratory system was developed to study the technique under a controlled range of conditions. In these experiments a 10 KV electron beam was injected into an experimental chamber containing slowly flowing nitrogen. The nitrogen temperature was controlled in the range 78°-300°K, and the nitrogen pressure was controlled over the range 0.001-1.0 Torr.

By photoelectric spectroscopic measurement of the rotational line intensities of a vibrational band a rotational temperature was measured and compared to the actual temperature of the nitrogen (which was the test chamber wall temperature) at various conditions of wall temperature, chamber pressure, beam current, and number of spectral lines used for the temperature determination. Vibrational band intensities were measured by electronic integration of the rotational line intensities of a vibrational band at room temperature and at pressures from 0.100 Torr to 1.0 Torr. Usually the intensities of two bands were measured at constant beam current and pressure and used to form a ratio that was plotted as a function of nitrogen pressure at 300°K.

CHAPTER II
INTENSITY EQUATIONS

For clarification the spectral intensity equations developed by Muntz (1) will be reviewed.

In the excitation transition, $N_2\ X^1\sum_g^+ \rightarrow N_2^+\ B^2\sum_u^+$, a change of multiplicity occurs which is accounted for by the ionization process. According to Herzberg (6) the two states $X^1\sum$ and $B^2\sum$ belong to Hund's case (b), and under moderate resolution the doublet states of $B^2\sum$ are unresolved. The rotational energy levels are then designated by the quantum number K. It is assumed that the selection rules for Hund's case (b) for $\sum - \sum$ transitions are valid for the excitation process, i.e., it is assumed that the fast electrons cause changes in the rotation quantum numbers equivalent to that of photoexcitation. The selection rules for the quantum number changes are $\Delta K = \pm 1$, $\Delta K = 0$ being forbidden. The selection rules therefore predict the existence of a P and R branch in the excitation (see Figure 2). For the emission process there are P and R branches with $\Delta K = \Delta J = \pm 1$; furthermore, there are satellite branches with $\Delta K \neq \Delta J = 0$ (see Figure 3). Again, under moderate resolution the doublet nature of the P and R and the satellite branches are not resolved. Therefore, as pointed out by Herzberg (6), the band structure appears the same as for $^1\sum - {}^1\sum$ bands, but with the rotational lines numbered by K instead of J.

In the following development of the intensity equations it

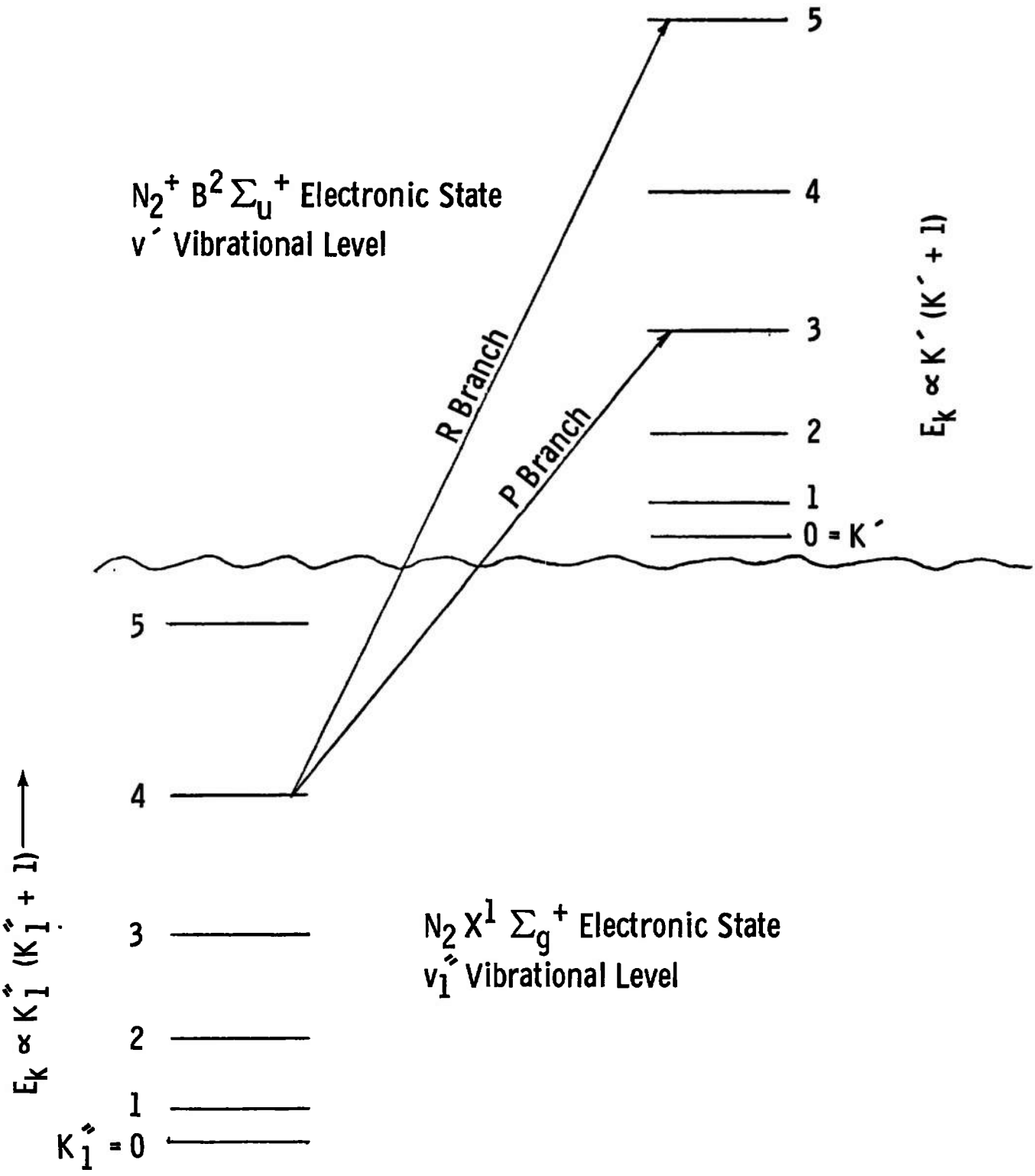

Fig. 2 More Detailed Diagram of Excitation Process

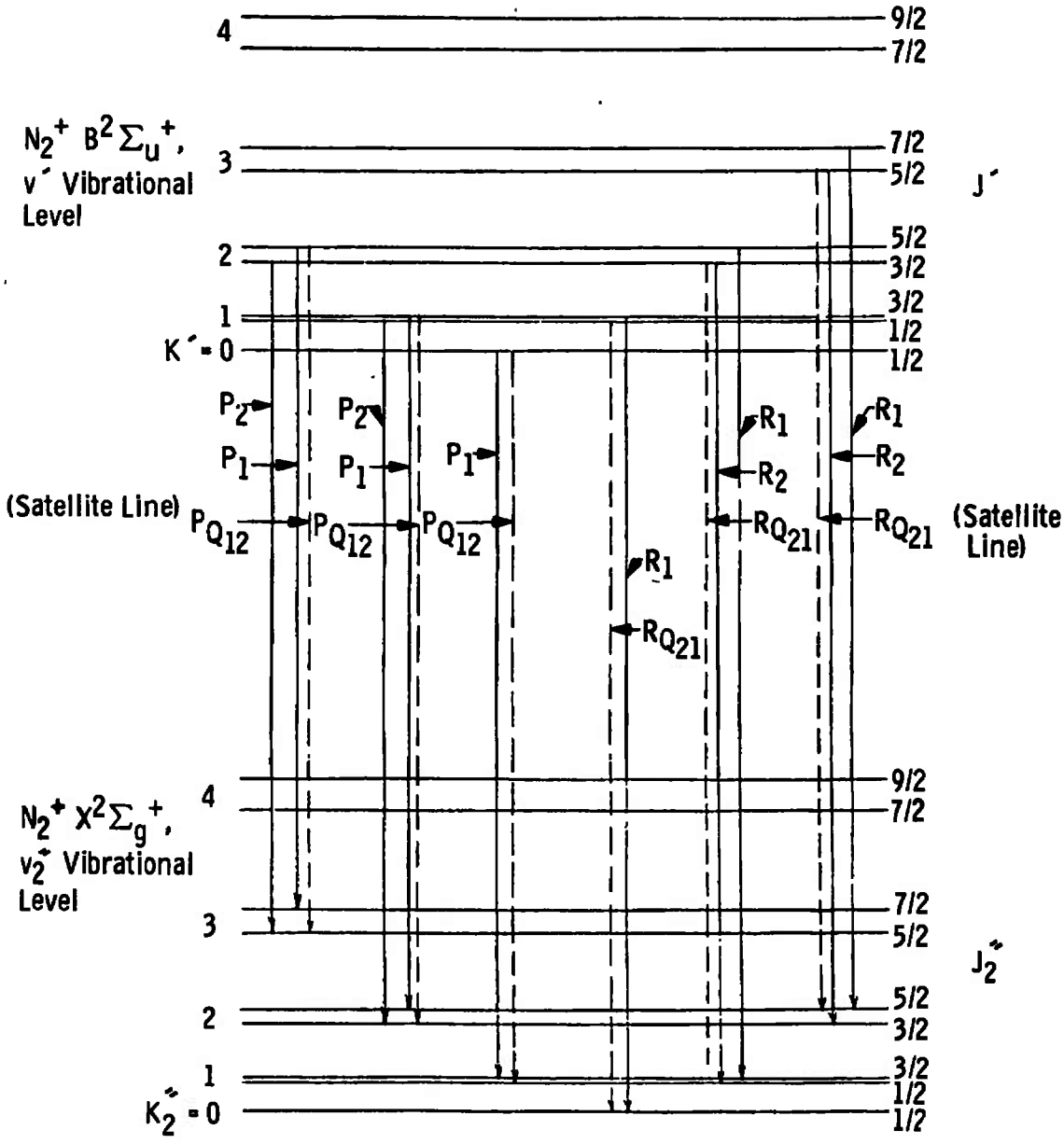

Fig. 3 More Detailed Diagram of Emission Process

will be assumed that the number density of the gas is sufficiently low, that collision effects are negligible and that the gas is pure nitrogen. The method of calculation follows that of Muntz (1) and procedures developed at AEDC.

The total number of molecules per unit volume being excited from the N_2 $X^1\sum$ state (level n) to the N_2^+ $B^2\sum$ state (level m) is given by

$$\frac{N_T\, J_b\, \sigma_{n\to m}}{-e\, \omega_n} = \frac{N_T\, I_b\, \sigma_{n\to m}}{-e\, \omega_n A_b} = \text{(number of } n\to m \text{ transitions (1) per second per unit volume)}$$

where

ω_n = the degeneracy of the electronic state n

I_b = beam current

A_b = beam cross-sectional area

$-e$ = electronic charge

N_T = neutral N_2 number density

J_b = beam current density

and

$\sigma_{n\to m}$ = the total inelastic cross-section for the N_2 $X^1\sum \to N_2^+$ $B^2\sum$ transition, irrespective of vibrational and rotational quantum numbers

The number of molecules per second making a P branch transition from v_1'', K_1'' will originate from v_1'', $K' + 1$ (since $K_1'' = K' + 1$ for a P branch transition), and this number is proportional to

$$p(v', v_1'') \cdot P_p \cdot N^n_{v_1'', K'+1} \tag{2}$$

where

$$p(v', v_1'') = q(v', v_1'')(R_e)^2 \tag{3}$$

and $$q(v',v_l'') \equiv \text{Franck-Condon factor} = \left[\int \psi^*(m,v')\psi(n,v_l'')d\tau\right]^2 \quad (4)$$

and $$R_e^2 = \left| \int \psi^*(m,v') < m|R_e(r)|n > \psi(n,v_l'')d\tau \right|^2 \quad (5)$$

and $R_e(r)$ is an assumed functional form of the electronic moment averaged over m and n.

P_p is the P branch Hönl-London factor which is proportional to the line-strength or rotational quantum number dependent portion of the transition probability. $p(v',v_l'')$ is a vibrational transition probability, and $N^n_{v_l'',K'+1}$ is the number of molecules in state n, v_l'', K' + 1.

Similarly, the number of molecules per second making an R branch transition is proportional to

$$p(v',v_l'') \cdot P_R \cdot N^n_{v_l'',K'-1} \quad (6)$$

The Hönl-London factors are those used for a $^1\Sigma - {}^1\Sigma$ transition. In terms of K' they are

$$P_p = \left.\frac{S^{K'}_{K_l''}}{2K_l''+1}\right|_{K_l''=K'+1} = \frac{K'+1}{2K'+3} \quad (7)$$

and

$$P_R = \left.\frac{S^{K'}_{K_l''}}{2K_l''+1}\right|_{K_l''=K'-1} = \frac{K'}{2K'-1} \quad (8)$$

The total number of transitions per second from n to m which originate in v_l'' and end in v' regardless of the initial and final value

of K is given by summing over both K_l'' and K'. However, since there is a relation between K_l'' and K' a single sum is sufficient. That is, a delta notation can be used such that

$$P_R = \delta[K_l'' - (K'-1)]\left(\frac{K'}{2K'-1}\right) \tag{9}$$

Then

$$P_R = \frac{K'}{2K'-1} \quad \text{if } K_l'' = K'-1 \tag{10}$$

otherwise, P_R is zero. Similarly,

$$P_p = \delta[K_l'' - (K'+1)]\left(\frac{K'+1}{2K'+3}\right) \tag{11}$$

Therefore, the total number of transitions per second from n to m which originate in v_l'' and end in v' regardless of the initial and final value of K is given by

$$\sum_{K'=0}^{\infty} p(v',v_l'')\left[P_p\, N_{v_l'',K'+1} + P_R\, N_{v_l'',K'-1}\right] \tag{12}$$

with the restriction that $K' - 1 \geq 0$ (i.e. for the R branch there is no K'=0 line).

The total number of transitions which originate from v_l'' and end in any v' per second

$$= \sum_{v'=0}^{\infty}\left\{\sum_{K'=0}^{\infty} p(v',v_l'')[P_p\, N_{v_l'',K'+1} + P_R\, N_{v_l'',K'-1}]\right\} \tag{13}$$

The total number of transitions per second which originate in any v''_l and any K''_l and end in any v' and any K'

$$= \sum_{v''_l=0}^{\infty} \sum_{v'=0}^{\infty} p(v',v''_l) \left\{ \sum_{K'=0}^{\infty} \left[P_p N_{v''_l,K'+1} + P_R N_{v''_l,K'-1} \right] \right\} \quad (14)$$

which is proportional to

$$\frac{j_b N_T \sigma_{n\to m}}{-e \omega_n}$$

The fraction populating the state represented by m, v', K' from all v''_l, K''_l levels of n

$$= \frac{\sum_{v''_l=0}^{\infty} p(v',v''_l) \left[P_p N_{v''_l,K'+1} + P_R N_{v''_l,K'-1} \right]}{\sum_{v''_l=0}^{\infty} \sum_{v'=0}^{\infty} p(v',v''_l) \left\{ \sum_{K'=0}^{\infty} \left[P_p N_{v''_l,K'+1} + P_R N_{v''_l,K'-1} \right] \right\}} \quad (15)$$

Therefore, the number of transitions per second, ζ, into m, v', K' due to excitation is

$$\zeta = \frac{j_b \sigma_{n\to m} N_T}{-e \omega_n} \left\{ \frac{\sum_{v''_l=0}^{\infty} p(v',v''_l) \left[P_p N_{v''_l,K'+1} + P_R N_{v''_l,K'-1} \right]}{\sum_{v''_l=0}^{\infty} \sum_{v'=0}^{\infty} p(v',v''_l) \left\{ \sum_{K'=0}^{\infty} \left[P_p N_{v''_l,K'+1} + P_R N_{v''_l,K'-1} \right] \right\}} \right\} \quad (16)$$

For a steady-state condition, neglecting molecular collisional effects, $\zeta \equiv$ the number of radiative de-excitations per second.

From m, v', K' there are transitions to all v_2'' levels of the ℓ state ($N_2^+ X^2 \Sigma$), since there is no selection rule for v. For each v' to v_2'' transition there is a P and R branch, and all these transitions must be summed over to find a quantity to balance ζ, the excitation rate.

From Herzberg (6), after a few manipulations, the number of emission transitions per second is

$$A_{\substack{m,v'K' \\ \ell,v_2'',K_2''}} = \frac{4 E^3_{v',K'} \; S^{m,v',K'}_{\ell,v_2'',K_2''} \; N^m_{v',K'}}{3 \hbar^4 c^3 \; \omega_m (2K'+1)} \tag{17}$$

where $\omega_m \equiv$ the degeneracy of the electronic state m

and $S^{m,v',K'}_{\ell,v_2'',K_2''} \equiv$ the band strength for the transition

$$S^{m,v',K'}_{\ell,v_2'',K_2''} = S^{K'}_{K_2''} \; p(v',v_2'') \tag{18}$$

$$S^{K'}_{K'-1} = K' \tag{19}$$

for the R branch; for the P branch

$$S^{K'}_{K'+1} = K'+1 \tag{20}$$

$$\sum_{K_2''=0}^{\infty} S^{K'}_{K_2''} = 2K'+1 \tag{21}$$

Therefore,

$$A_{\substack{v',K' \\ v''_2,K''_2}} = \left\{ \sum_{v''_2=0}^{\infty} \sum_{K''_2=0}^{\infty} 4 E^3_{\substack{v',K' \\ v''_2,K''_2}} \frac{S^{K'}_{K''_2} p(v',v''_2)}{3\hbar^4 c^3 \omega_m (2K'+1)} \right\} N_{v',K'} \tag{22}$$

$$A_{v',K'} = \frac{4N_{v',K'}}{3\hbar^4 c^3 \omega_m (2K'+1)} \sum_{v''_2=0}^{\infty} p(v',v''_2) h^3 c^3 \left[\frac{S^{K'}_{K'+1}}{\lambda^3_{\substack{v',K' \\ v''_2,K'+1}}} + \frac{S^{K'}_{K'-1}}{\lambda^3_{\substack{v',K' \\ v''_2,K'-1}}} \right] \tag{23}$$

$$A_{v',K'} = \frac{64\pi^4}{3h\omega_m} \frac{N_{v',K'}}{2K'+1} \sum_{v''_2=0}^{\infty} p(v',v''_2) \left[\frac{K'+1}{\lambda^3_{\substack{v',K' \\ v''_2,K'+1}}} + \frac{K'}{\lambda^3_{\substack{v',K' \\ v''_2,K'-1}}} \right] \tag{24}$$

Since $\zeta = A_{v',K'}$ the following expression for the steady-state number density, $N_{v',K'}$, is obtained.

$$N_{v',K'} = \frac{(2K'+1)\left(\frac{3h\omega_m}{64\pi^4}\right)(\zeta)}{\sum_{v''_2=0}^{\infty} p(v',v''_2) \left[\frac{K'+1}{\lambda^3_{\substack{v',K' \\ v''_2,K'+1}}} + \frac{K'}{\lambda^3_{\substack{v',K' \\ v''_2,K'-1}}} \right]} \tag{25}$$

From Herzberg (6), again with a little manipulation, the intensity of a rotational line in emission is

$$I_{\substack{v',K' \\ v''_2,K''_2}} = \frac{4 E^4_{v',K'} p(v',v''_2) S^{K'}_{K''_2} N_{v',K'}}{3\hbar^4 c^3 \omega_m (2K'+1)} \tag{26}$$

For R branch transitions $K''_2 = K'-1$ and $S^{K'}_{K''_2} = S^{K'}_{K'-1} = K'$.

Therefore, for the R branch

$$I_{\substack{v',K' \\ v''_2,K'-1}} = \frac{\zeta_{K'} \frac{hc}{\lambda_R^4} p(v',v''_2)}{\sum_{v''_2=0}^{\infty} p(v',v''_2)\left[\frac{K'+1}{\lambda_P^3} + \frac{K'}{\lambda_R^3}\right]} \tag{27}$$

Using Equation 16 for ζ, Equation 27 becomes

$$\cdot_{\substack{v',K' \\ v''_2,K'-1}} = \frac{N_T\, j_b\, \sigma_{n\to m}\, hc}{e\, \omega_n\, \lambda^4_{\substack{v',K' \\ v''_2,K'-1}}} \left\{\left[\frac{K'\, p(v',v''_2)}{\sum_{v''_2=0}^{\infty} p(v',v''_2)\left[\frac{K'+1}{\lambda_P^3} + \frac{K'}{\lambda_R^3}\right]}\right]\right.$$

$$\left.\times\left[\frac{\sum_{v''_1=0}^{\infty} p(v',v''_1)\,(P_p\, N_{v''_1,K'+1} + P_R\, N_{v''_1,K'-1})}{\sum_{v'=0}^{\infty}\sum_{v''_1=0}^{\infty} p(v',v''_1)\left(\sum_{K'=0}^{\infty}\left\{P_p\, N_{v''_1,K'+1} + P_R\, N_{v''_1,K'-1}\right\}\right)}\right]\right\} \tag{28}$$

Therefore,

$$I_{\substack{v',K' \\ v''_2,K'-1}} = \frac{c_1\, p(v',v''_2)}{\lambda^4_{\substack{v',K' \\ v''_2,K'-1}} \left\{\tau_{v',v''_2}\right\}} \quad \frac{K'}{2K'+1}$$

$$\times \sum_{v''_1=0}^{\infty} p(v',v''_1)\left[P_p\, N_{v''_1,K'+1} + P_R\, N_{v''_1,K'-1}\right] \tag{29}$$

where

$$c_1 = \frac{j_b \sigma_{n\to m} hc N_T}{-e \omega_n \left\{ \sum_{v'=0}^{\infty} \sum_{v_1''=0}^{\infty} p(v', v_1'') \left[\sum_{K'=0}^{\infty} (P_p N_{v_1'', K'+1} + P_R N_{v_1'', K'-1}) \right] \right\}} \tag{30}$$

$$\left\{ \tau_{v', v_2''} \right\} = \sum_{v_2''=0}^{\infty} \frac{p(v', v_2'')}{\lambda^3_{v', v_2''}} \equiv \frac{1}{c_2} \tag{31}$$

and the approximation $\lambda^3_{\substack{v', K' \\ v_2'', K'+1}} \approx \lambda^3_{\substack{v', K' \\ v_2'', K'-1}}$ (32)

is enforced.

For the non-rigid rotor anharmonic oscillator model of the homonuclear diatomic molecule the energy of vibration and rotation is

$$W_{v,K} = E_v + E_{v,K} \tag{33}$$

That is, in a first approximation the energy eigenvalue may be written as a sum of vibrational energy and a vibrational-rotational interaction term.

From Rushbrooke (7) it may be shown that

$$\frac{N_{v,K}}{N_T} = g_K \frac{e^{-(E_v + E_{v,K})/kT}}{(p.f.)_t} \tag{34}$$

where

$$(p.f)_t = \sum_{v=0}^{\infty} \sum_{K=0}^{\infty} g_K \, e^{-(E_v + E_{v,K})/kT} \tag{35}$$

It may be shown using Rushbrooke (7) and AEDC information that

$$(p.f.)_t = \sum_{v=0}^{\infty} e^{-E_v/kT_v} \left\{ \sum_{K=0}^{\infty} g_K \, e^{-E_{v,K}/kT_R} \right\} \tag{36}$$

may be correctly written while

$$\frac{N_{v,K}}{N_T} = \frac{\left[e^{-E_v/kT_v}\right]\left[e^{-E_{v,K}/kT_R}\right]}{(p.f.)_t} \tag{37}$$

even if $T_v \neq T_R$. Therefore,

$$N_{v_1'',K'+1} = \frac{N_T}{(p.f.)_t} (2K'+3) e^{-E_{v_1''}/kT_v} \, e^{-E_{v_1'',K'+1}/kT_R} \tag{38}$$

Using Equation 38 and Equation 7

$$P_p \, N_{v_1'',K'+1} = \frac{N_T}{(p.f.)_t} e^{-E_{v_1''}/kT_v} \, (K'+1) e^{-E_{v_1'',K'+1}/kT_R} \tag{39}$$

Similarly,

$$P_R \, N_{v_1'',K'-1} = \frac{N_T}{(p.f.)_t} e^{-E_{v_1''}/kT_v} \, (K') e^{-E_{v_1'',K'-1}/kT_R} \tag{40}$$

Therefore, from Equations 39 and 40

$$P_p \, N_{v_1'',K'+1} + P_R \, N_{v_1'',K'-1} = \frac{N_T}{(p.f.)_t} e^{-E_{v_1''}/kT_v}$$

$$\times \left[(K'+1) e^{-E_{v_1'',K'+1}/kT_R} + (K') e^{-E_{v_1'',K'-1}/kT_R} \right] \tag{41}$$

From Herzberg (6)

$$E_{v_1'',K'+1} = B_{v_1''}(K'+1)(K'+2)hc \tag{42}$$

and

$$E_{v_1'',K'-1} = B_{v_1''}(K')(K'-1)hc \tag{43}$$

Therefore,

$$p(v',v_1'')[P_p N_{v_1'',K'+1} + P_R N_{v_1'',K'-1}] = \frac{N_T}{(p.f.)_t} \times p(v',v_1'')e^{-E_{v_1''}/kT_v}\left[(K'+1)e^{-B_{v_1''}(K'+1)(K'+2)hc/kT_R} + (K')e^{-B_{v_1''}(K')(K'-1)hc/kT_R}\right] \tag{44}$$

Now,

$$I_{\substack{v',K' \\ v_2'',K'-1}} = \left[\frac{c_1\, p(v',v_2'')}{\lambda^4_{\substack{v',K' \\ v_2'',K'-1}}\left(\sum_{v_2''=0}^{\infty}\frac{p(v',v_2'')}{\lambda^3_{v',v_2''}}\right)}\right]\frac{N_T}{(p.f.)_t} \times\left[\sum_{v_1''=0}^{\infty} p(v',v_1'')e^{-G(v_1'')hc/kT_v}(H)_{v_1''}\left(\frac{K'}{2K'+1}\right)\right] \tag{45}$$

where

$$(H)_{v_1''} = (K'+1)e^{-B_{v_1''}(K'+1)(K'+2)hc/kT_R} + (K')e^{-B_{v_1''}(K')(K'-1)hc/kT_R} \tag{46}$$

For the laboratory conditions T_v is sufficiently low to neglect

all but $v_1'' = 0$ levels of N_2 $X^1\Sigma$. By defining

$$\frac{(H)_o}{2K'+1} = (G)_o e^{-B_o K'(K'+1)hc/kT_R} \tag{47}$$

where

$$(G)_o = \frac{(K'+1)e^{-2B_o(K'+1)hc/kT_R} + (K')e^{2B_o(K')hc/kT_R}}{(2K'+1)} \tag{48}$$

and where $(H)_o$ is $(H)_{v_1''=0}$, $(G)_o$ is $(G)_{v_1''=0}$, and $(B)_o$ is $(B)_{v_1''=0}$. Then,

$$\frac{I_{v',K'}^{v_2'',K'-1}\lambda^4_{v',K'}}{K'(G)_o} = \frac{c_1 c_2 N_T}{(p.f.)_t} e^{-B_o(K')(K'+1)hc/kT_R} \tag{49}$$

Therefore,

$$\ln\left[\frac{I_{v',K'}^{v_2'',K'-1}\lambda^4_{v',K'}}{K'(G)_o}\right] = \ln\left(\frac{c_1 c_2 N_T}{(p.f.)_t}\right) - B_o K'(K'+1)hc/kT_R \tag{50}$$

Equation 50 is the equation derived by Muntz (1). This equation may be solved by iteration to find T_R using measured values of $I_{v',K'}^{v_2'',K'-1}$.

Equation 29 gives the intensity of the R branch line of a band for a given K'. The same equation will yield the intensity of a P branch line of the band for the same K' when K'+1 is substituted for K' in the numerator. By adding these two equations

$$I_{pK'}+I_{RK'} = \frac{c_1\, p(v',v_2'')}{\lambda^4_{\substack{v',K'\\ v_2'',K'-1}}\left\{\tau_{v',v_2''}\right\}} \sum_{v_1''=0}^{\infty} p(v',v_1'')(P_p N_{v_1'',K'+1} + P_R N_{v_1'',K'-1}) \quad (51)$$

$$I_{pK'}+I_{RK'} = \frac{c_1\, p(v',v_2'')}{\lambda^4_{\substack{v',K'\\ v_2'',K'-1}}\left\{\tau_{v',v_2''}\right\}} \sum_{v_1''=0}^{\infty} \sum_{K_1''=0}^{\infty} p(v',v_1'') \left(\frac{S^{K'}_{K_1''}}{2K_1''+1}\right) N_{v_1'',K_1''} \quad (52)$$

The total intensity of a vibrational band is obtained by summing Equation 52 over all values of K. To sum over K' select and fix a value of K_1''. Therefore, assuming $\lambda_{\substack{v',K'\\ v_2'',K'-1}}$ can be replaced by $\lambda_{v',v_2''}$

$$I(v',v_2'') = \frac{c_1\, p(v',v_2'')}{\lambda^4_{v',v_2''}\left\{\tau_{v',v_2''}\right\}} \left[\sum_{K_1''=0}^{\infty} \sum_{v_1''=0}^{\infty} \frac{p(v',v_1'')\, N_{v_1'',K_1''}}{2K_1''+1} \sum_{K'=0}^{\infty} S^{K'}_{K_1''}\right] \quad (53)$$

Then

$$I(v',v_2'') = \frac{c_1\, p(v',v_2'')}{\lambda^4_{v',v_2''}\left\{\tau_{v',v_2''}\right\}} \sum_{K_1''=0}^{\infty} \sum_{v_1''=0}^{\infty} p(v',v_1'') N_{v_1'',K_1''} \quad (54)$$

Since

$$N_{v_1''} = \frac{N_T}{(p.f.)_v} e^{-G(v_1'')hc/kT_v} \quad (55)$$

then

$$I_{v',v_2''} = \frac{c_1 N_T}{(p.f.)_v} \frac{p(v',v_2'')}{\lambda^4_{v',v_2''}} \frac{\sum_{v_1''=0}^{\infty} p(v',v_1'')e^{-G(v_1'')hc/kT_v}}{\sum_{v_2''=0}^{\infty} \frac{p(v',v_2'')}{\lambda^3(v';v_2'')}} \tag{56}$$

Then the intensity ratio of the two bands $(a_{v'},b_{v_2''})$ and $(c_{v'},d_{v_2''})$ is seen to be

$$I_{R_{T_v}} = \frac{I(a_{v'},\ b_{v_2''})}{I(c_{v'},\ d_{v_2''})} = \left(\frac{\lambda_{cd}}{\lambda_{ab}}\right)^4 \frac{p(a_{v'},\ b_{v_2''})}{p(c_{v'},\ d_{v_2''})} \frac{\sum_{v_1''=0}^{\infty} p(a_{v'},v_1'')e^{-G(v_1'')hc/kT_v}}{\sum_{v_1''=0}^{\infty} p(c_{v'},v_1'')e^{-G(v_1'')hc/kT_v}}$$

$$\times \left[\frac{\sum_{v_2''=0}^{\infty} p(c_{v'},v_2'')/\lambda^3_{c_{v'},v_2''}}{\sum_{v_2''=0}^{\infty} p(a_{v'},v_2'')/\lambda^3_{v',v_2''}}\right] \tag{57}$$

From a theoretical plot of $I_{R_{T_v}}$ versus T_v and an experimental measure of $I_{R_{T_v}}$ a value of T_v of nitrogen may be found. Therefore, it is seen that using Equation 57 the vibrational temperature of nitrogen can be determined by performing the measurement of the relative band strengths of at least two bands of the N_2^+ $[I^-]$ system.

CHAPTER III
BRIEF REVIEW OF THE WORK OF OTHER INVESTIGATORS

Muntz (1), using an equation similar to Equation 50, calibrated an electron beam probe in slowly flowing nitrogen (∿ 0.5 meters per second) at room temperature and 373°K with a film spectrograph and found it accurate (± two per cent) for pressures less than approximately 0.5 Torr. A maximum of nineteen rotational lines was used for the temperature determination. The beam current was 0.085-0.25 milliamperes at 17 KV with gas pressures of 0.155-0.470 Torr. The measured temperature was shown to be independent of beam energy in the range 12.5-17.5 KV and independent of pressure from 0.200-0.470 Torr. Muntz also pointed out that rotational temperatures measured from beam emission of stagnant room temperature nitrogen indicated that the nitrogen in the vicinity of the beam was heated.

For vibrational temperatures Muntz calculated an intensity ratio of two bands as a function of vibrational temperature using

$$\frac{I(a_{v'},\, b_{v_2''})}{I(c_{v'},\, d_{v_2''})} = \left(\frac{\lambda_{cd}}{\lambda_{ab}}\right)^4 \frac{q(a_{v'},\, b_{v_2''})}{q(c_{v'},\, d_{v_2''})} \frac{\sum_{v_1''=0}^{\infty} q(a_{v'}, v_1'') e^{-G(v_1'')hc/kT_v}}{\sum_{v_1''=0}^{\infty} q(c_{v'}, v_1'') e^{-G(v_1'')hc/kT_v}} \tag{58}$$

which is Equation 57 with Franck-Condon factors instead of the more appropriate vibrational band strengths. By measuring the ratio and using the calculated curve vibrational temperature was measured.

Muntz concluded that his model for excitation and emission was the correct one and that point low density rotational temperature measurements could be made in nitrogen (with a majority of molecules in the N_2 $X^1\sum$ state) with an accuracy of ± two per cent. On this basis further work of Muntz was directed toward development of a Rotational Temperature Apparatus (RTA) which was essentially a two-color pyrometer for observing portions of the rotational structure of a vibrational band (2). This device was shown to be capable of measuring rotational temperatures.

Due to the apparent simplicity of the EBT using the RTA, an RTA device was fabricated by this author for use in transient hypervelocity flow measurements.

Muntz also reported a ± ten per cent accuracy for vibrational temperature measurements.

Petrie (5) conducted validation experiments for the EBT in slowly flowing air. At room temperature the difference between measured and known temperature was within ± three per cent. The temperature measurements were also found to be independent of pressure to 0.400 Torr. Beam current was 0.010-0.50 milliamperes at 10-20 KV.

For vibrational temperature validation the intensity ratios I_{01}/I_{12} and I_{02}/I_{13} were measured by Petrie at room temperature. The measured values are shown in Figures 4 and 5. The ratios were obtained from film spectra, and the discrepancies between theory and experiment were attributed to uncertainties in intensities determined with a densitometer. The vibrational temperature measurement accuracy was

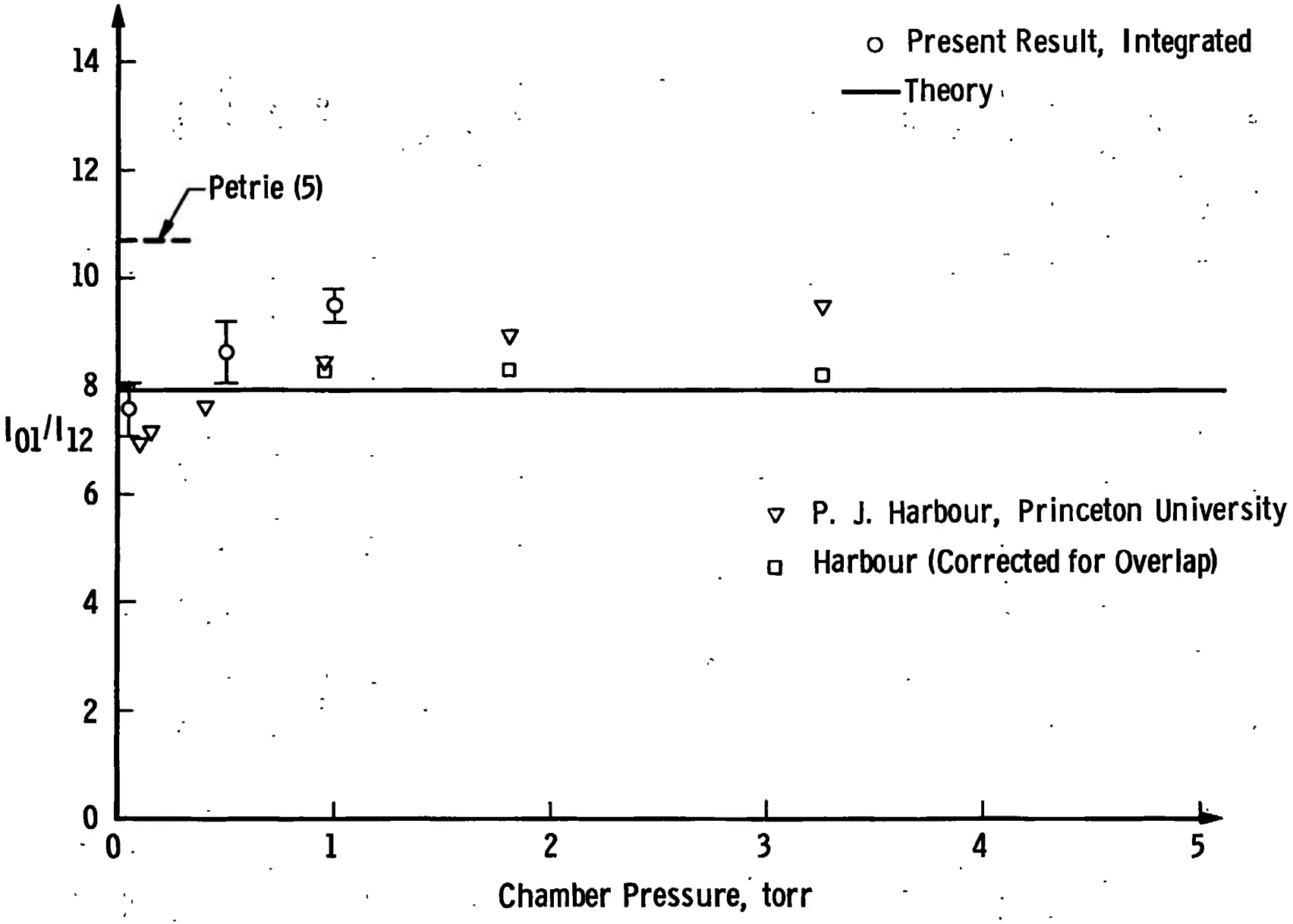

Fig. 4 I_{01}/I_{12} versus Chamber Pressure

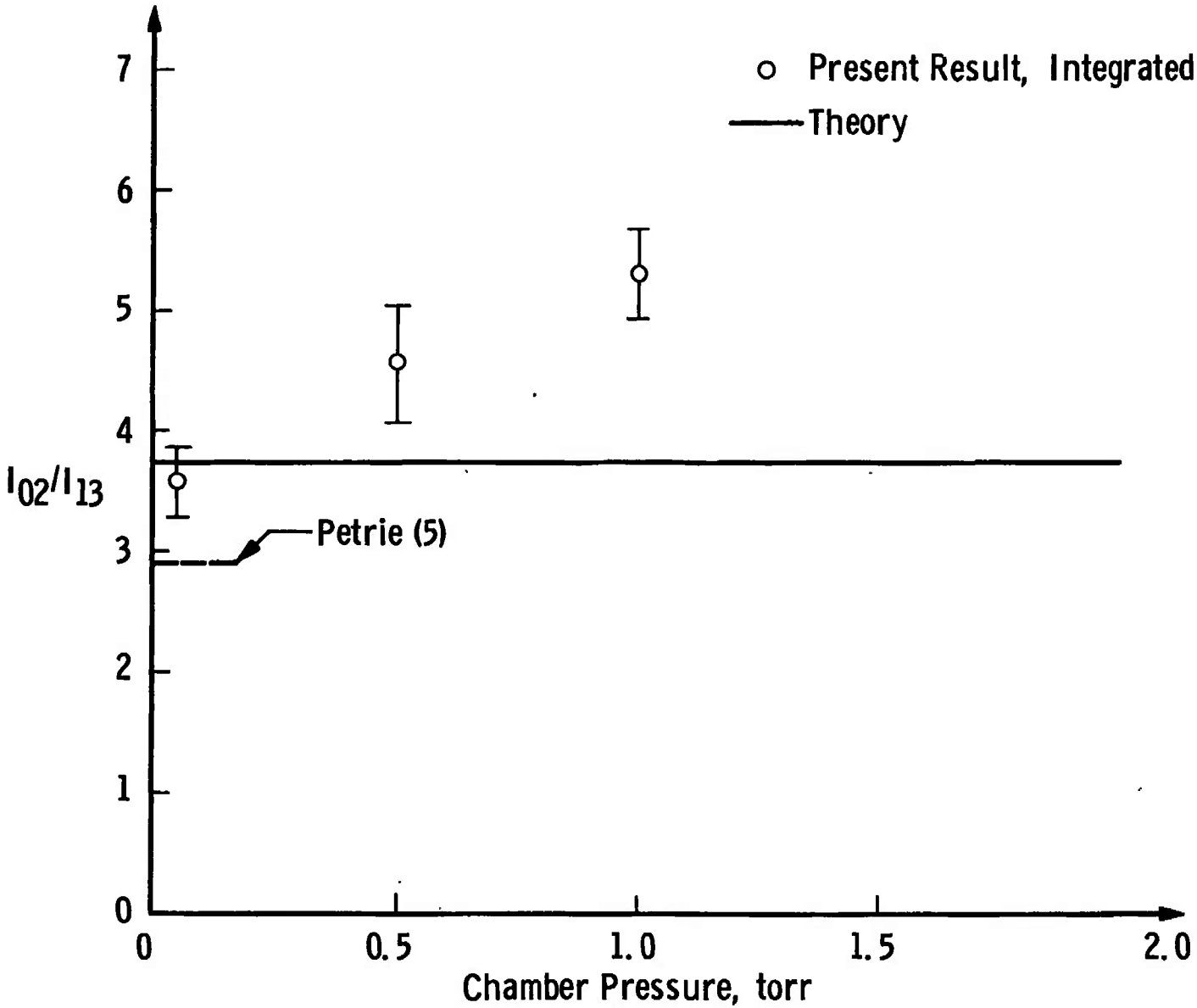

Fig. 5 I_{02}/I_{13} versus Chamber Pressure

predicted to be within ± 15 per cent. However, Petrie neglected completely the effect of the decay channels in emission by omitting the last factor of Equation 57.

Robben and Talbot (8) carried out a series of rotational temperature measurements in a subsonic nozzle, a Mach 4 nozzle, and a free jet expansion. The measurements were shown to be about three per cent high at 280°K with a progressively increasing error at lower temperatures (see Figure 6). These measurements were made with the electron gun operating at 30 KV and with beam currents of 1-10 milliamperes. The beam was imaged perpendicular to the spectrometer slit.

Robben and Talbot suggested empirically correcting electron beam rotational temperature measurements to account for the difference between spectrally measured and calculated temperatures. It was believed that the error was due to secondary electrons since a small dependence on slit height was observed in their data; and it was pointed out that the halo surrounding the beam was caused by secondary electrons which might not obey the optical selection rules when exciting N_2^+ [1⁻].

They also found (as did Muntz) that in slowly flowing nitrogen at 300°K the measured temperatures were higher by as much as 50°K. This error was found to be highly density dependent, but at 0.04 Torr the error had decreased to the flowing gas error. Robben and Talbot thought this might be due to metastable atoms not being able to diffuse to the walls at high pressures.

Marrone (9) used the electron beam probe to obtain measurements in supersonic nitrogen jets expanding from room temperature. The

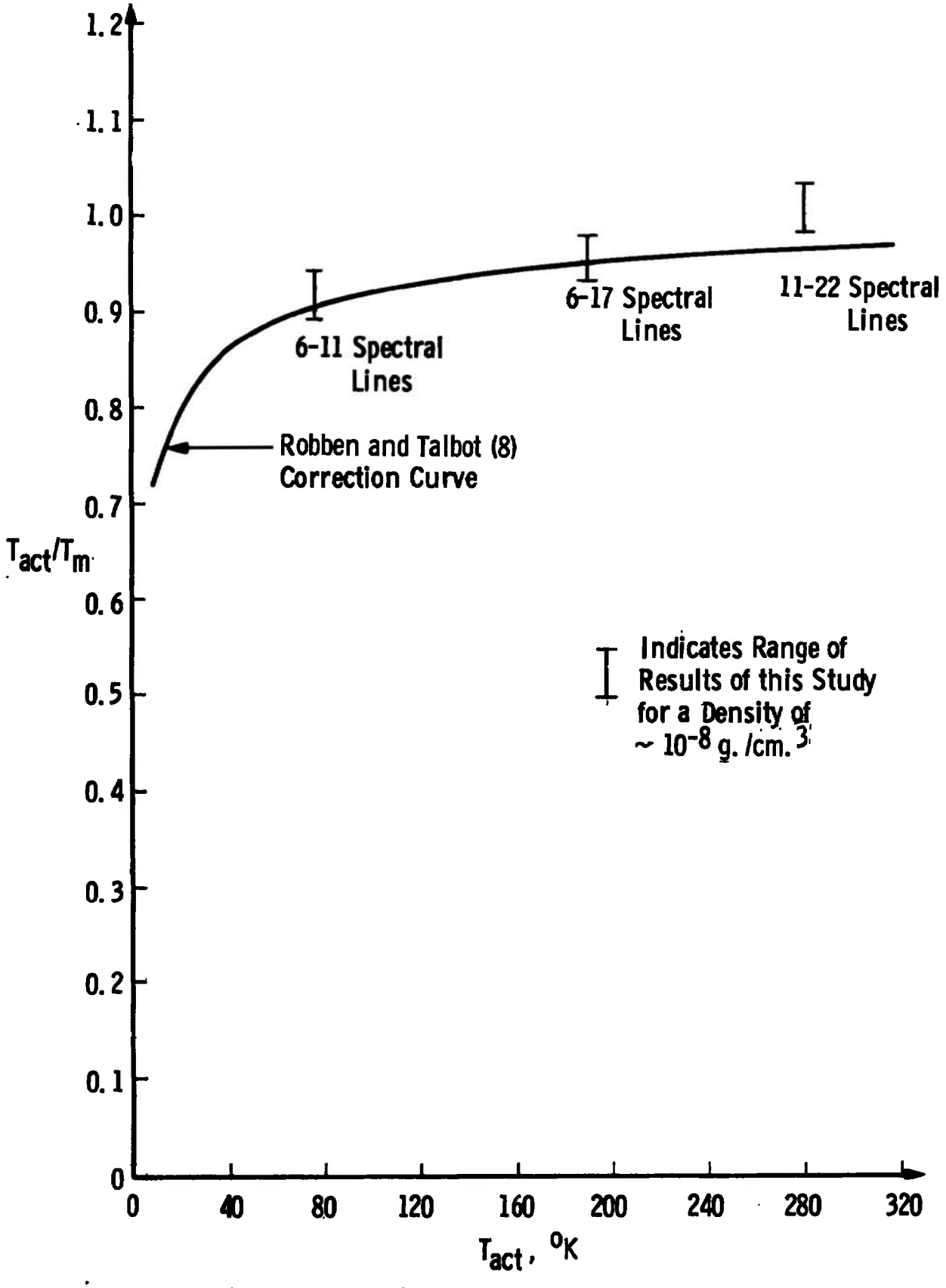

Fig. 6 Actual Temperature Divided by Measured Temperature versus Actual Temperature

electron gun was operated at 17.5 KV and 0.100-0.250 milliamperes beam current. The rotational temperature values obtained experimentally agreed with the predicted values down to about 50°K. That is, the Boltzmann plots of rotational line intensities were linear using the majority of observed rotational lines, and Marrone proceeded to re-interpret Robben and Talbot's tunnel data as rotational freezing phenomena. However, the higher K' rotational lines always indicated a higher intensity than was consistent with the straight line plot. This led Marrone to believe that perhaps this effect was produced by the electron beam itself, and again the effect of the secondary electrons was under question. Ashkenas (10) investigated the rotational spectra of nitrogen in thermodynamic equilibrium at 300°K and 78°K and observed a non-linear line intensity plot. It was observed that the rotational temperature defined by a straight line varied with the number of spectral lines used and that the spectrally measured rotational temperature was dependent on the dry nitrogen density at which the measurement was made. There was doubt expressed concerning the validity of the Muntz excitation model. Figures 7, 8, and 9 illustrate the findings of Ashkenas.

Ashkenas's pressure range was 0.02-2.0 Torr. The electron gun was operated at 15 KV at maximum current output. The beam current measured at the collector plate varied with the density of the gas in the chamber; and beam currents up to 0.200 milliamperes and as low as 0.010 milliamperes were recorded. Judging from this author's own experience, the current in the chamber was probably an order of magnitude higher; however, Ashkenas's work indicated no beam effect on

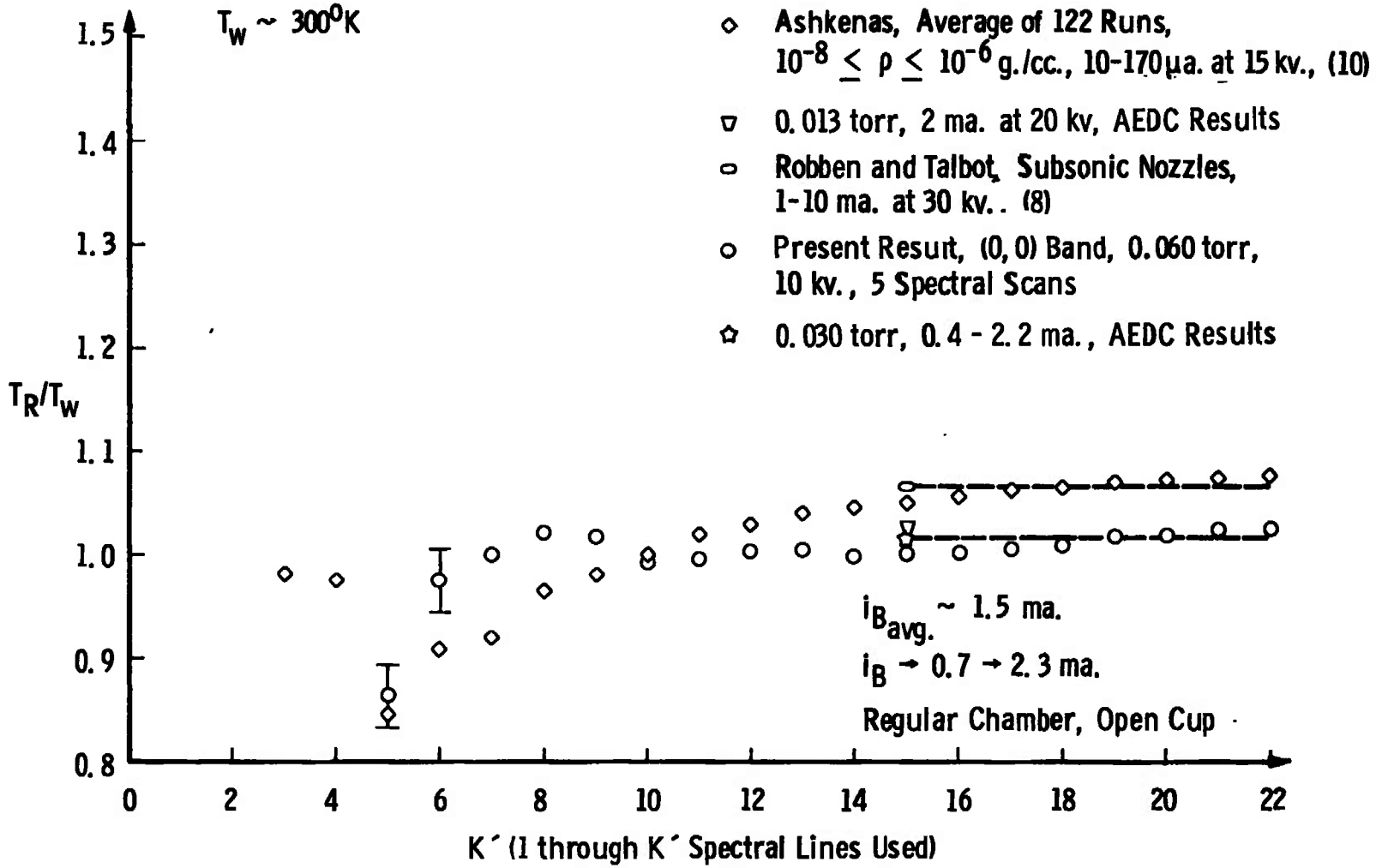

Fig. 7 Ratio of Measured Rotational Temperature to Chamber Wall Temperature versus Number of Spectral Lines Used for the Temperature Determination, $T_w \approx 300°K$, $P_c = 0.060$ Torr

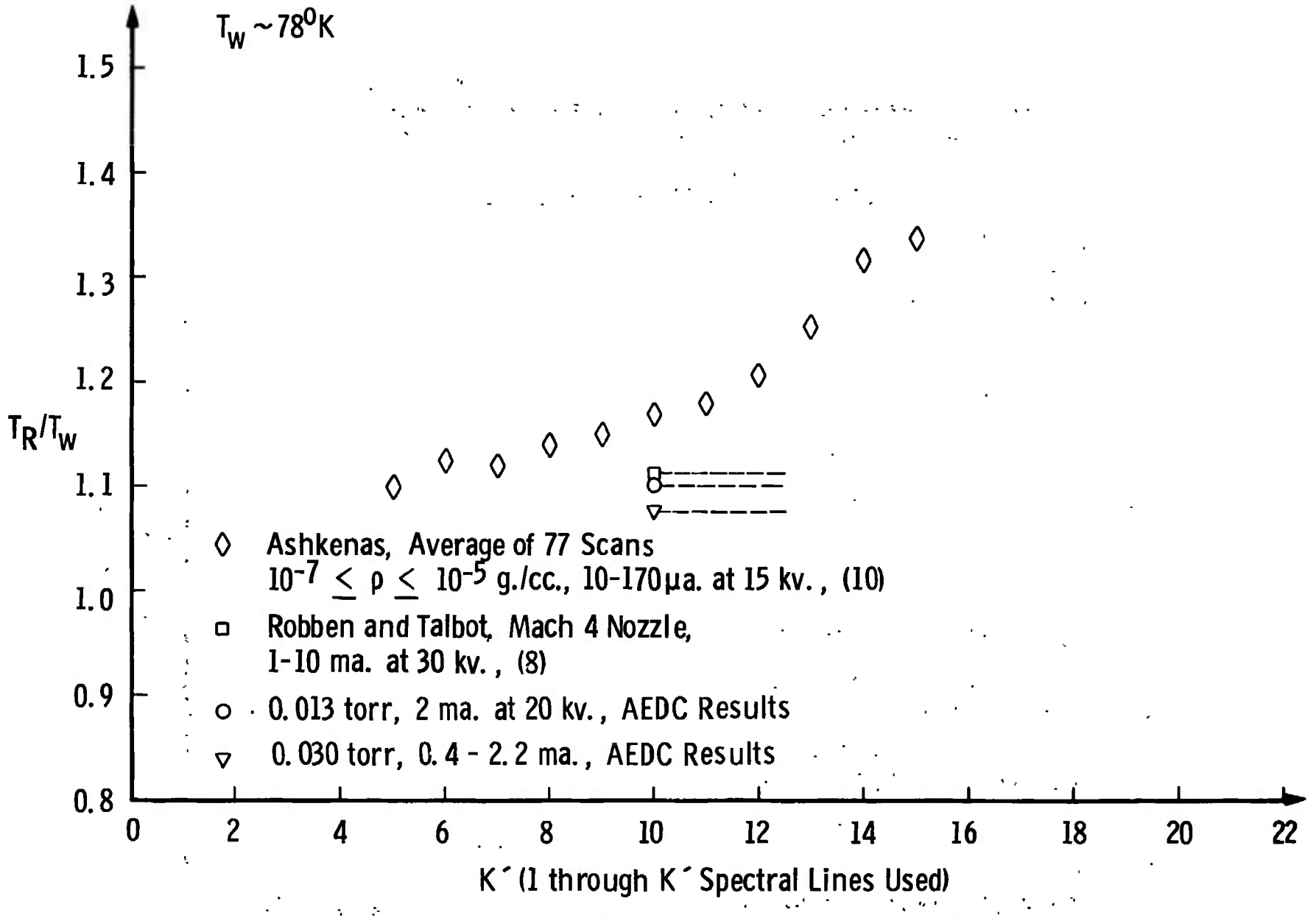

Fig. 8 Ratio of Measured Rotational Temperatures to Chamber Wall or Actual Temperature from Other Investigations, $T_w \approx 78°K$

AEDC-TR-68-265

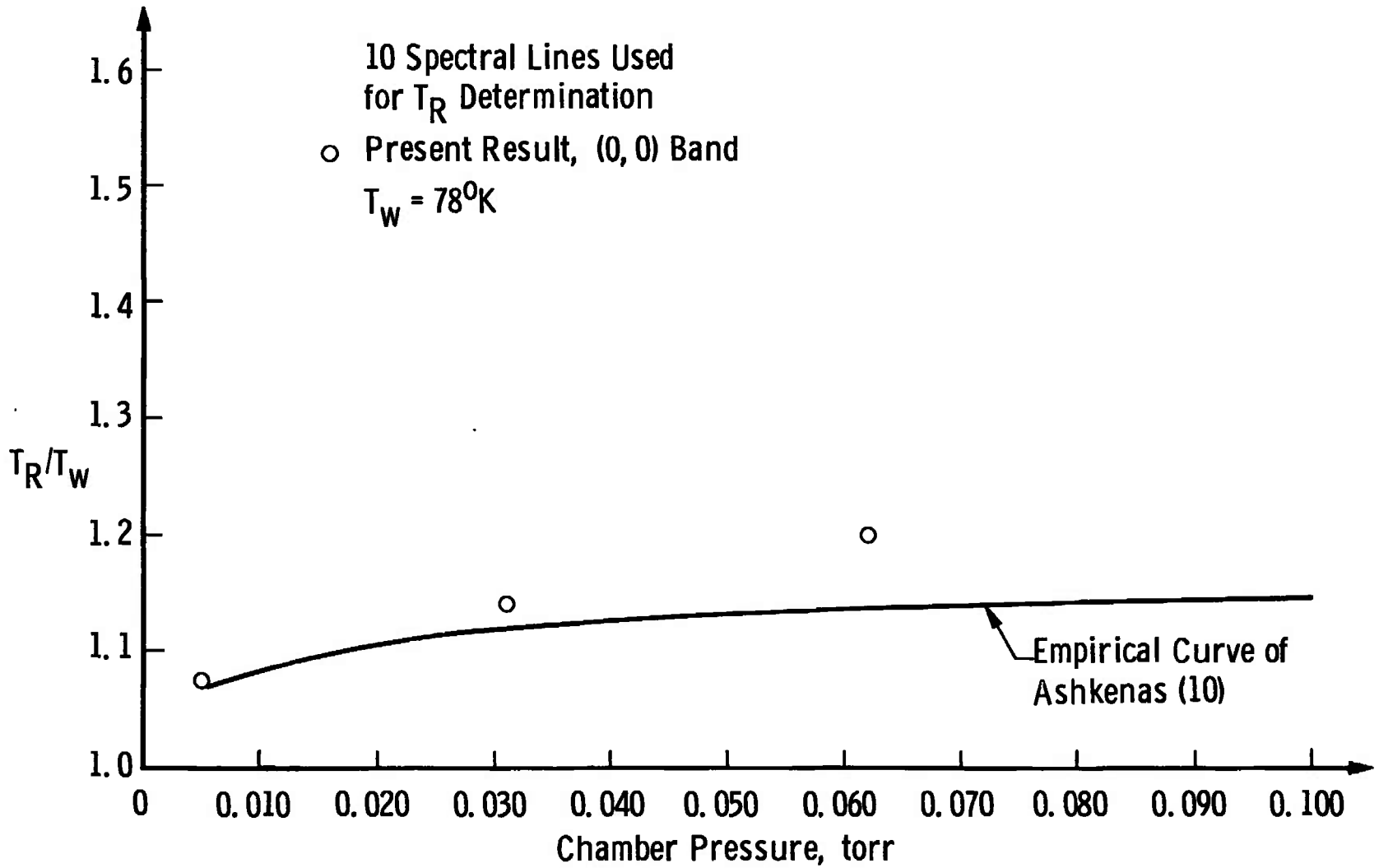

Fig. 9 Ratio of Measured Rotational Temperature to Chamber Wall Temperature versus Chamber Pressure, T_w . 78 °K, 10 Spectral Lines Used

temperature measurements since a thirtyfold increase in the beam current at the lowest mass flow rate resulted in a temperature change of less than five per cent. The flow rates in the test chamber were varied from 0.02-1.2 grams per minute.

In contrast, data developed at AEDC showed that in a completely static calibration channel at 80°K the spectrally measured values of temperature varied directly with beam current. This was shown to be consistent with a local heating within the beam volume due to inelastic collisions between beam and atomic electrons. The electron gun was operated at 20 KV and 0.2-3.0 milliamperes. However, at 300°K the difference between measured temperatures and wall temperatures could not be explained by local heating; and, furthermore, agreed with the Robben and Talbot correction curve.

In an effort to observe qualitatively the effect of low energy electrons on apparent rotational temperatures the cathode region of a glow discharge tube was spectroscopically investigated at Princeton by Harbour. Especially near the cathode in the cathode glow region a marked overpopulation in the upper rotational levels was found.

The intensity ratio of the (0,1) and (1,2) bands of N_2^+ $[1^-]$ was measured by Harbour and found to have a density dependence as shown in Figure 4, page 23. Even accounting for the contribution from the N_2 $[2^+]$ (1,5) band did not eliminate the density variation in the lower pressure region.

CHAPTER IV
THE ELECTRON BEAM LABORATORY SYSTEM

A. THE VACUUM SYSTEM

In order to inject an electron beam originating from an electron gun at a pressure of less than 0.1×10^{-3} Torr into a gas at pressures ranging from a few thousandths Torr to several Torr a dynamic pumping system was fabricated. The system consists of a four-inch oil diffusion pump ($\sim$ 700 liters per second) and associated mechanical forepump (140 liters per minute) that provide low pressure for the electron gun section. The electron gun section is separated by an orifice or system of orifices from the test chamber into which the beam is injected through the orifice. With a single orifice (0.080 inches in diameter and 0.0625 inches in length) a maximum pressure of 0.100 Torr is attainable in the test section without exceeding 0.1×10^{-3} Torr in the electron gun. With a triple stage orifice internally pumped by two mechanical pumps (each 140 liters per minute) the maximum test chamber is approximately 10 Torr. The lowest pressure attained in the system was 7×10^{-7} Torr (measured with an ion gauge) with a leak rate of less than 0.15×10^{-3} Torr per minute.

The electron gun is separated from the high vacuum "T" section (see Figure 10) by a vacuum valve which allows gun changes without venting the entire system to atmosphere. A water-cooled baffle is directly

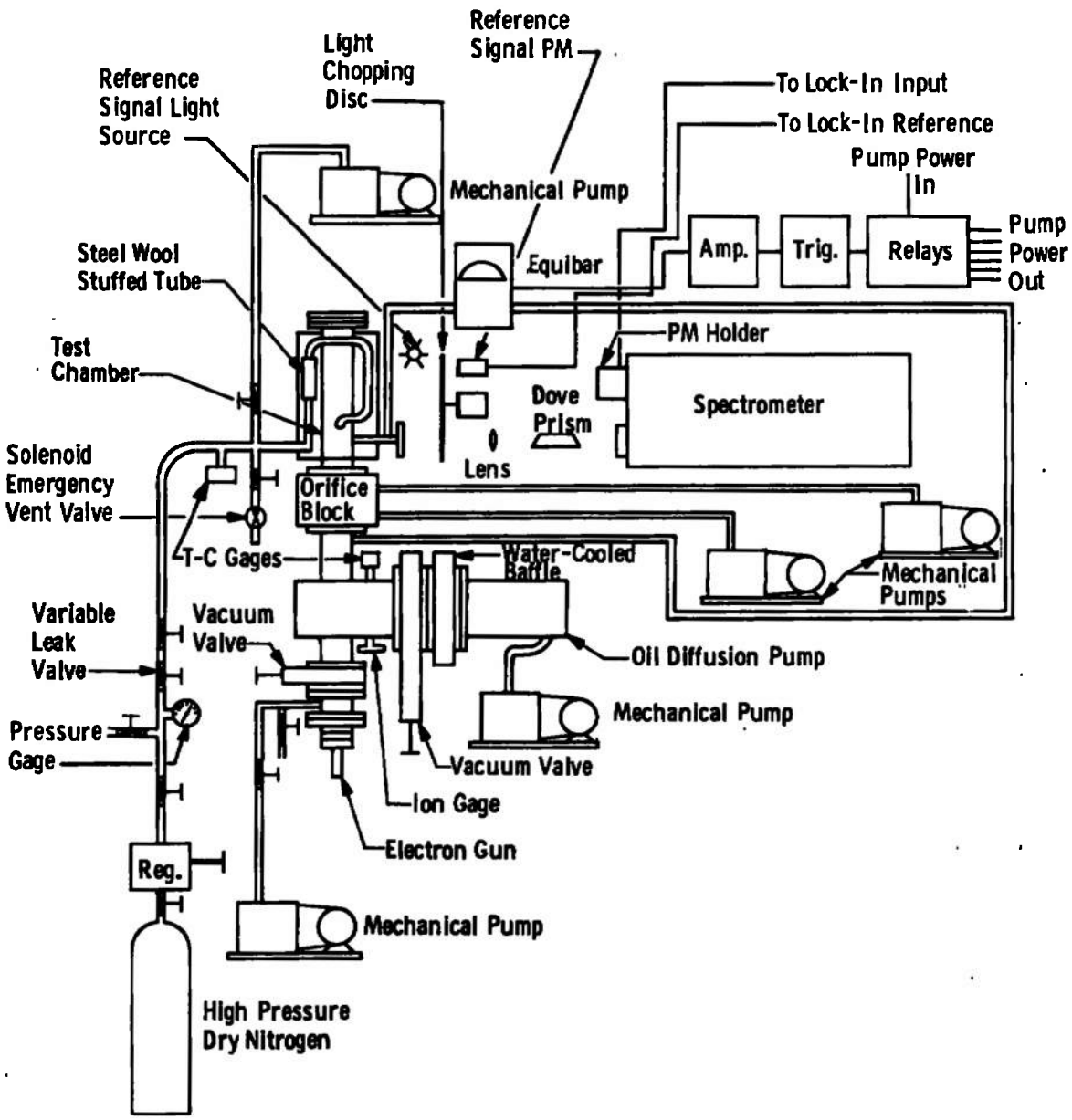

Fig. 10 Simplified Diagram of Laboratory System

connected to the diffusion pump to help prevent oil vapor from back-streaming into the electron gun, and a large vacuum valve is used across the baffle and diffusion pump combination.

The test chamber is an 18-inch length of thin wall (0.032-inch thick) stainless steel tubing. An observation port is located four inches from the point of injection of the electron beam. Dry nitrogen is leaked into the system from a high pressure bottle through a series of regulators and valves and copper tubing. The flow of nitrogen passes through a six-inch length 3/4-inch diameter piece of stainless steel tubing packed with very fine steel wool; then the nitrogen flows through another foot of copper tubing before entering the test chamber. The steel wool packed tubing and last foot of copper tubing are all contained within an insulated trough built around the test chamber. This trough holds whatever coolant is used in the experiments.

Inner wall and coolant temperatures were measured with copper-constantan thermocouples and a potentiometer.

The vacuum seals between the test chamber and orifice and observation port are effected with teflon "O"-rings to withstand the low temperatures brought about by the test chamber coolants. In addition, due to the nearness of all the flanges to the coolant, the flanges are heated with nichrome heating elements in order to maintain a vacuum seal during several hours of coolant operation.

Test chamber pressures are monitored on a Type 128 Transonics Equibar Pressure Meter, which is a portable, differential, variable

capacitance type micromanometer operating over eight full scale ranges from 0.01-30 Torr. The reference pressure is the electron gun section pressure.

The Equibar also provides an 0.5 volt 60 Hz output at full scale on each scale. The signal is amplified and fed into a trigger circuit which controls a vacuum system solenoid bleed valve and vacuum pump power. This circuit and valving system is activated during periods in which no personnel are near the system. If for any reason the test chamber pressure rises above 0.050 Torr, the pumps will shut down, and the system will slowly vent to atmospheric pressure automatically.

B. THE ELECTRON BEAM SOURCE AND RECEIVER CUP

The electron gun high voltage power supply was a 0-50 KV at 0-5 milliampere universal Voltronics supply. At present, this supply has been replaced by a 0-100 KV at 0-5 milliampere, ripple filtered supply of the same make. Voltage supplied to guns is negative with respect to ground potential.

The electron guns are General Electric Type 33. These guns are television type, oxide cathode models modified for a maximum of 50 KV operation. The accelerator grid of these guns is also modified by having its opening enlarged to 3/16-inch diameter. Magnetic focusing and deflection are used with these guns. The filament is battery powered at 6-18 V.

The electron gun system is capable of injecting up to ≥ 4.5 milliampere beam into the test chamber at 10-35 KV.

Basically the beam receiver cup is a four-inch length of 1-3/4-inch diameter stainless steel tubing capped with a brass, water-cooled plate. The interior of the cup was coated with carbon to reduce the number of secondary electrons ejected from the cup's interior surface. The cup is installed in the end of the test chamber. It is electrically isolated from the test chamber with the use of a plexiglass flange between the cup flange and the test chamber flange.

Two other cup designs have been used. One simply had a negatively biased brass grid screen across the entrance to the basic cup. The grid screen opening spacing was 1/16-inch and the wire diameter 0.02-inch. Difficulties were experienced in passing the beam into the cup without a direct hit onto the grid.

The present cup design is shown in Figure 11. Both the front and second grids are made of the brass wire mesh described above. The opening in both grids is 3/4-inch diameter. The first grid is grounded, and the second is negatively biased at about 20 V for optimum operation.

Since the highest beam voltage used in data runs was 10 KV, the current measurements were certainly not realistic above about 0.100 Torr at 300°K due to beam spreading. Also, at 0.100 Torr at 300°K the second grid would apparently begin to collect ions at grid voltages near -20 V. A diode was placed in the circuit (as shown in Figure 11) to prevent this from affecting the current reading.

Since there was still some difficulty experienced in evading the front grid of this cup, a view port was made near the entrance to the cup so centering of the beam into the cup could easily be accomplished

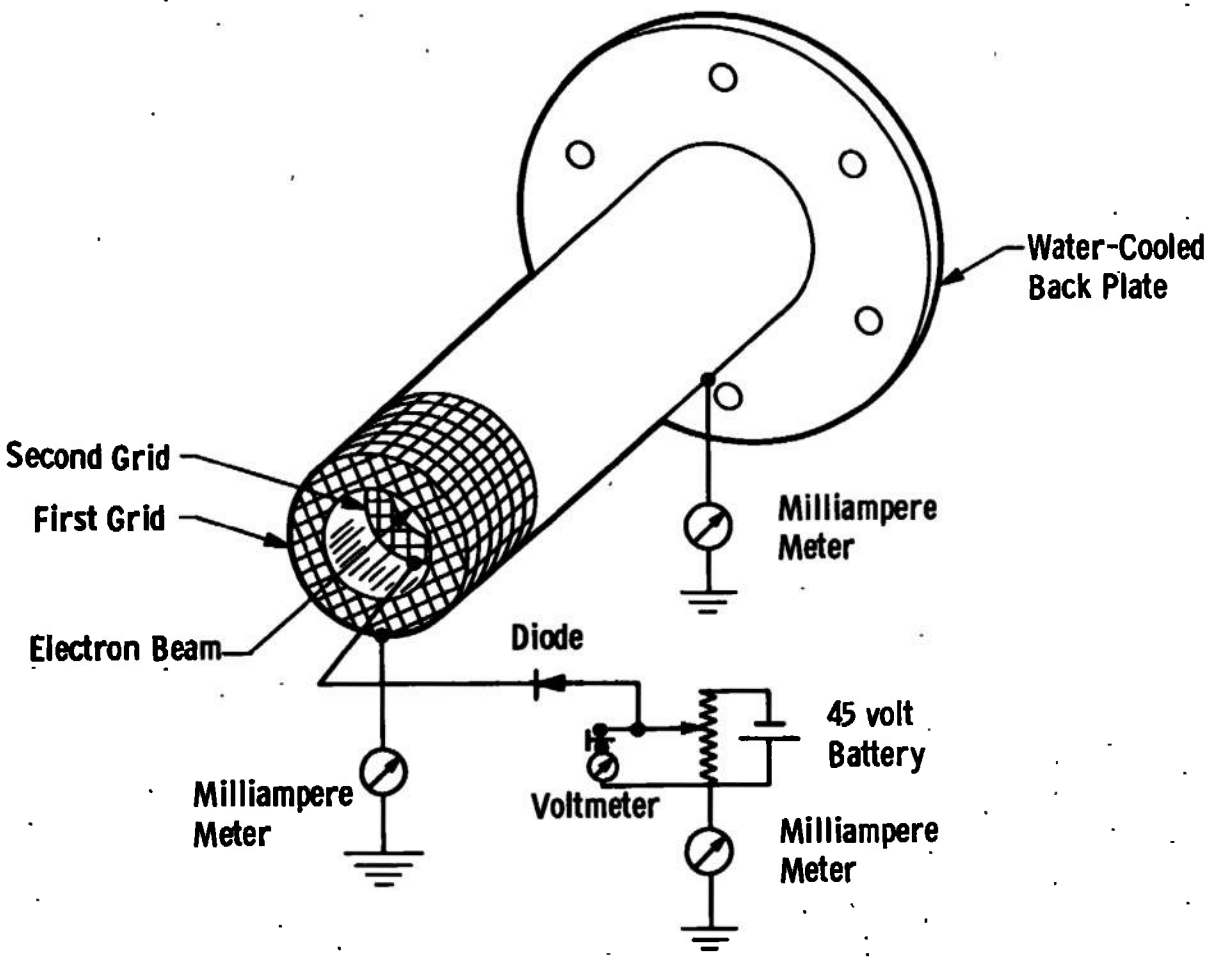

Fig. 11 Diagram of Beam Receiver Cup and Its Electrical Connections

using a small permanent magnet.

C. OPTICS (See Figure 10, Page 33)

A Wollensak, 135 millimeter Raptar lens and shutter assembly focuses the electron beam image parallel onto the entrance slit of the spectrometer. Although this made the data more sensitive to any relative motion between the beam and slit, the gain in amount of light gathered was needed for low density data. The f/number of the lens and spectrometer is matched at f/6.8. A dove prism is used between the lens and spectrometer slit to rotate the beam image parallel to the slit.

The spectrometer is a 3/4-meter Spex (1700-11) with a Czerny-Turner mount. The grating is 102 x 102 millimeters with 1200 lines per millimeter and blaze at 5000 Å. With a 20 micron by 10 millimeter slit the resolution in the first order is 0.24 Å which is sufficient for resolution of the R branch lines of most of the prominent N_2^+ [1^-] bands. Scanning speeds for rotational spectra are normally 2-2.5 Å per minute and for vibrational band integration 10-15 Å per minute.

D. SIGNAL DETECTION AND RECORDING

An RCA 1P28 photomultiplier tube mounted at the exit slit of the spectrometer is used as the detection element. The voltage divider network for the tube is shown in Figure 12. The high voltage applied to the tube is normally -700 VDC which is supplied by a Fluke 405B Power Supply. Electrostatic and magnetic shielding and cooling of the tube are not used at the present time. Signals from the photomultiplier are

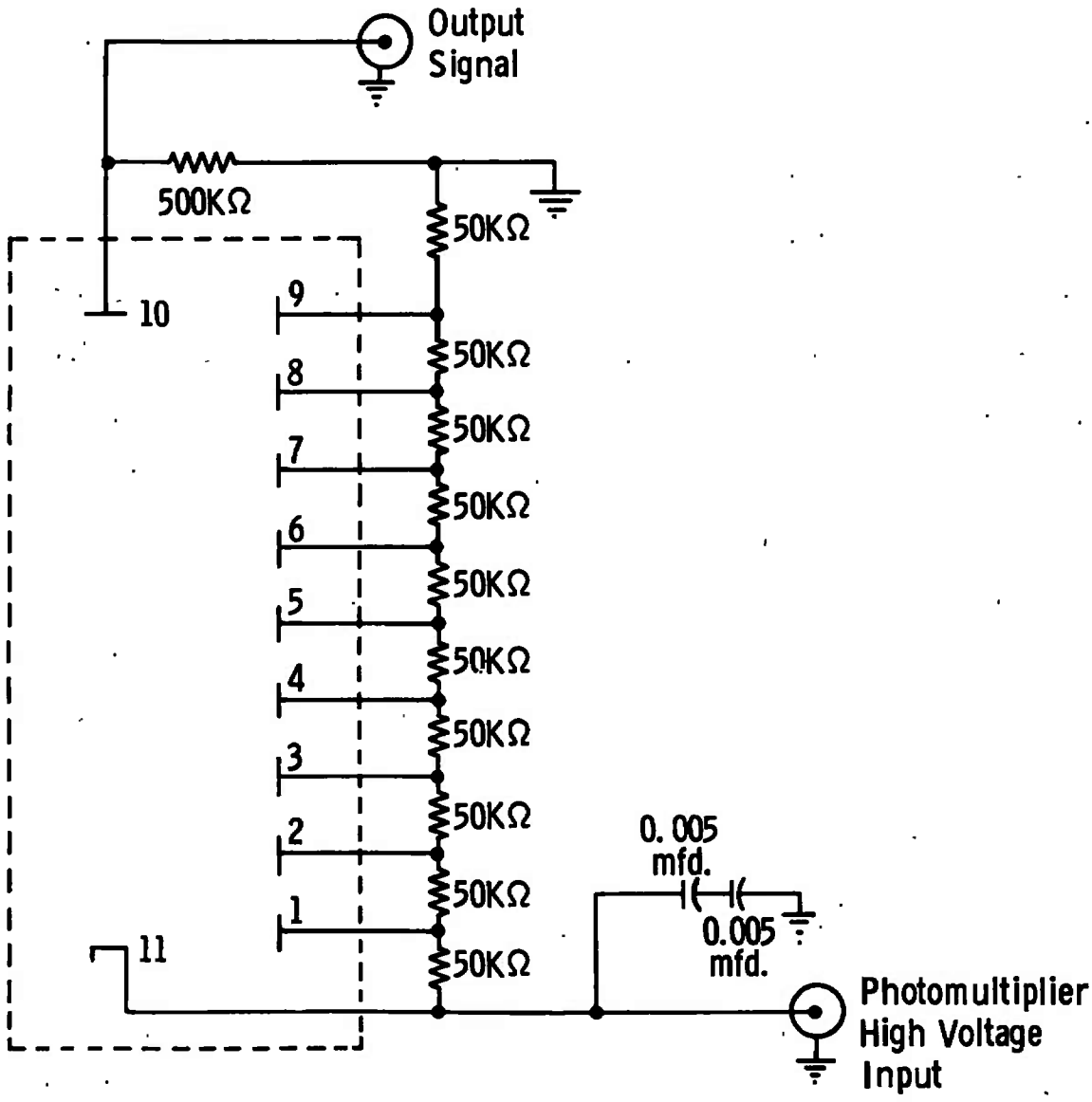

Fig. 12 IP28 Photomultiplier Voltage Divider Circuit

fed into a PAR Model HR-8 Precision Lock-In Amplifier for amplification and noise rejection and attenuation.

In order to take advantage of the capabilities of a lock-in amplifier the light beam received by the spectrometer photomultiplier must be modulated in some manner. The simplest and best way to achieve this appeared to be modulation of the electron beam itself. An audio oscillator and power amplifier provided a modulation voltage to the control grid of the electron gun (see Figure 13). However, the necessary addition of the control grid resistor caused the 60 Hz ripple of the power supply (1-1/2 per cent at 50 KV) to almost completely modulate the beam by itself. The injected modulation appeared as a high frequency component "riding" the 60 Hz modulation signal.

The addition of a large capacitor (28 microfarad rated at 10 KV) across the output of the power supply essentially eliminated the 60 Hz ripple. However, the capacitor itself presented quite a problem. Any small high voltage arc in the electron gun resulted in a discharge of the capacitor, subsequent heating and cracking of the gun's glass envelope, and implosion and ejection of the gun's internal parts into the vacuum system. This problem was eliminated by fusing the capacitor with exploding wire fuses developed by Mr. D. S. Bynum of ARO, Inc. However, due to the impromptu nature of any arcing during a period of data recording, the large capacitor filter was abandoned and a high voltage regulator tube was employed that somewhat reduced the 60 Hz ripple and stabilized the electron beam also. The gun modulation used was 20 KHz, and a 20 KHz pass filter was used to reject the 60 Hz signal component before it

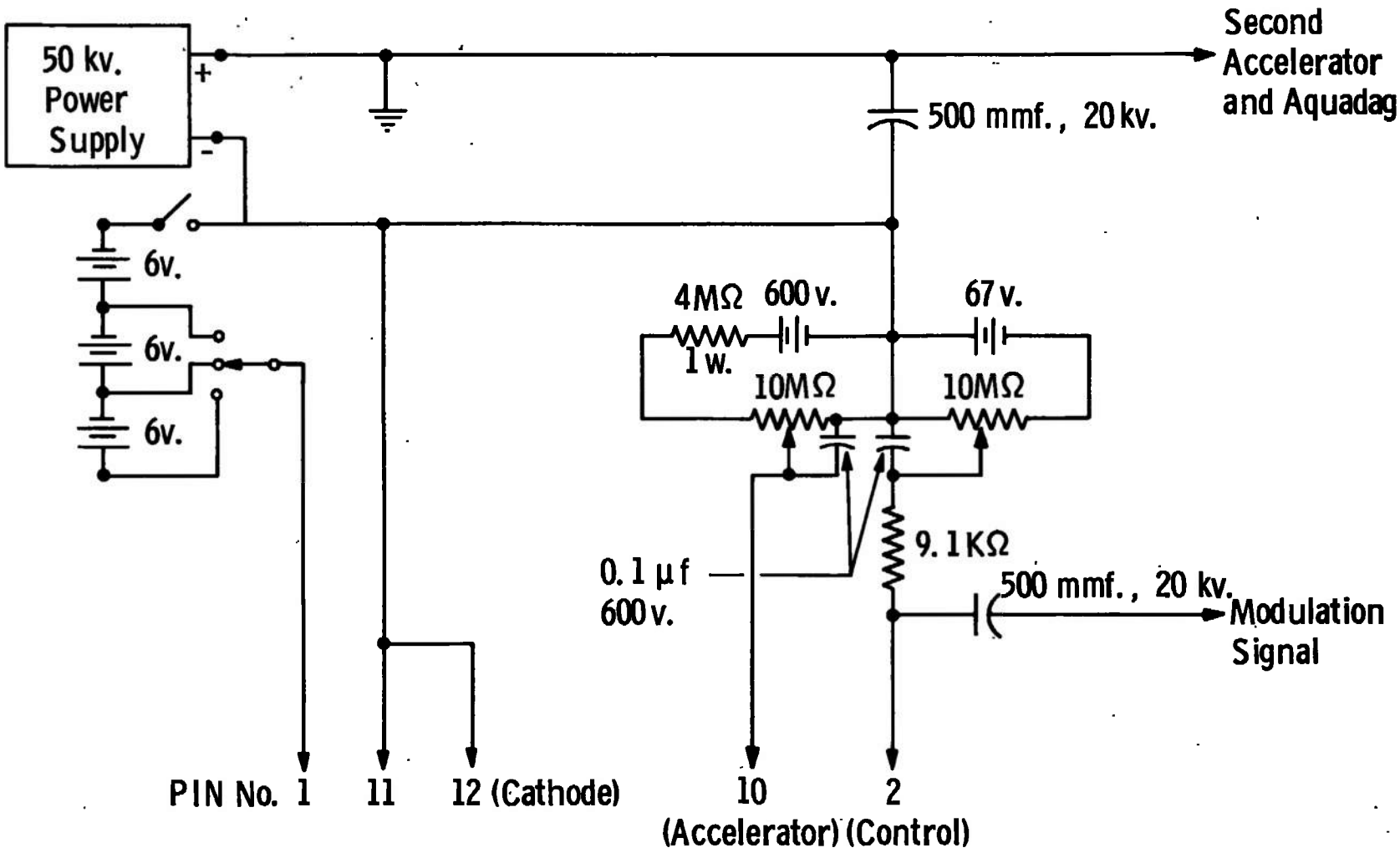

Fig. 13 Electron Gun Connections

reached the lock-in amplifier. Data quality was not as good as when the large filter capacitor was used, therefore the beam modulation scheme was later abandoned in favor of the present beam light chopping.

A 5000 rpm motor was equipped with a stainless steel coupling to an 8-inch diameter plexiglass disc with alternating pie-shaped opaque and transparent sections. The coupling and disc were dynamically balanced and are used to modulate the beam light intercepted by the lens (Figure 10, page 33) at ∿ 700 Hz. A reference signal to the lock-in is provided at the same frequency by a small light bulb (6 V) and RCA IP28 photomultiplier (see Figure 10). This simpler arrangement was observed to produce the best quality data.

The lock-in amplifier is, of course, the heart of the data recording system. As pointed out by the manufacturer (11) the lock-in is basically a phase-sensitive detector in which the modulated photomultiplier signal is mixed with a reference voltage to produce sum and difference frequencies. A low-pass filter at the output of the mixer rejects the high frequency components (sum frequencies), and it passes the difference frequencies that lie within its passband. The difference frequency due to components of the signal at the reference is zero or DC. Difference frequencies resulting from components of the signal at frequencies differing from the reference frequency by more than the cut-off frequency of the low-pass filter will be attenuated. Therefore, the lock-in selects a band of frequencies from a signal spectrum applied to its input circuit and converts the information therein to an equivalent bandwidth at DC.

The sensitivity of the lock-in is usually operated at 20

microvolts to 2 millivolts for rotational line spectra and 1-50 millivolts for vibrational band integration. A 0.3 or 1 second lock-in time constant is normally used.

The spectra are recorded on chart paper by a Sargent, multirange, precision recorder.

The schematic of the electronic integrator used for vibrational band intensity measurements is shown in Figure 14. It is an active integrator with a 1 second time constant, and it has an accuracy of ± one per cent provided the integration time is no longer than about 200 seconds.

For band integration the output of the lock-in is fed to the integrator input. The integrator output is then recorded on chart paper. The recorded peak output is then proportional to the area under a corresponding spectral line trace of the band and is thus proportional to the total intensity of the band.

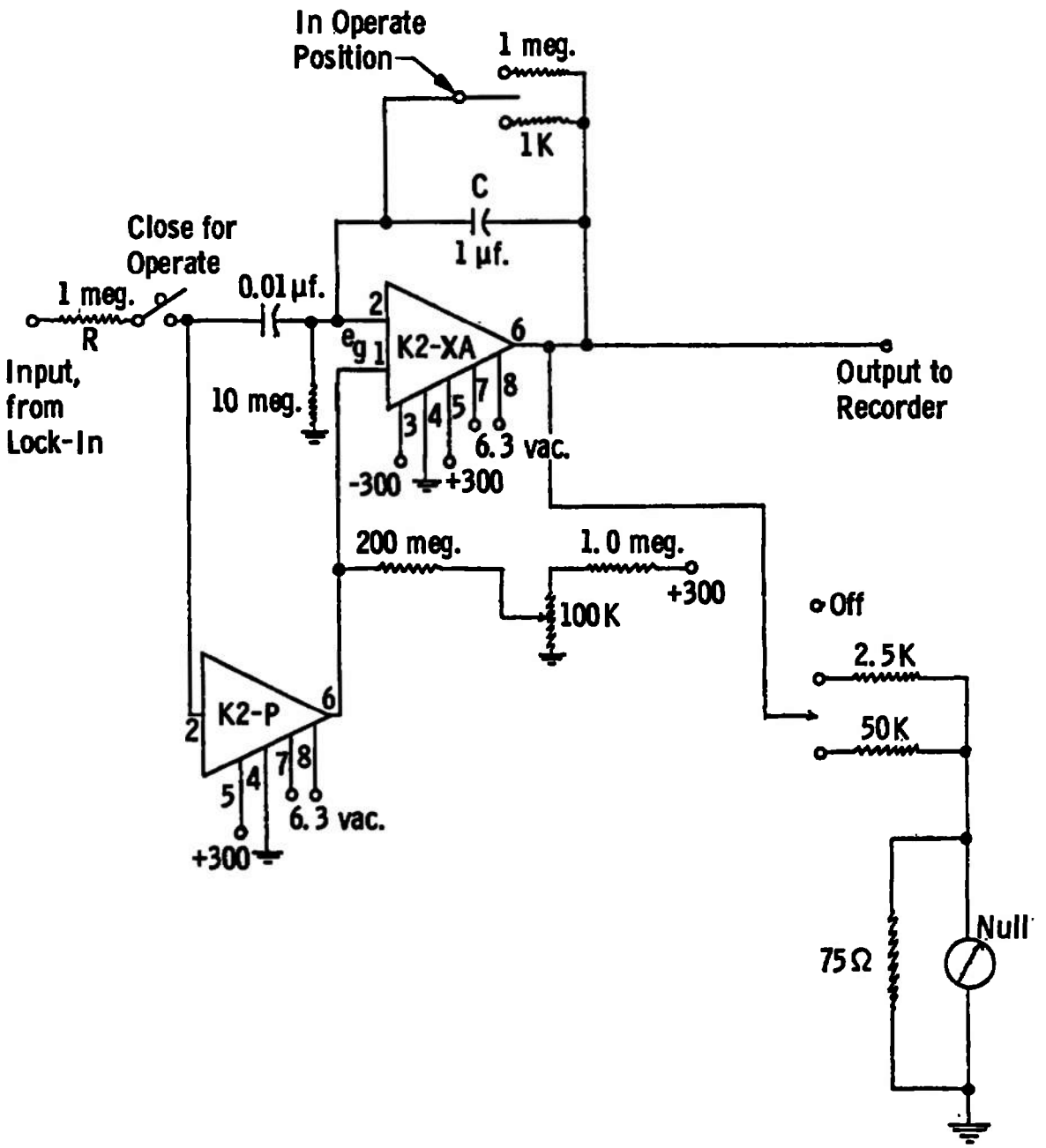

Fig. 14 Electronic Integrator

CHAPTER V
DISCUSSION OF DATA

A. ROTATIONAL TEMPERATURE DATA

Several rotational scans were made at each data condition with never less than four spectral scans averaged for a given data point. The spectrometer scans were always made in alternating directions across the band. Beam and test chamber conditions were always checked before every scan to assure their proper setting.

It should be pointed out here that current measurements in this investigation cannot be used for comparison except when specifically indicated, because throughout these measurements the beam current measurement technique was varied due to change in beam receiver design and beam alignment with respect to the cup. Change in modulation technique also affected the beam current measurement. In all cases in which the test chamber pressure was above 0.100 Torr the beam current measurement was quantitatively worthless due to beam spreading.

The quality of the rotational scans was very good due to a lack of noise and was well resolved as can be seen in Figures 15, 16, and 17 which are actual, typical spectral scans. In comparison to the spectra recorded by other investigators the spectral data obtained in this investigation are superior. Data taken in the beam "halo" region were generally of better quality than the normal beam spectra taken in

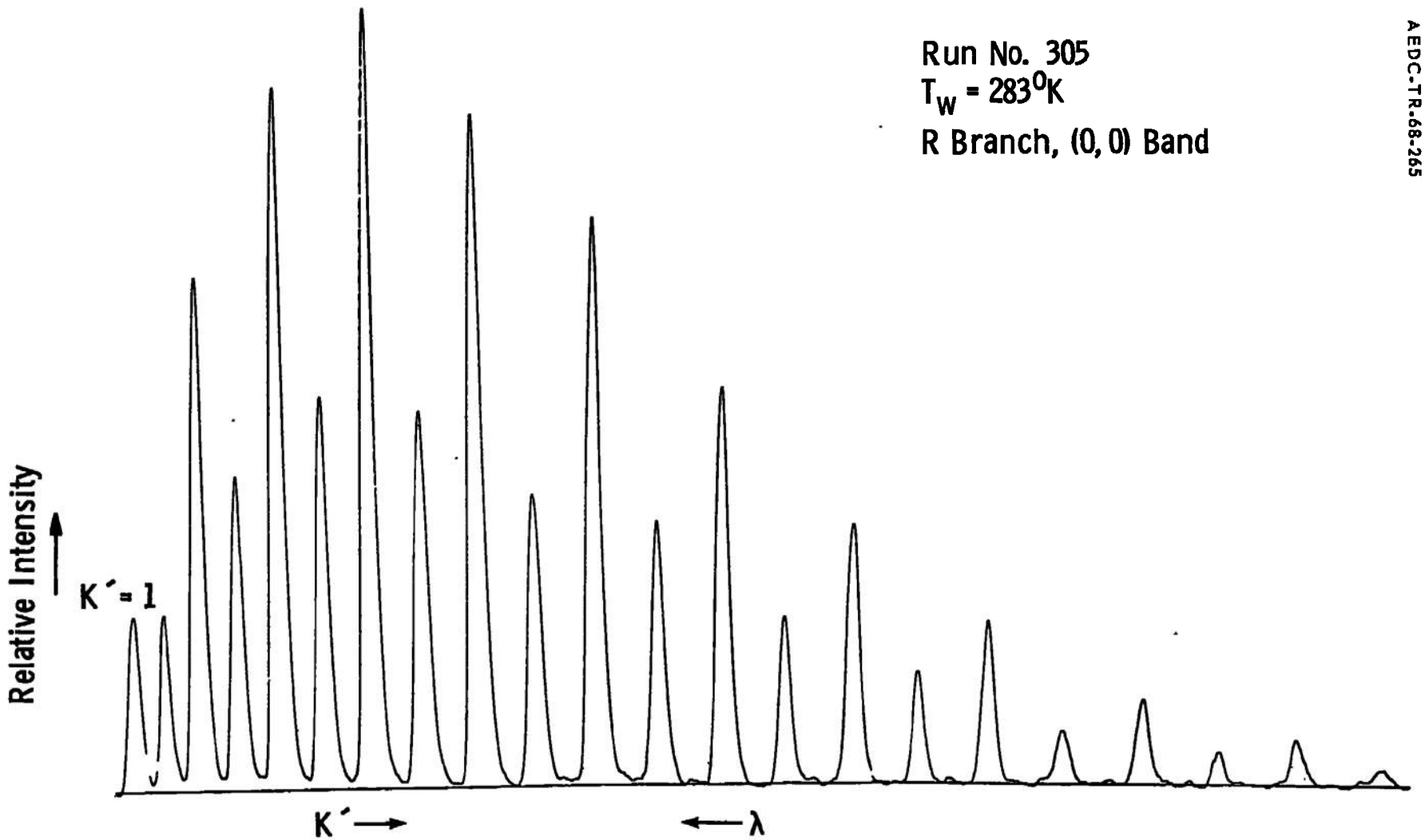

Fig. 15 Typical Spectral Scan, $T_w = 283^{o}K$

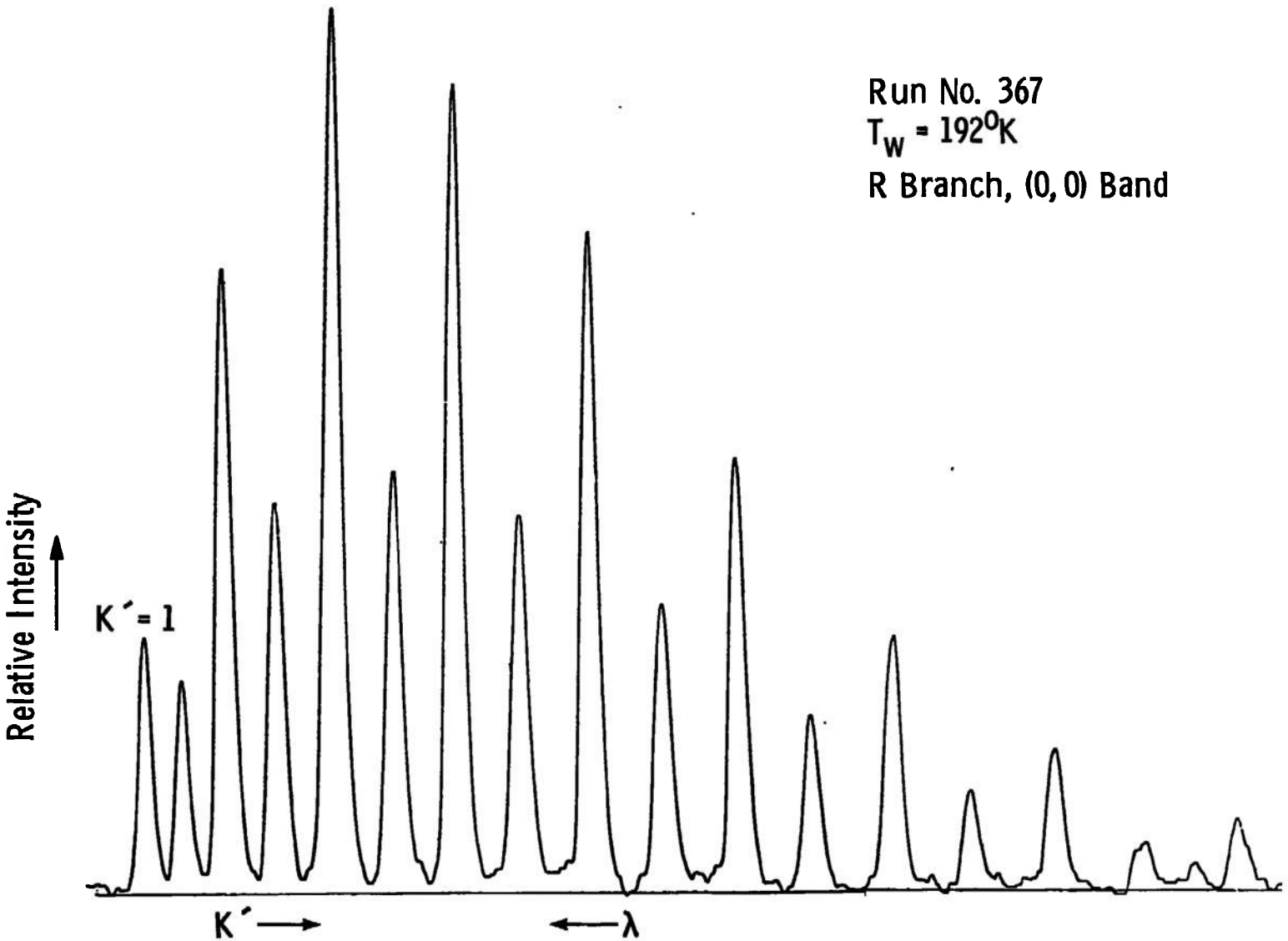

Fig. 16 Typical Spectral Scan, T_w = 192°K

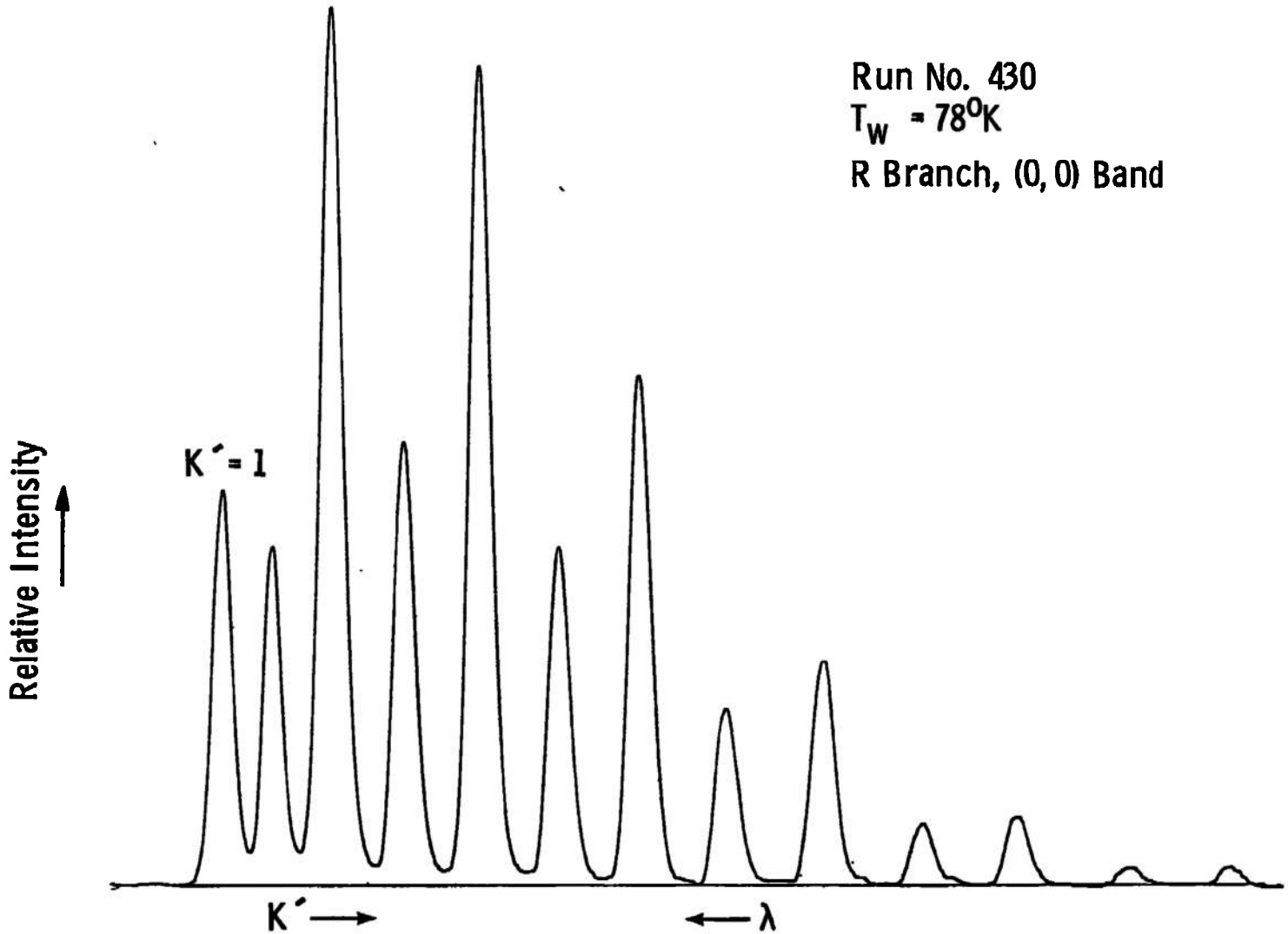

Fig. 17 Typical Spectral Scan, T_w = 78°K

other investigations. Rotational scans were not only made in the more intense (0,0) band, but also in some of the weaker bands such as (1,2), (1,1), and (0,1).

Using Equation 50 and the methods outlined in Appendix A, the rotational spectral scans were reduced to rotational temperatures at various conditions of test chamber pressure, temperature, and beam current. Data are generally presented as a ratio of measured temperature (T_R) to wall temperature as a function of the number of spectral lines used in the temperature determination.

Initial room temperature data were taken without a coolant around the chamber, and it was observed that the channel wall heated up as much as 6°K. This heating of a static test chamber was also observed at AEDC and was accounted for by considering the large-angle scattering of the high energy beam electrons resulting in their impacting with the test chamber wall. Figure 7, page 28, shows the non-coolant room temperature results at 0.060 Torr which agree within 2.5 per cent with AEDC data assuming 15-22 lines were used in determining their temperatures. The Robben and Talbot (8) value and an average of Ashkenas's (10) results are seen to be approximately five per cent higher. By using 10-22 lines the spectrally measured temperature was within ± 2.5 per cent of the wall temperature. However, a slight increase in measured temperature with the number of spectral lines used past K' = 10 is surely noticeable.

Further, near room temperature measurements were made using cold, circulating water as a test chamber coolant. Results of these

scans at 0.056 Torr at high and low currents are shown in Figure 18. Using 10-22 lines the spectrally measured temperatures are in agreement with the wall temperature within ± 2.5 per cent. A "high" beam current indicates a current on the order of a couple of milliamperes and a "low" beam current is on the order of a few hundred microamperes. There is little indication of a beam current effect at the conditions of Figure 18 except at the lower K' numbered lines where there was an obvious breaking away of the high and low current data points. However, the data quality is observed to deteriorate with the smaller number of spectral lines used. At 0.160 Torr and 283°K (see Figures 19 and 20) the measured temperature is generally higher than the wall temperature. For 11-22 spectral lines the measured temperatures are about 1-5 per cent high. Again there is little indication of a beam current effect except when using only lower numbered rotational lines. At 299°K and 0.160 Torr (see Figure 21) the measured temperature is about 0-4 per cent high with no indication of a beam current effect. Low current scans at 0.525 Torr and 283°K (Figure 22) essentially agree with the 0.160 Torr measurements. However, at high current at 0.525 Torr the measured temperatures are 9-11 per cent high for 12-22 lines used. Thus a beam current effect appeared present at moderate pressure at 283°K, but the variation of measured temperature with number of spectral lines used was only slight for 10-22 lines.

Figure 8, page 29, displays the results of a few other investigators at 78°K. All the results shown are laboratory measurements except for those of Robben and Talbot (8) which were obtained with a

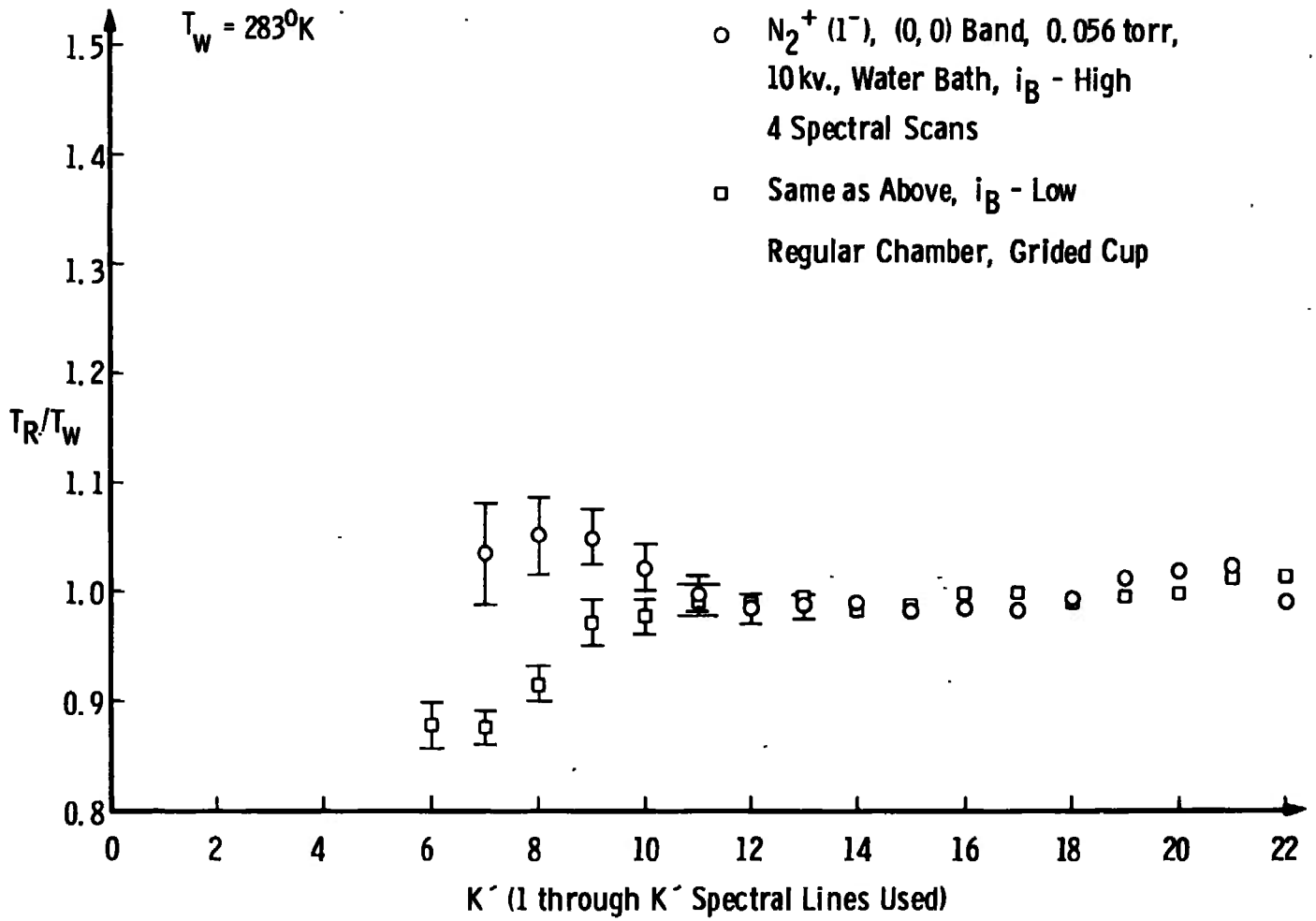

Fig. 18 Ratio of Measured Rotational Temperature to Chamber Wall Temperature versus Number of Spectral Lines Used for the Temperature Determination with Beam Current as a Parameter, T_w = 283°K, P_c = 0.056 Torr

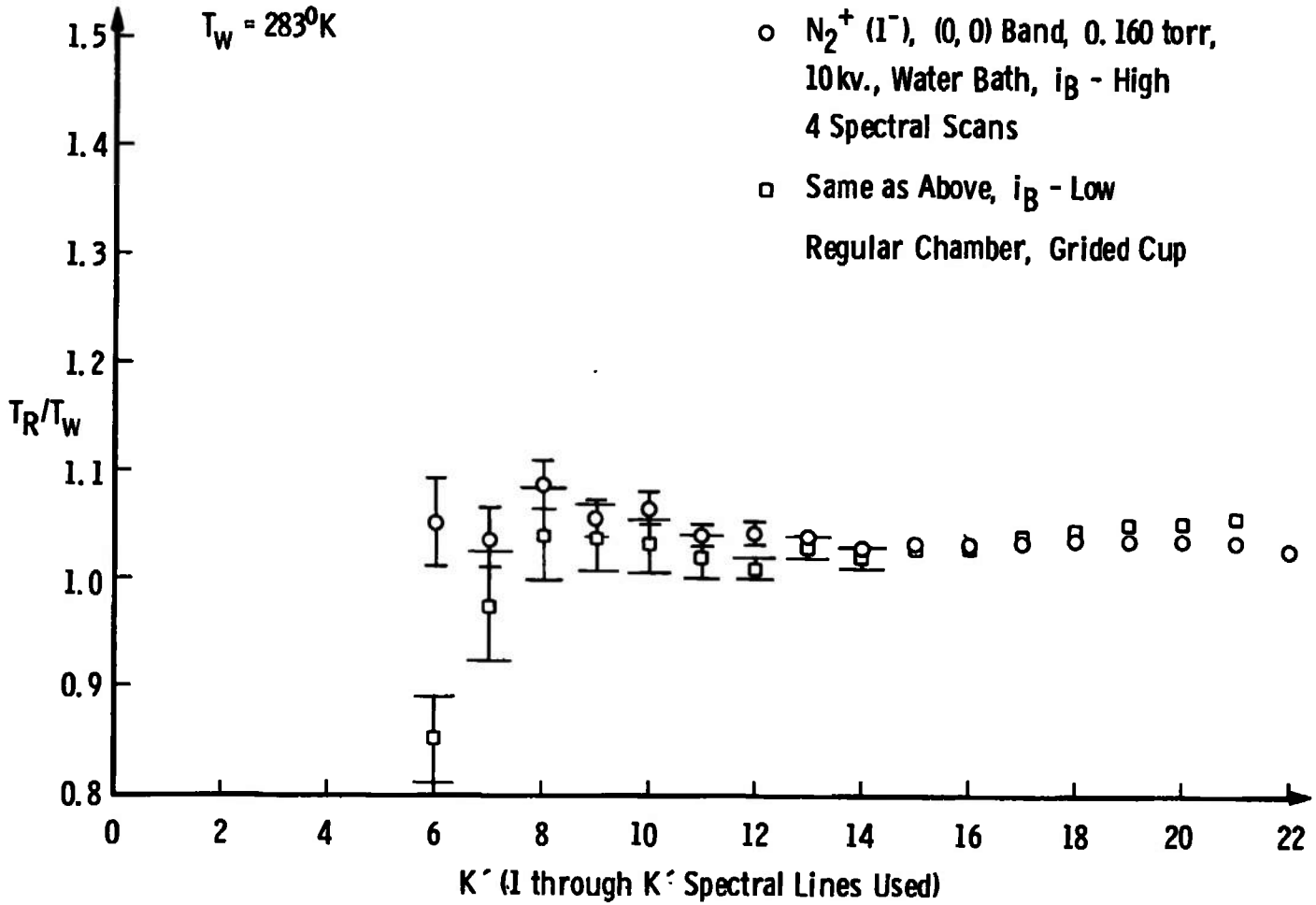

Fig. 19 Ratio of Measured Rotational Temperature to Chamber Wall Temperature versus Number of Spectral Lines Used for the Temperature Determination with Beam Current as a Parameter, T_w = 283°K, P_c - 0.160 Torr

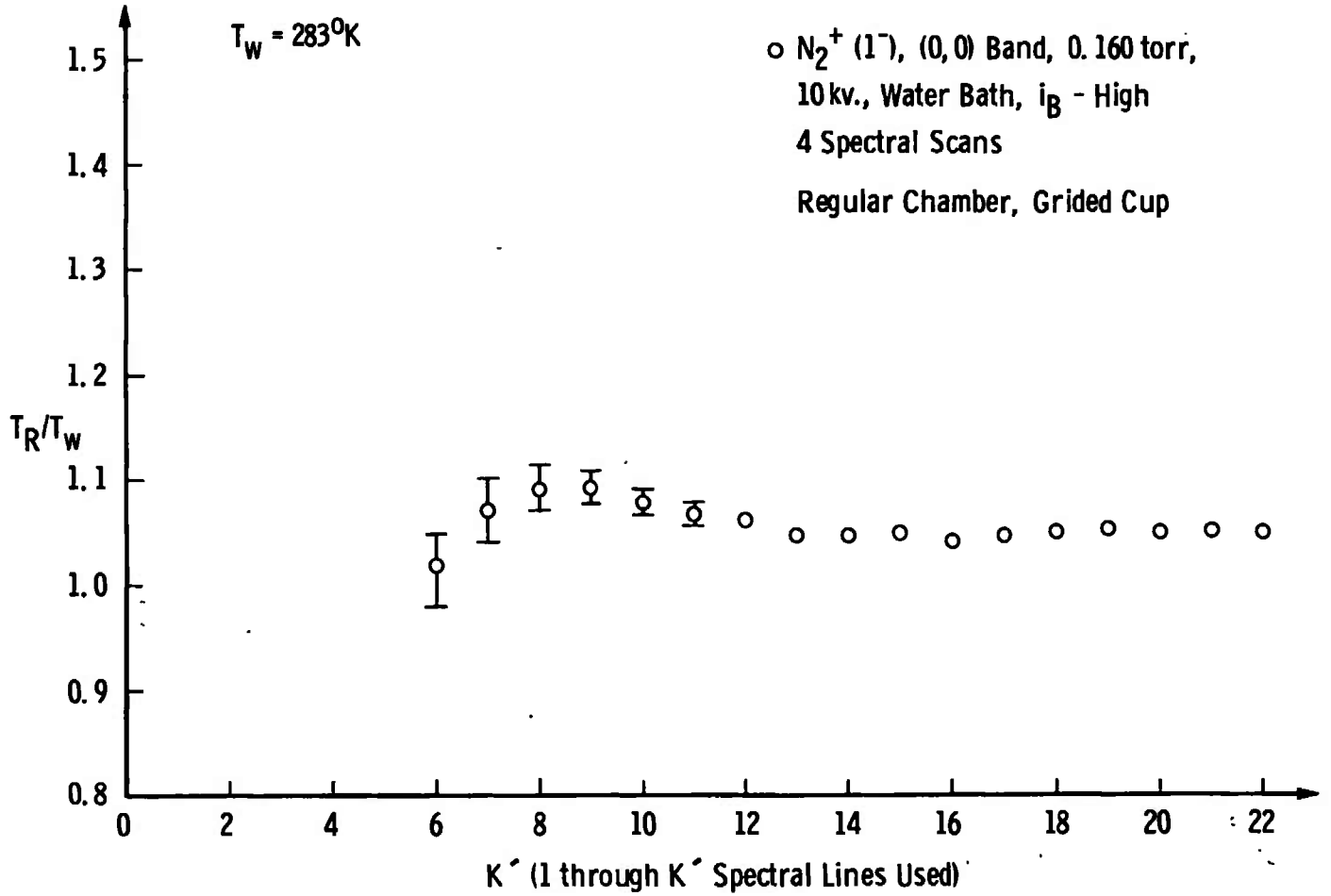

Fig. 20 Ratio of Measured Rotational Temperature to Chamber Wall Temperature versus Number of Spectral Lines Used for the Temperature Determination, T_w = 283 °K, P_c = 0.160 Torr

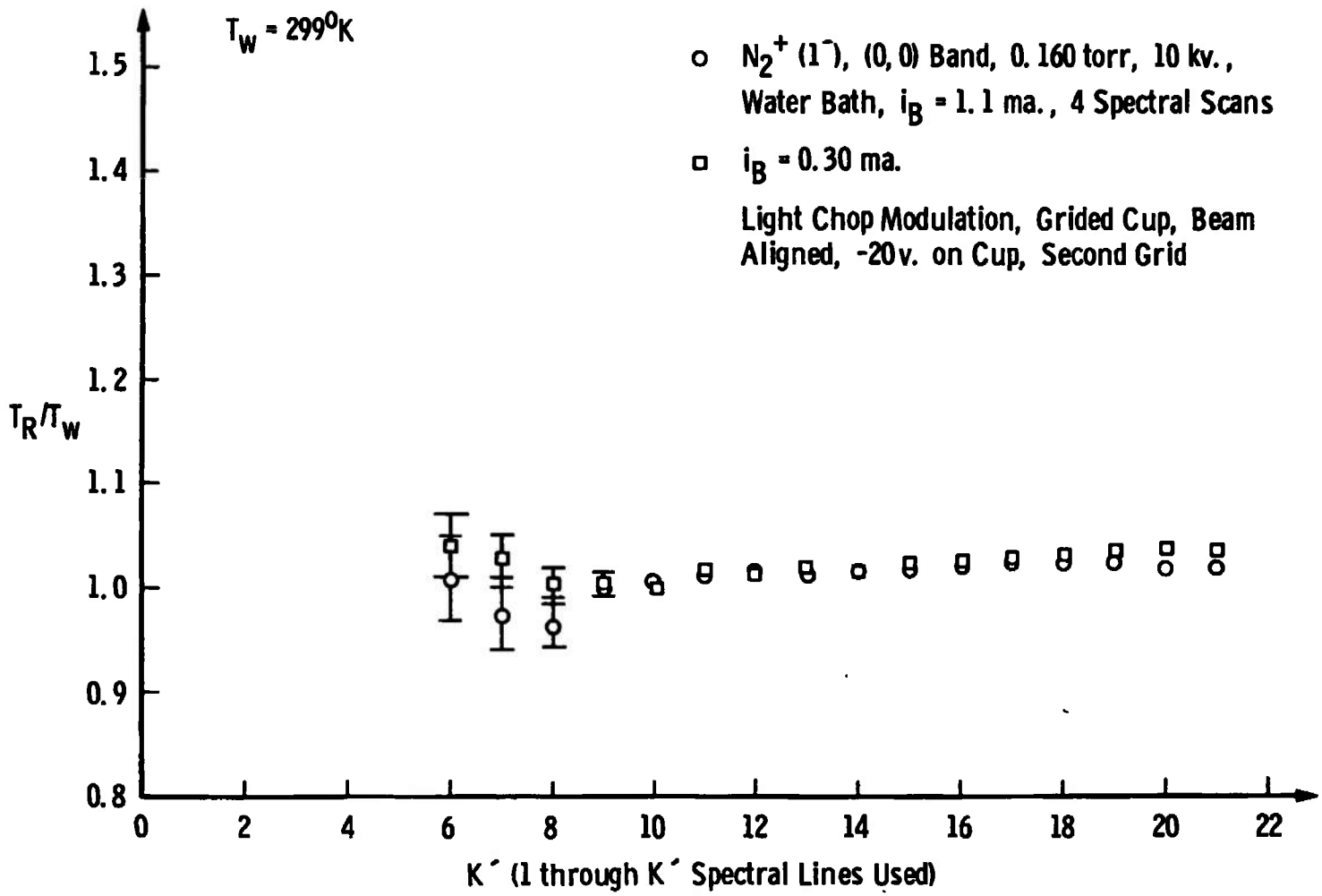

Fig. 21 Ratio of Measured Rotational Temperature to Chamber Wall Temperature versus Number of Spectral Lines Used for the Temperature Determination with Beam Current as a Parameter, T_w = 299°K, P_c = 0.160 Torr

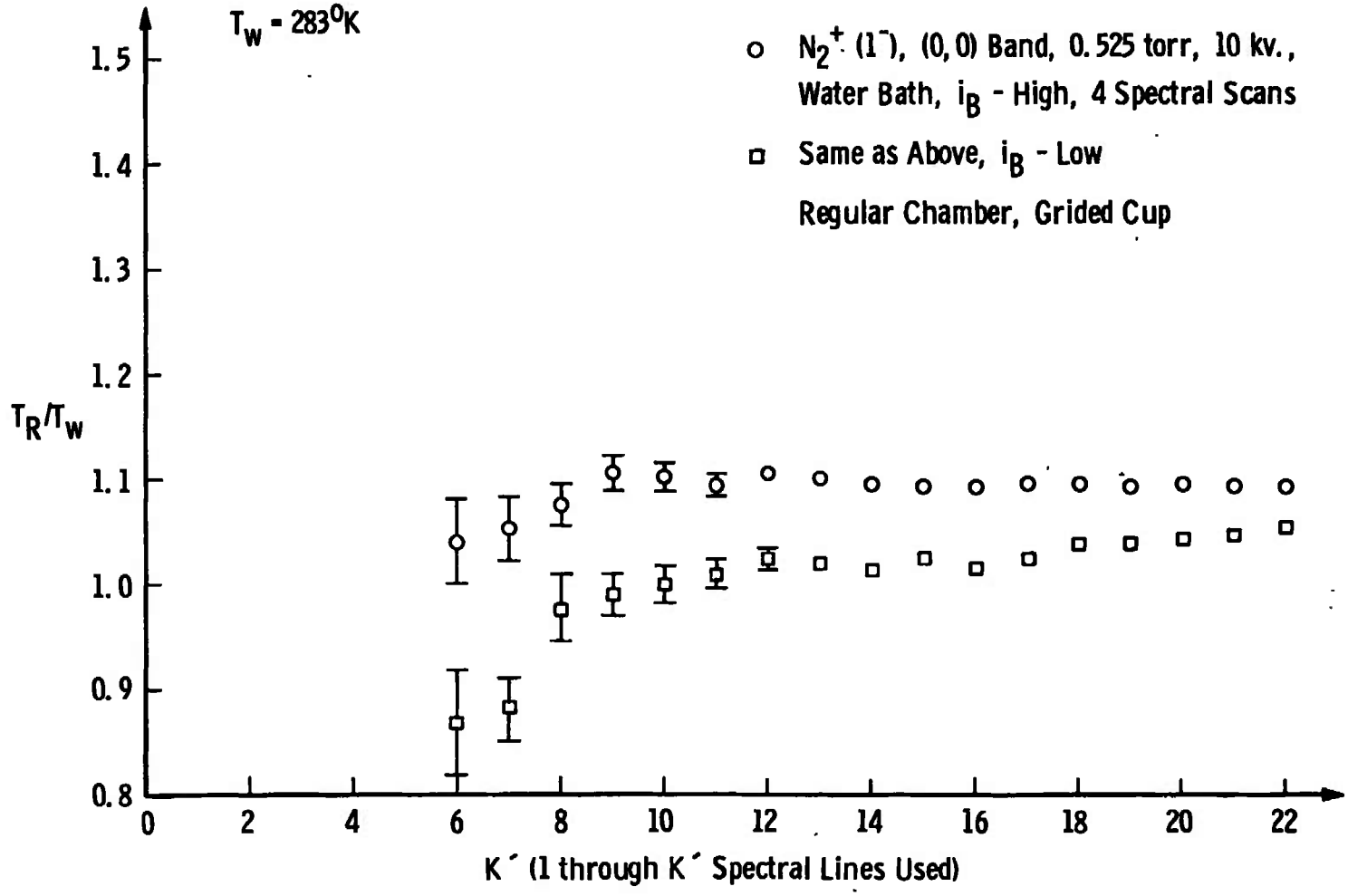

Fig. 22 Ratio of Measured Rotational Temperature to Chamber Wall Temperature versus Number of Spectral Lines for the Temperature Determination with Beam Current as a Parameter, T_w = 283°K, P_c = 0.525 Torr

Mach 4 nozzle flow measurement. The results of Ashkenas show a dramatic variation of measured temperature with number of spectral lines at this low temperature.

Figure 23 shows results of scans at 0.003 Torr and 78°K using liquid nitrogen as a coolant. Generally the measured temperature is approximately 7.5 per cent (± 2.5 per cent) higher than the wall temperature for 5-13 lines used. A slight increase of measured temperature with K' is also evident.

Figures 24, 25, 26, 27, and 28 show results of scans at 0.005 Torr and 78°K. At this pressure the temperature is essentially independent of beam current and flow rate as shown in Figures 24, 25, and 26. The flow rate was increased by putting a 140 liter per minute mechanical pump onto the test chamber opposite the spectrometer view port. However, even this increased flow rate was at least an order of magnitude below the minimum flow rate used by Ashkenas (10). The data of Figures 24, 25, 26, 27, and 28 agree well. Generally the measured temperature is about 8 per cent (± 2.5 per cent) higher than the wall temperature for 6-11 spectral lines used. However, Figure 27 surely depicts the increase of the measured temperature with K', especially for K' greater than eleven.

Scans at 0.024 Torr and 78°K show a definite beam current dependence as seen in Figures 29, 30, and 31. Figure 30 also shows that the faster flow rate is not enough to prevent the beam current dependence at this pressure. For ten spectral lines used measured temperatures range from 10-18 per cent higher than the wall temperature (see Figure 29).

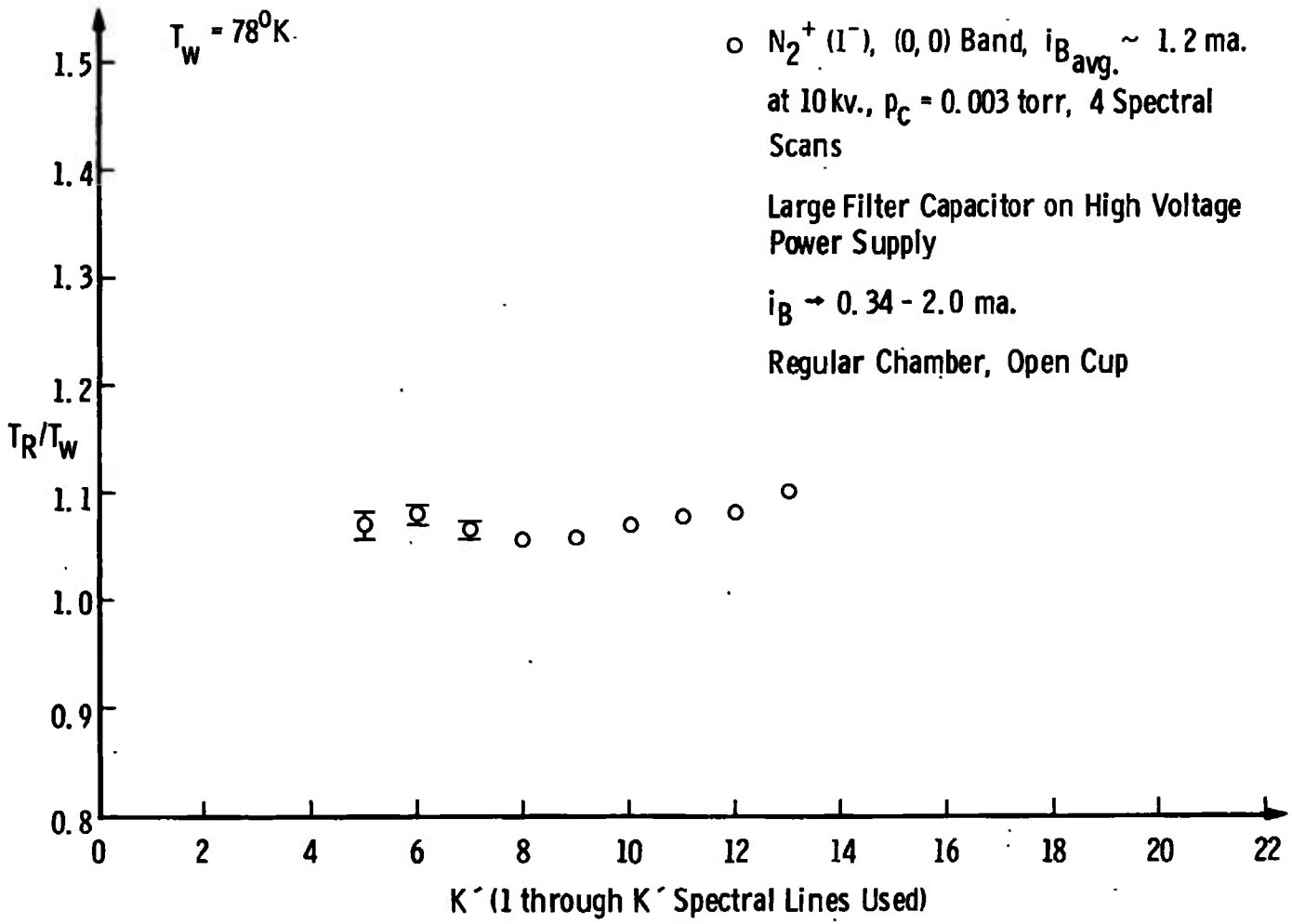

Fig. 23 Ratio of Measured Rotational Temperature to Chamber Wall Temperature versus Number of Spectral Lines for the Temperature Determination, T_w = 283°K, P_c = 0.003 Torr

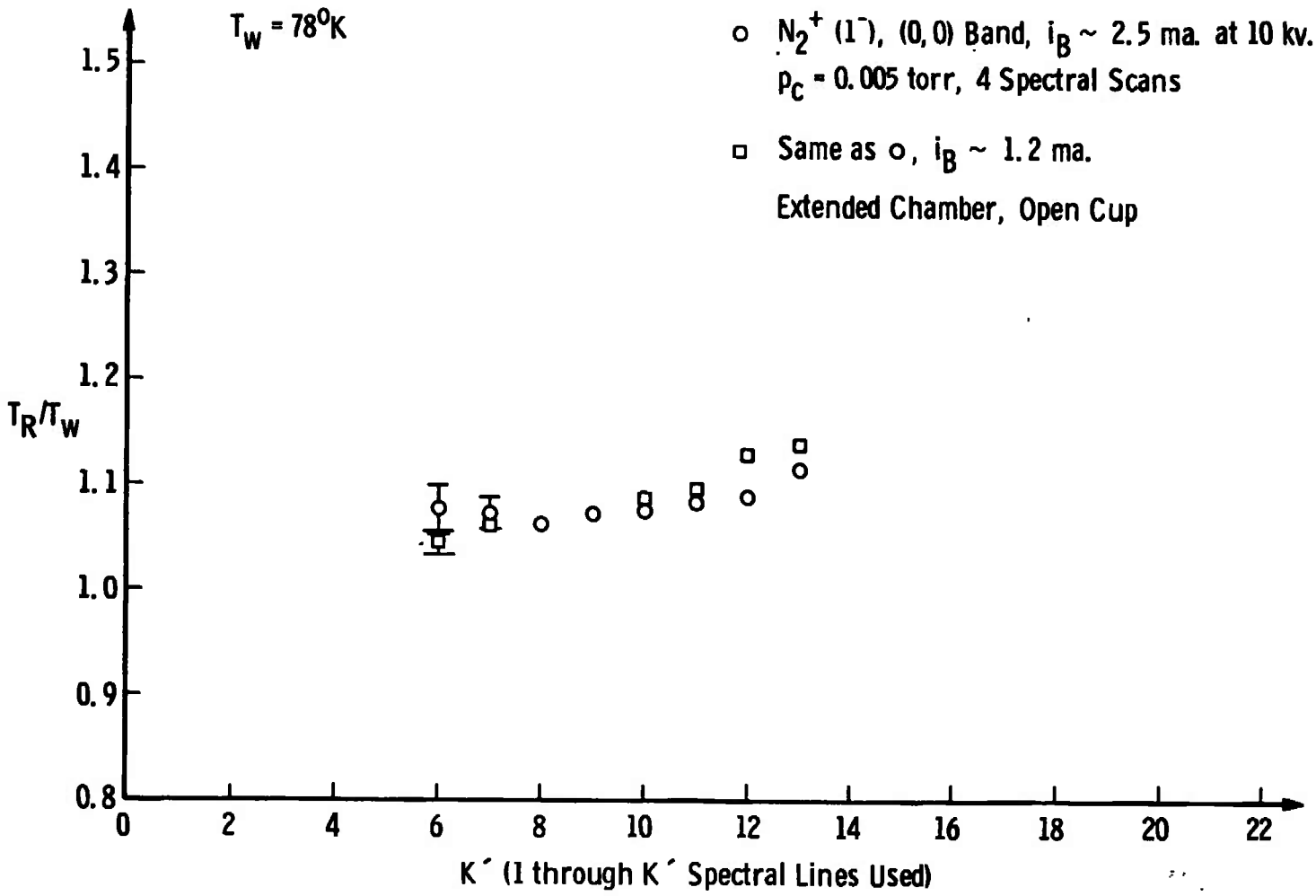

Fig. 24 Ratio of Measured Rotational Temperature to Chamber Wall Temperature versus Number of Spectral Lines Used for the Temperature Determination with Beam Current as a Parameter, $T_w = 78°K$, $P_c = 0.005$ Torr

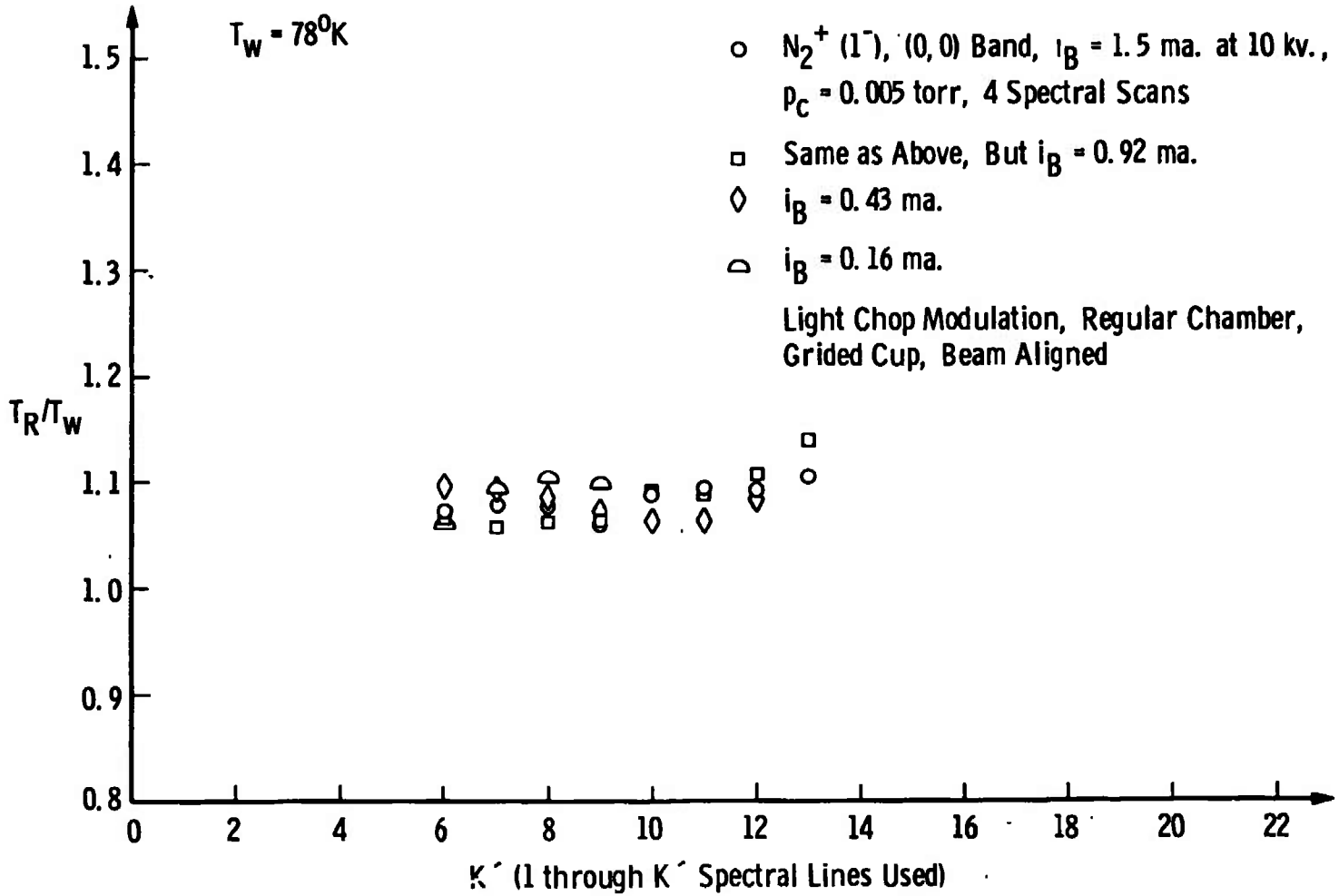

Fig. 25 Ratio of Measured Rotational Temperature to Chamber Wall Temperature versus Number of Spectral Lines Used for the Temperature Determination with Beam Current as a Parameter, T_w = 78°K, P_c = 0.005 Torr

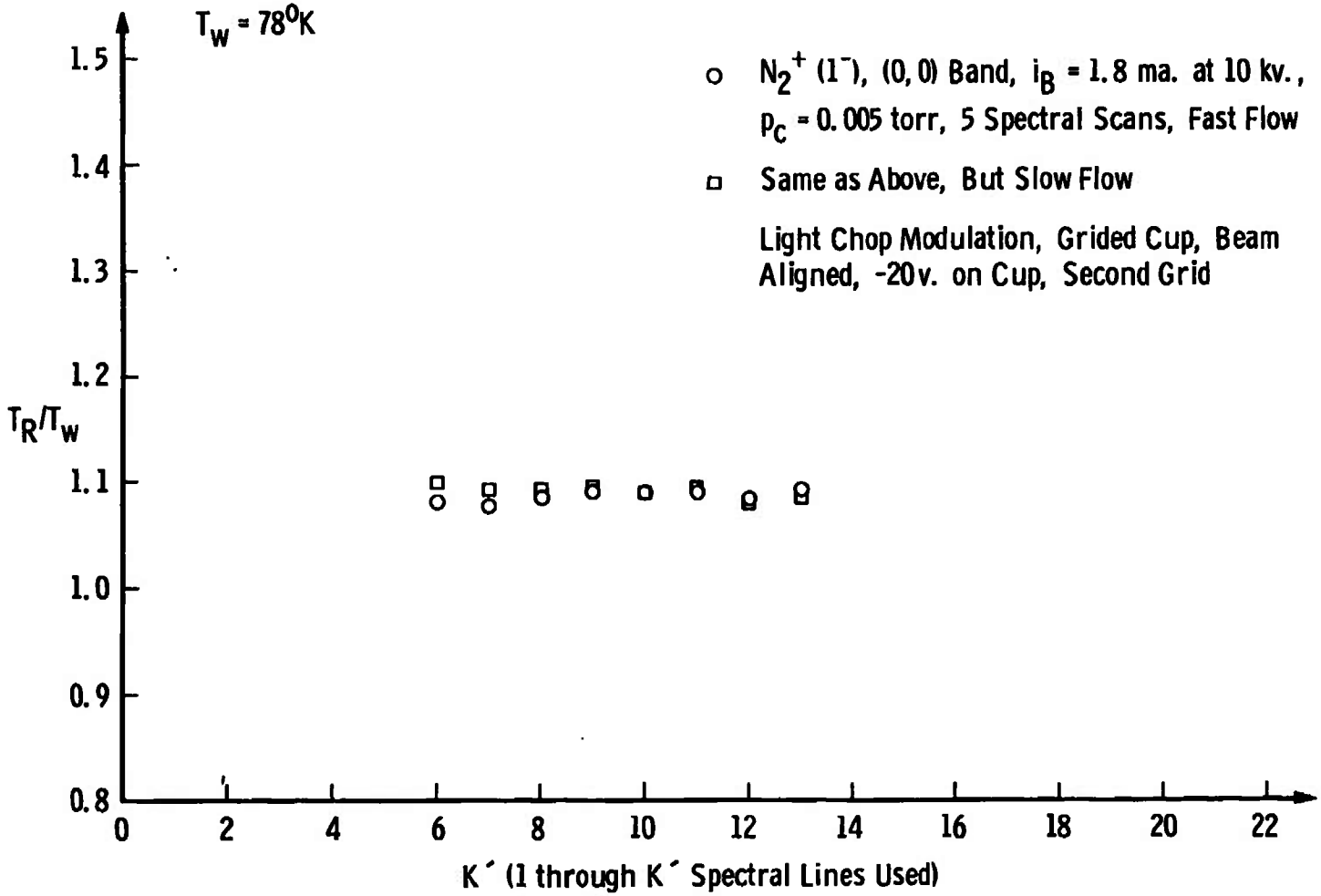

Fig. 26 Ratio of Measured Rotational Temperature to Chamber Wall Temperature versus Number of Spectral Lines Used for the Temperature Determination with Flow Rate as a Parameter, T_w = 78°K, P_c = 0.005 Torr

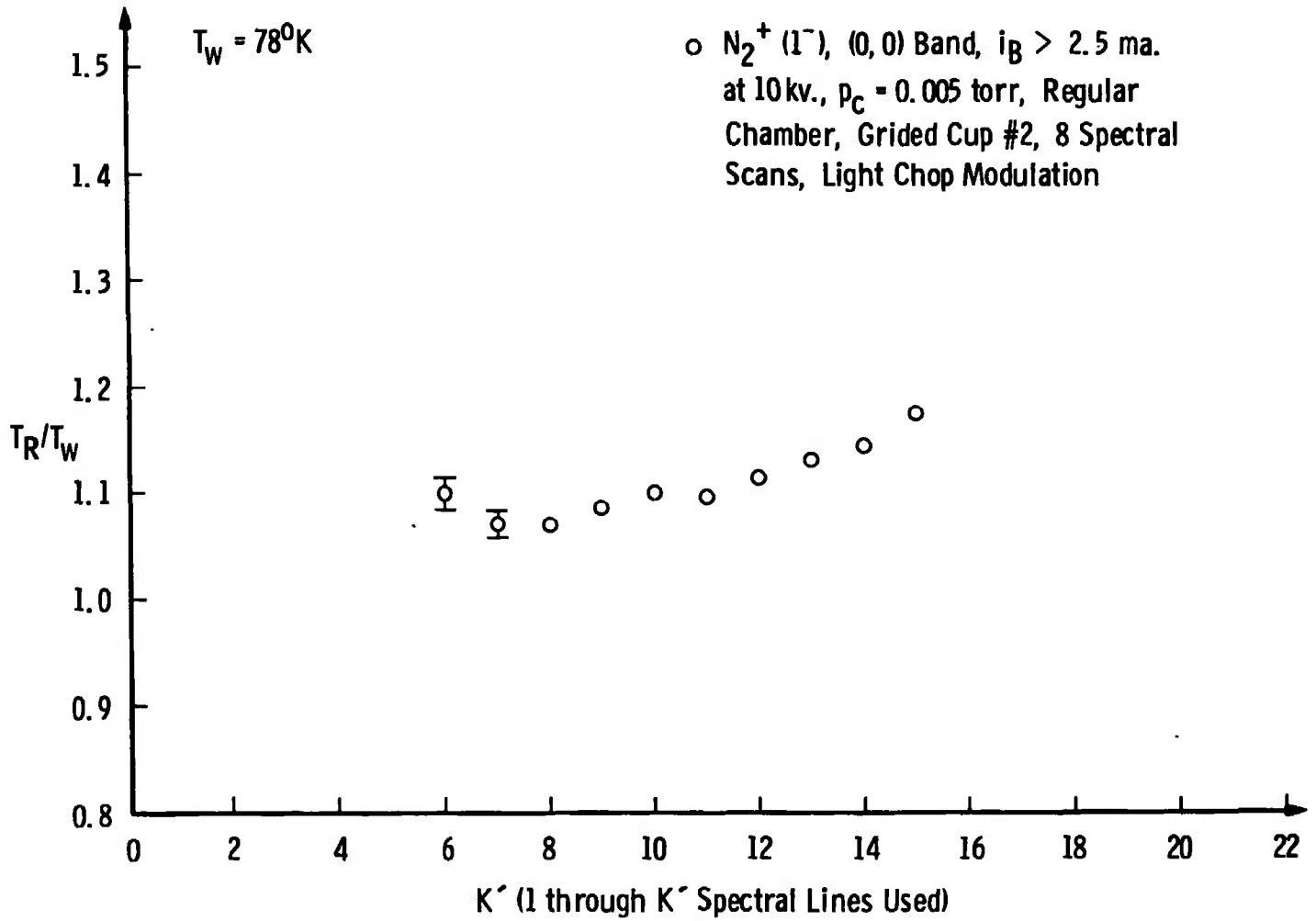

Fig. 27 Ratio of Measured Rotational Temperature to Chamber Wall Temperature versus Number of Spectral Lines Used for the Temperature Determination, $T_w = 78°K$, $P_c = 0.005$ Torr

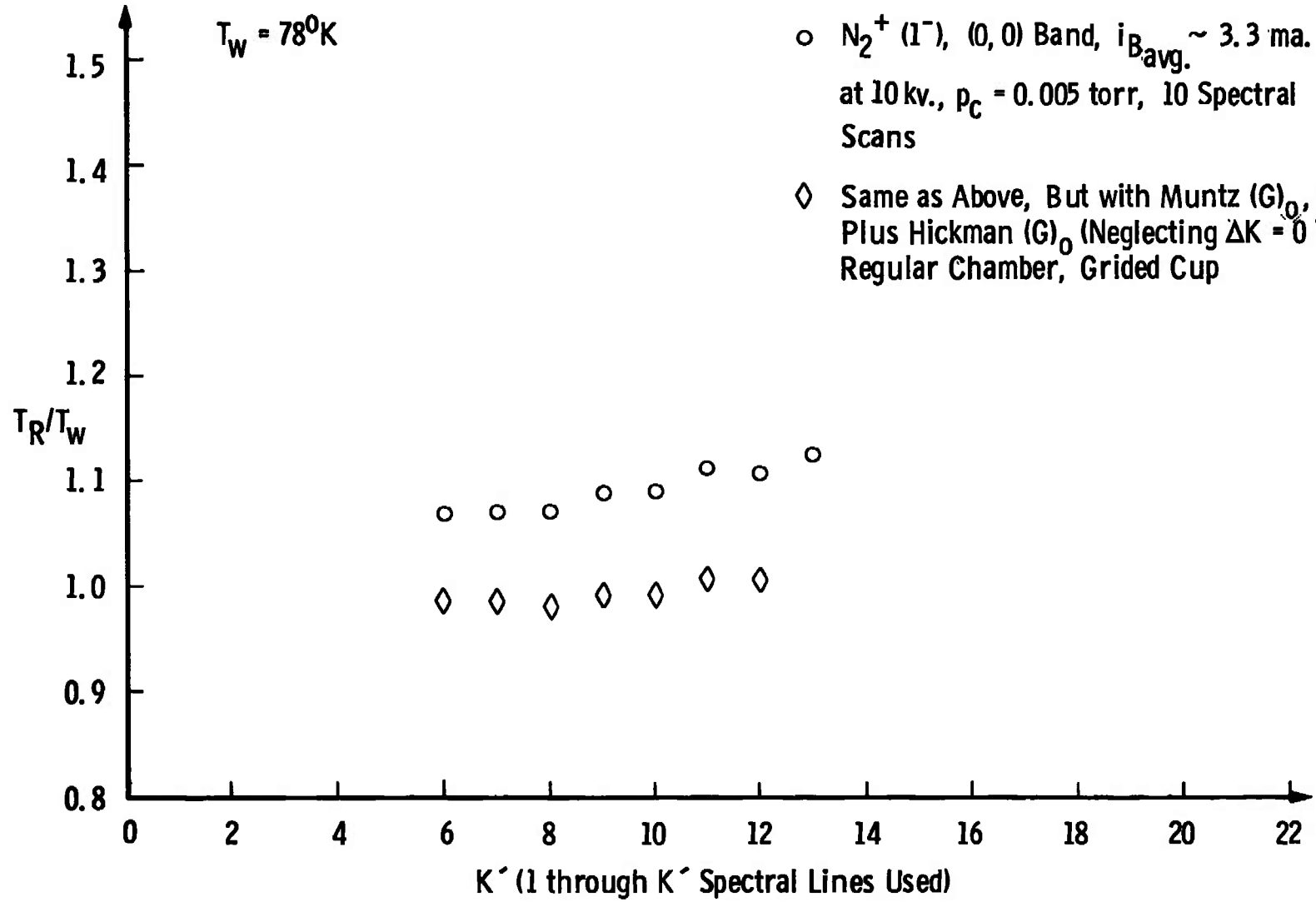

Fig. 28 Ratio of Measured Rotational Temperature to Chamber Wall Temperature versus number of Spectral Lines Used for the Temperature Determination, T_w = 78°K, P_c = 0.005 Torr

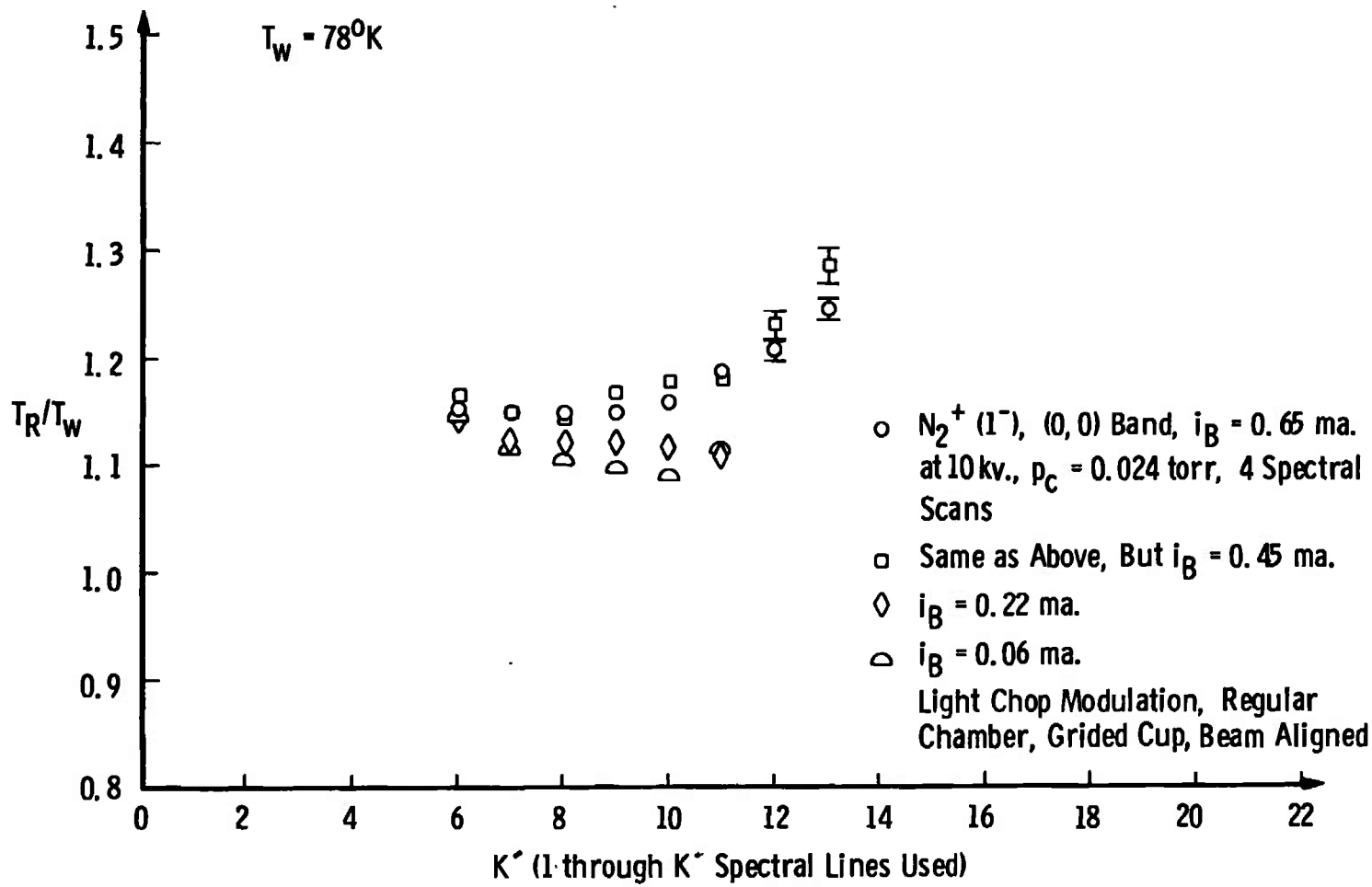

Fig. 29 Ratio of Measured Rotational Temperature to Chamber Wall Temperature versus Number of Spectral Lines Used for the Temperature Determination with Beam Current as a Parameter, T_w = 78°K, P_c = 0.024 Torr

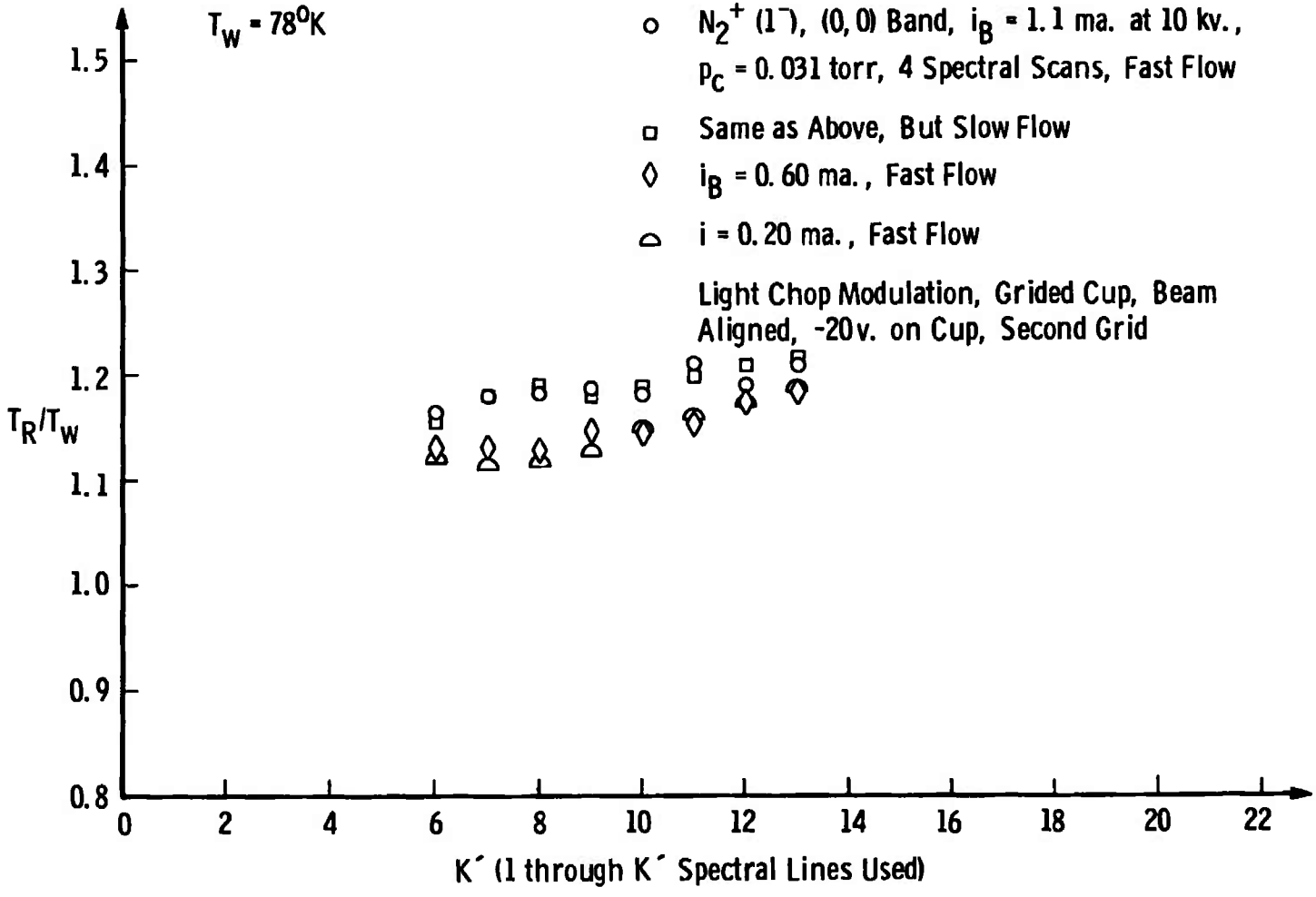

Fig. 30 Ratio of Measured Rotational Temperature to Chamber Wall Temperature versus Number of Spectral Lines Used for the Temperature Determination with Beam Current and Flow Rate as Parameters, T_w = 78°K, P_c = 0.031 Torr

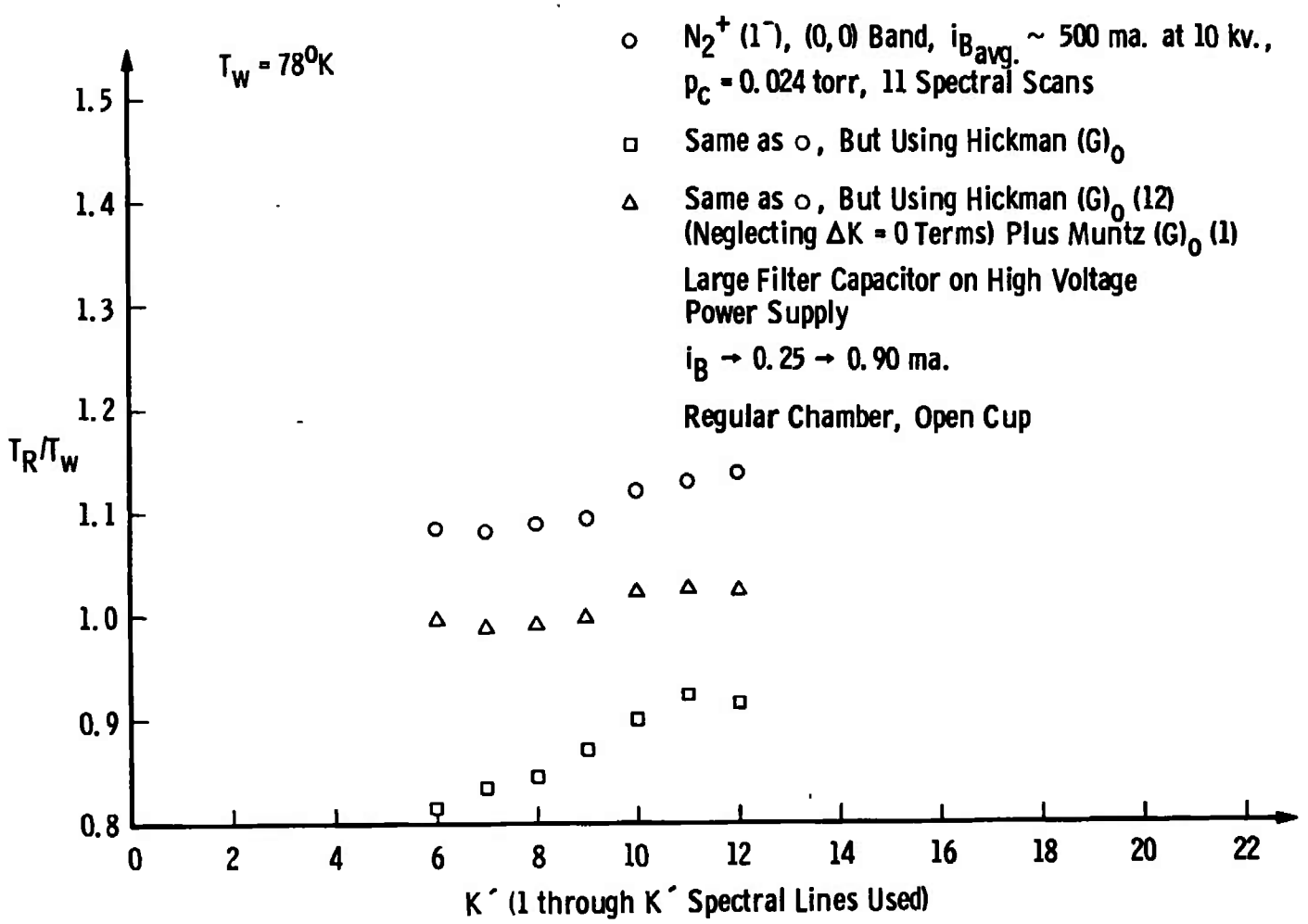

Fig. 31 Ratio of Measured Rotational Temperature to Chamber Wall Temperature versus Number of Spectral Lines Used for the Temperature Determination, $T_w = 78°K$, $P_c = 0.024$ Torr

Data at 0.062 Torr and 78°K show an increasing difference between the measured temperature and the wall temperature (see Figures 32 and 33). Both figures also show an increasing dependence of measured temperature on number of spectral lines. For a given condition of current the measured value of temperature was found to range from 36 per cent high using one through six spectral lines to 58 per cent high using one through seventeen spectral lines. For ten spectral lines used the measured temperature ranges from 23-34 per cent high for various values of beam current.

Data taken at 0.130 Torr and 0.200 Torr at 78°K serve only to show more distinctly the density-current effect on the temperature measurement and the dependence of measured temperature on number of spectral lines (see Figures 34 and 35). Figure 34 also shows the result of scans made using beam "halo" light, and it is seen that observation in the halo yields the same temperature result as observation of the main part of the beam in agreement with a finding of Ashkenas (10).

Using a dry ice and acetone mixture as a coolant, spectral scans were made at 191-192°K. At 0.0044 Torr the measured temperature is about 3.0 per cent (± 1 per cent) high for 8-17 lines used, and there is little dependence on K' for K' as high as 17 (see Figure 36). For 0.120 Torr at 192°K the measured temperature is 9 per cent (± 1 per cent) high for 8-17 lines used. However, there is a definite increase of measured temperature with K' for K' greater than 16. For 22 lines, for example, the temperature is 15 per cent high (see Figure 36).

Thus, there appear to be possibly several effects on the beam

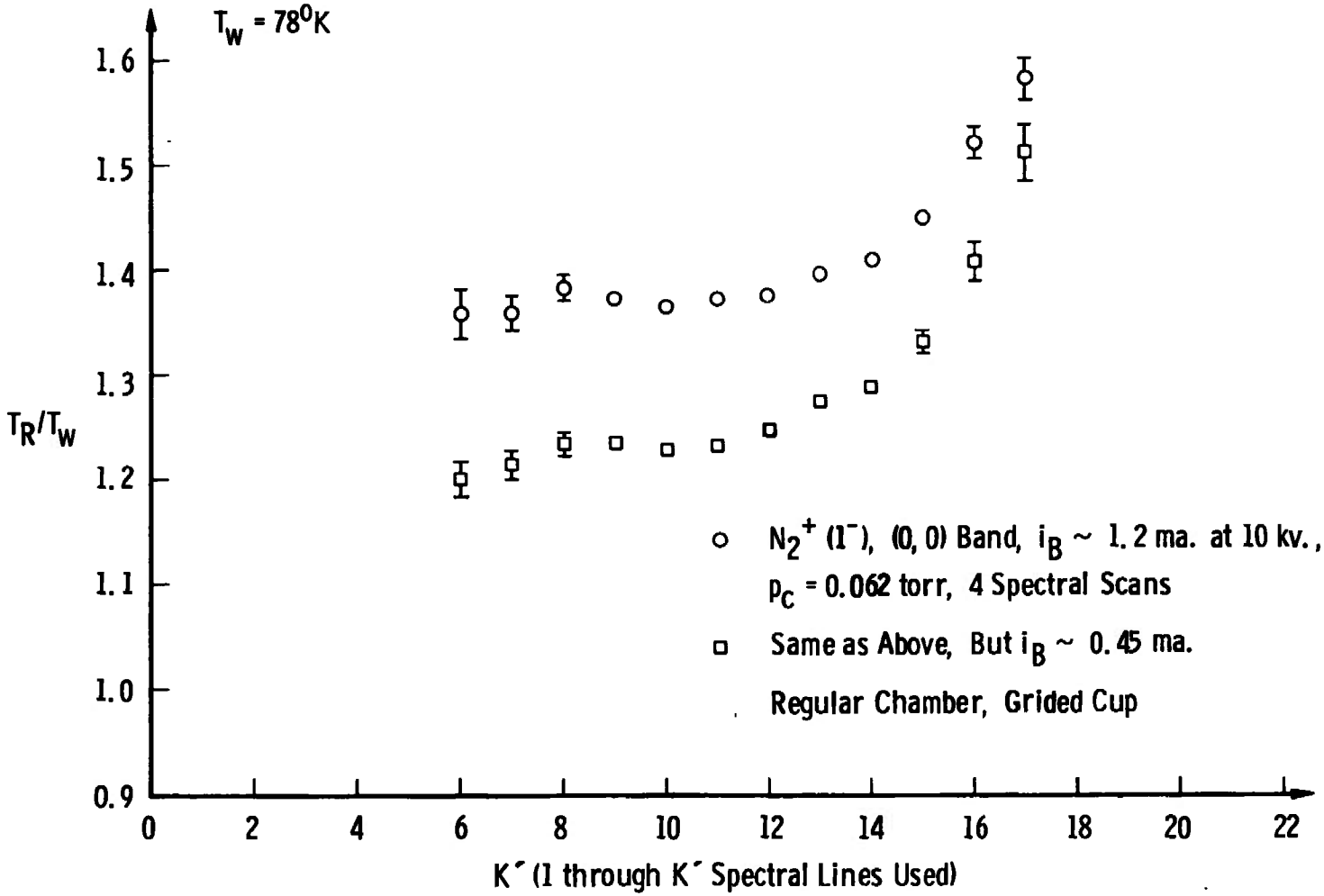

Fig. 32 Ratio of Measured Rotational Temperature to Chamber Wall Temperature versus Number of Spectral Lines Used for the Temperature Determination with Beam Current as a Parameter, $T_w = 78°K$, $P_c = 0.062$ Torr

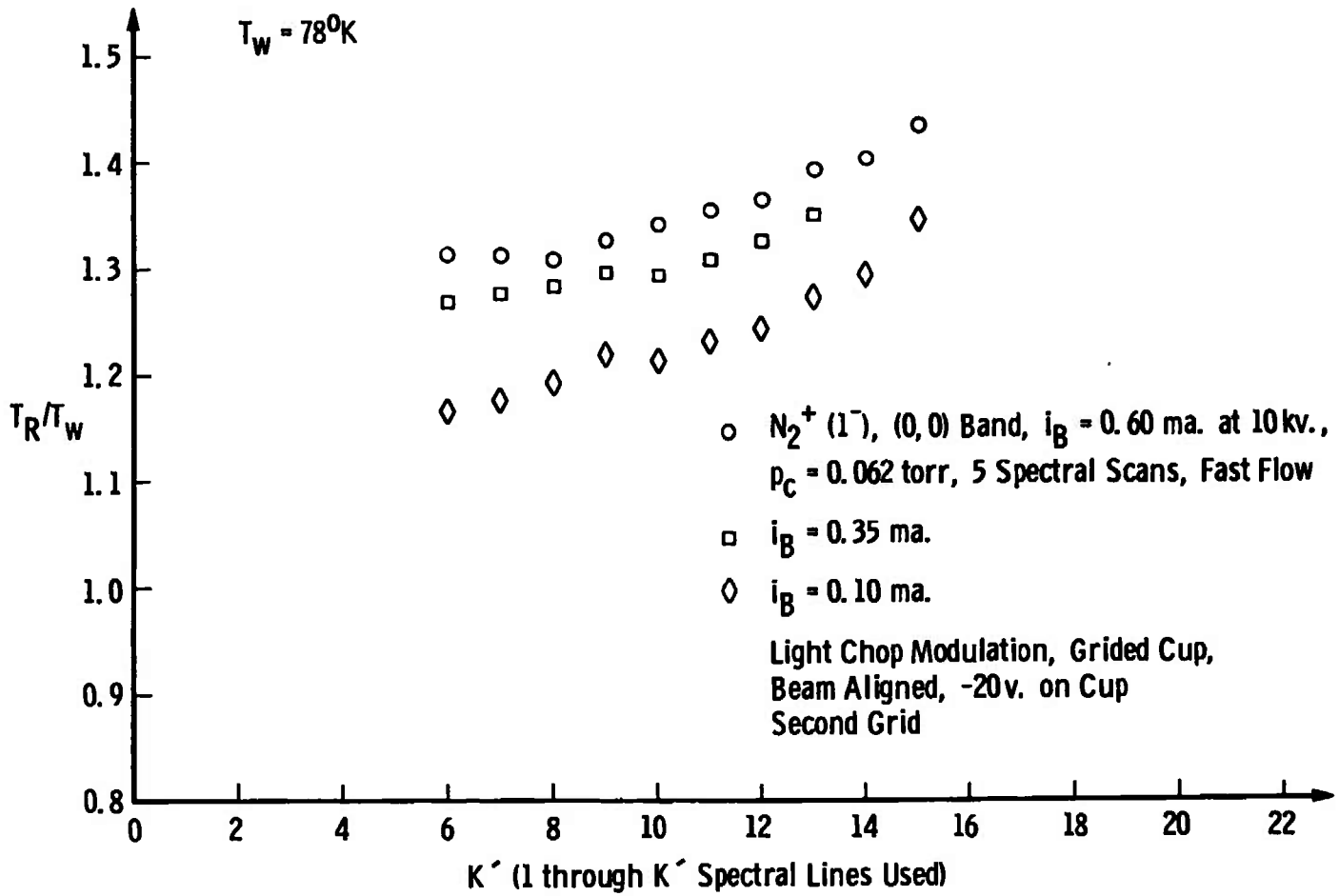

Fig. 33 Ratio of Measured Rotational Temperature to Chamber Wall Temperature versus Number of Spectral Lines Used for the Temperature Determination with Beam Current as a Parameter, T_w = 78°K, P_c = 0.062 Torr

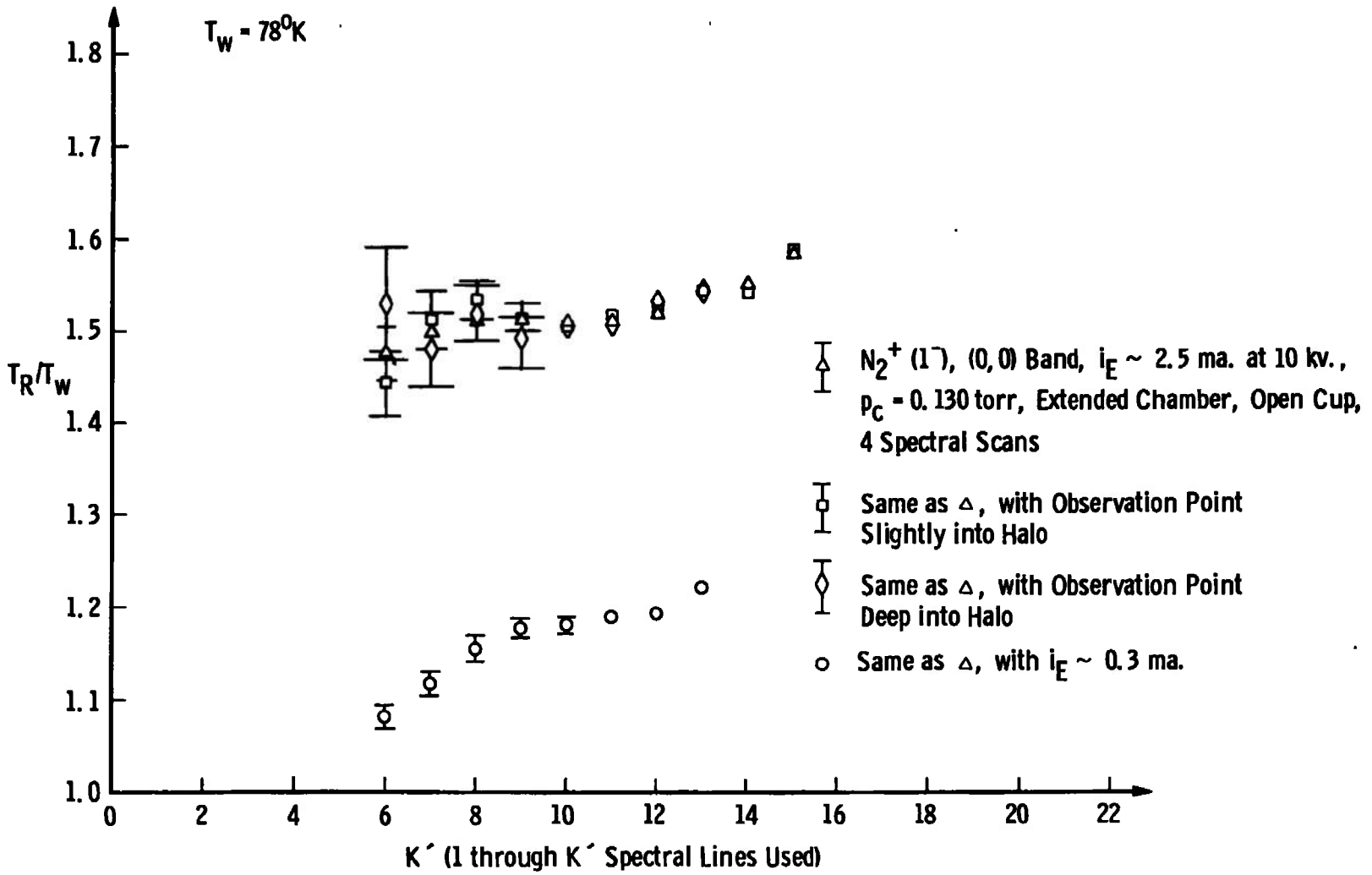

Fig. 34 Ratio of Measured Rotational Temperature to Chamber Wall Temperature versus Number of Spectral Lines Used for the Temperature Determination with Beam Current and "Halo" Observation as Parameters, T_w = 78°K, P_c = 0.130 Torr

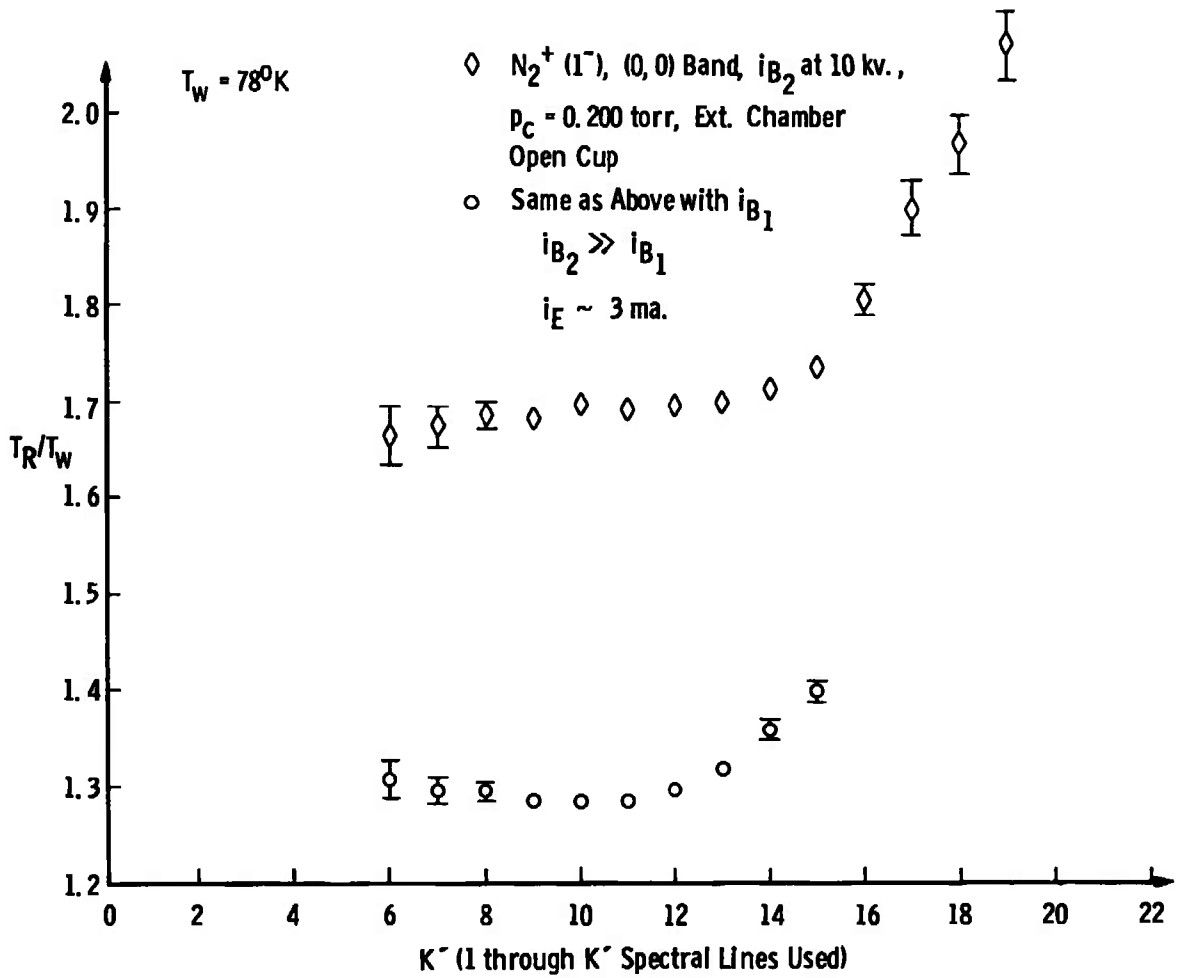

Fig. 35 Ratio of Measured Rotational Temperature to Chamber Wall Temperature versus Number of Spectral Lines Used for the Temperature Determination with Beam Current as a Parameter, T_w = 78°K, P_c = 0.200 Torr

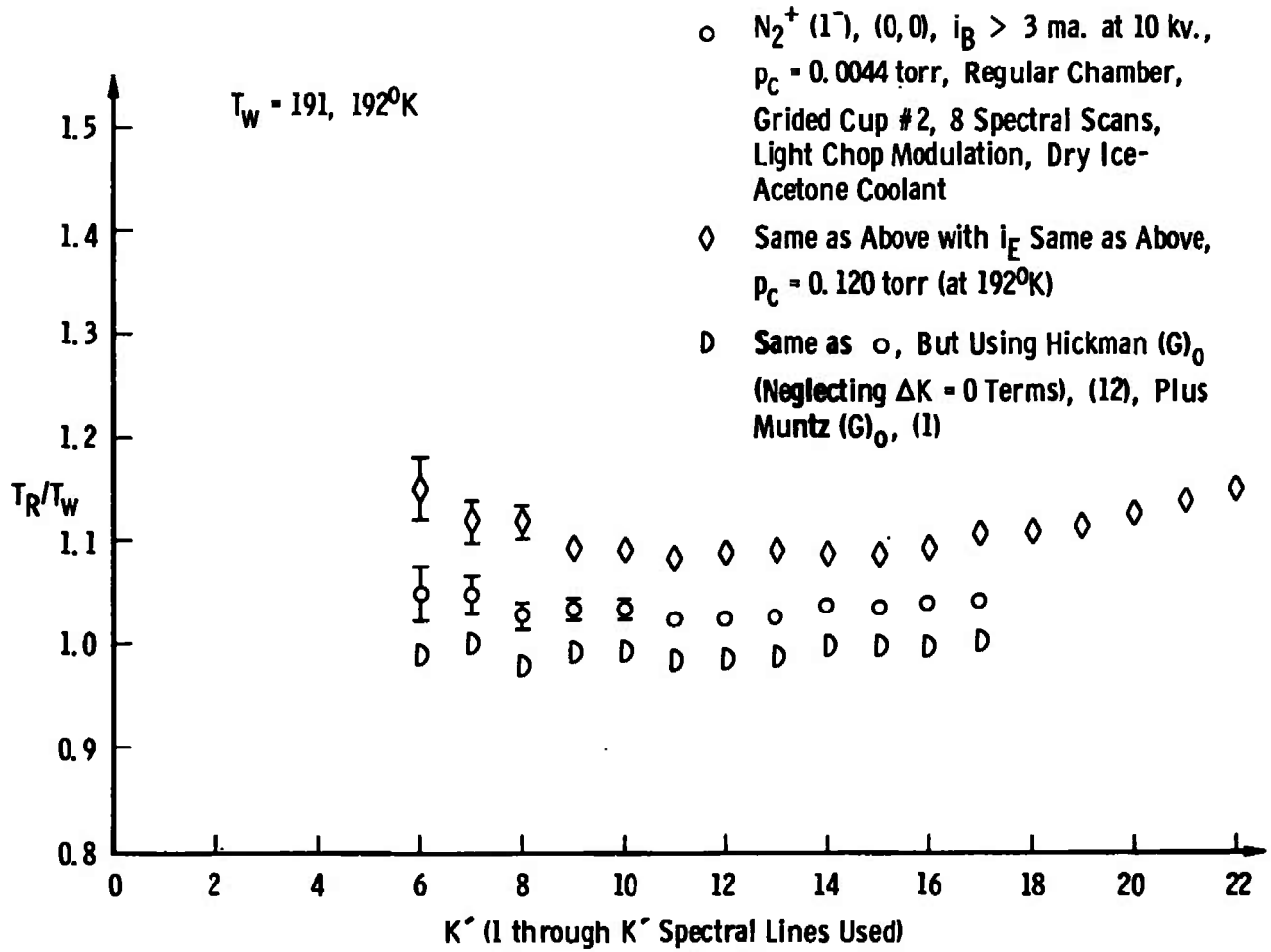

Fig. 36 Ratio of Measured Rotational Temperature to Chamber Wall Temperature versus Number of Spectral Lines Used for the Temperature Determination with Chamber Pressure a Parameter, T_w = 192°K

temperature measurements:

1. A temperature effect - evidenced by increasing error between measured temperature and wall temperature as the wall temperature decreases and by increased non-linearity of Boltzmann plots at lower temperatures.

2. A density effect which, at a given temperature, causes increasing temperature error and non-linearity of Boltzmann plots with increasing density.

3. A beam current or localized heating effect dependent on the temperature, density, and flow rate of the test gas and also dependent on the beam energy and current density.

4. A possible band overlap effect due to the presence of the N_2 $[2^+]$ system (3,6) band at approximately 3895 Å within the N_2^+ $[1^-]$ system (0,0) band rotational structure (a possibility also noted by Ashkenas (10)).

The possibility of band overlap was definitely noticeable in the spectral data shown in Figure 37 for $K' \geq 14$. Any significant overlap will, of course, make the Boltzmann plots non-linear and, in this case, make the measured temperature higher than the actual temperature when the overlapped lines are used in the temperature determination. It is believed that this overlap effect will certainly prevent quality rotational spectra from being observed with a moderate resolution spectrometer at high densities due to the strong intensity dependence of the N_2 $[2^+]$ system on nitrogen density. The N_2 $[2^+]$ system is also easily excited by secondaries. Therefore the overlap effect will be

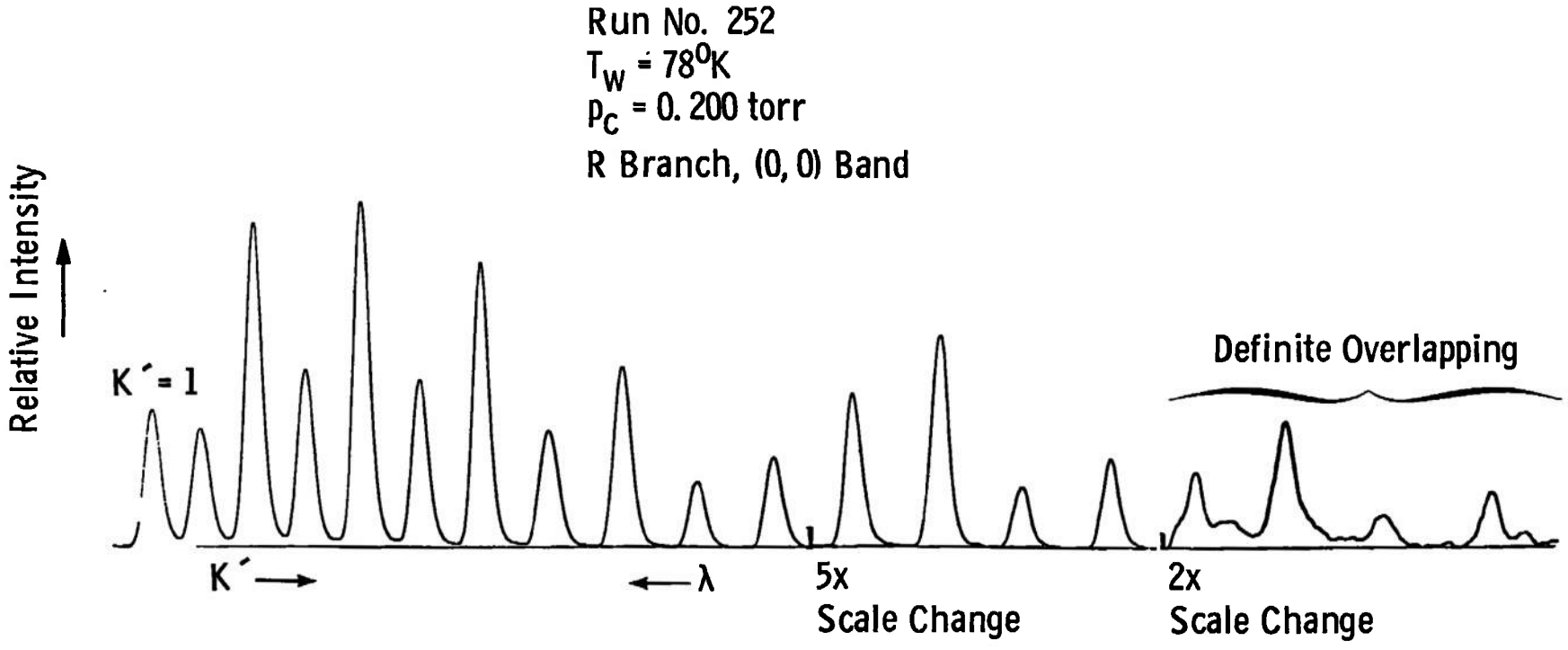

Fig. 37 Spectra Showing Possible Band Overlap

strongly coupled to density and possibly influenced by beam energy and current density. For low temperature and/or high density conditions it will be necessary to exclude all rotational lines for $K' \geq 14$. Another possibility for avoiding overlap will be to search for a band of the N_2^+ [I^-] system that is free from overlap. The (0,2) and (0,3) bands appear to be excellent possibilities; but, of course, these bands are considerably weaker than the (0,0) band.

A beam heating effect has been reported by others, as pointed out previously, for static and slowly flowing gas electron beam temperature measurements. Beam heating is partially analyzed in Appendix B, and the result is that beam heating is definitely possible to a noticeable degree for the 78°K conditions of this investigation even at low values of pressure (see Table I). Experimentally, however, no confirmation of beam current dependence has been observed at the low pressure conditions, but at the higher pressures (even at room temperature) it has been noticed. Elimination of beam heating will have to be accomplished by the use of higher energy beams and higher test gas flow rate. Judging from the results of Ashkenas (10) flow rates on the order of 0.01-1.00 grams per minute will be necessary.

The density effect on T_R/T_W observed by Ashkenas (10) is plotted in Figure 9, page 30, for T_W = 78°K and K' = 10. Data points from this investigation are plotted for comparison. The 0.005 Torr data point agrees very well with the result of Ashkenas (10) as it should. The second point at 0.031 Torr is high as expected due to apparent beam heating. However, it should be pointed out that all these

TABLE I
RESULTS OF BEAM HEATING CALCULATIONS FOR A FEW SELECTED TEST CHAMBER CONDITIONS

Gas	Chamber Pressure (Torr)	Beam Current (milliamperes)	Beam Energy (KV)	Wall Temperature (°K)	Approximate Temperature Increase at the Beam Center (°K)
N_2	0.0015	3	10	78	2
N_2	0.0044	3	10	192	1
N_2	0.050	3	10	300	0.6
N_2	0.005	3	10	78	7
N_2	0.013	2	20	78	8
N_2	0.013	2	20	300	0.6

points are well within the scatter of the data used by Ashkenas (10) to determine the density dependent curve. The data of Figure 33, page 68, were used in Figure 38 in an attempt to extrapolate to zero current the beam current dependence and to then obtain a pure density effect point at 0.062 Torr for plotting in Figure 9, page 30. The data point so obtained also lies above the curve of Ashkenas (10). The reliability of the point is certainly questionable and should serve to emphasize the necessity of eliminating any possible beam heating so that a true measure of density dependence can be determined.

The pure temperature effect calibration curve for T_w/T_R or $T_{actual}/T_{measured}$ proposed by Robben and Talbot (8) is shown in Figure 6, page 26. Data points from this investigation have been plotted in comparison to the Robben and Talbot (8) curve. Conditions for the data were 283°K at 0.56 Torr, 192°K at 0.0044 Torr, and 78°K at 0.005 Torr, and the density of these conditions is on the order of 10^{-8} grams per cubic centimeter. There is a definite lack of agreement between the Robben and Talbot (8) curve and the data from this investigation. Although the 192°K point agrees very well the 78°K and 283°K points surely do not. It should be pointed out, however, that the Robben and Talbot (8) curve was formulated without a knowledge of a density dependence of the temperature measurements. The density of the Robben and Talbot (8) 78°K points was given as equivalent to approximately 0.300 Torr at 300°K. This is equivalent to about 0.080 Torr at 78°K, and as can be seen from the data in Figure 9 there is a very significant density effect at this density which would invaildate the low temperature points

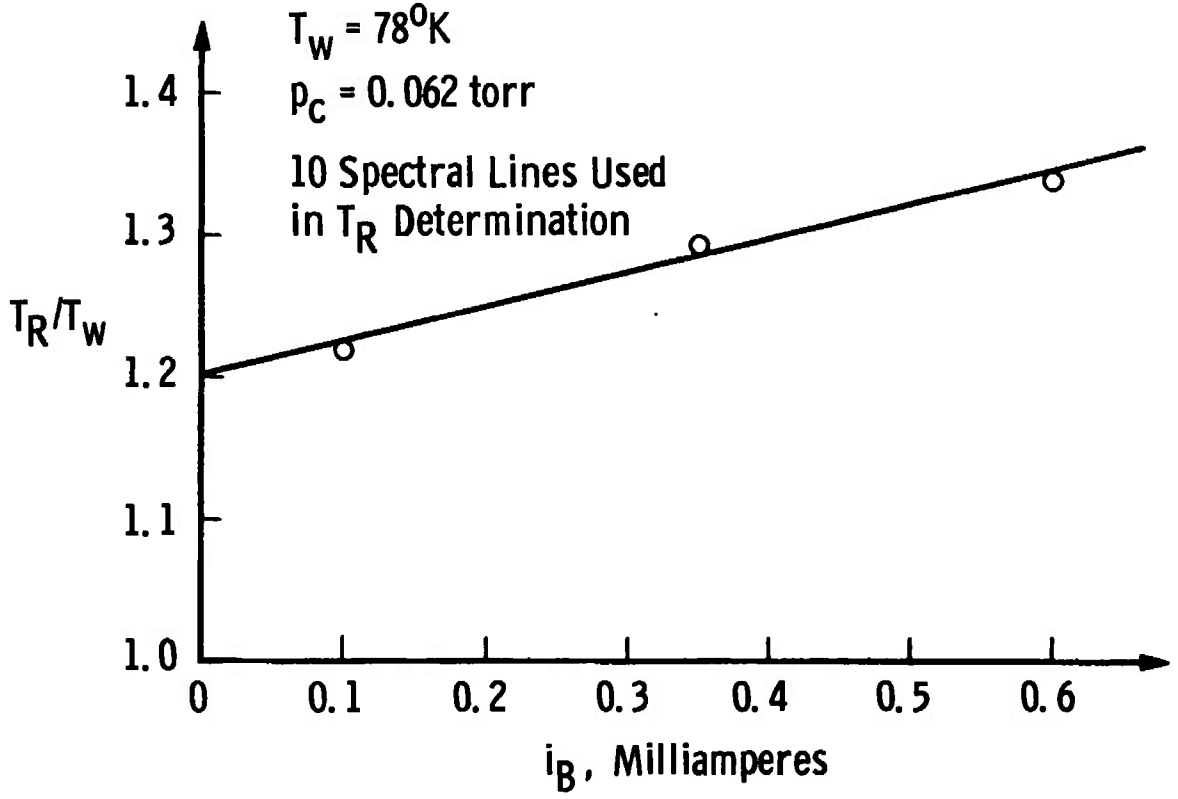

Fig. 38 Ratio of Measured Rotational Temperature to Chamber Wall Temperature Extrapolated to Zero Beam Current, $T_w = 78°K$, $P_c = 0.062$ Torr, 10 Spectral Lines Used

of the Robben and Talbot (8) curve. Furthermore, as pointed out by Marrone (9), there also exists the possibility of rotational relaxation effects in the Robben and Talbot (8) experiments.

An explanation of the disagreement at 283°K is difficult to make, since the Robben and Talbot (8) density was nearly the same as the density for the 283°K point at 0.056 Torr. The result of this investigation at the 283°K point would agree closely, however, with the findings of Muntz (1), Petrie (5), and AEDC results.

There have been several attempts to modify the Muntz excitation model in order to account for the temperature dependence and the variation of temperature with number of spectral lines used. Robben and Talbot (8) attempted to use a model wherein a relatively small number of $\Delta K = \pm 3$ transitions (10 per cent of the total transitions) were allowed to take place and were caused by secondary electrons that did not follow the optical selection rules assumed for the primaries. This attempt was abandoned, however, because of inconsistencies at low temperatures, lack of knowledge of proper Hönl-London factors, and lack of knowledge of the mean free path of the secondaries as a function of density.

Hickman (12) introduced a model which was a composite of two processes. It was proposed that an intermediate neutral $\sum_g^+$ state of the excited molecule was populated by collisions with secondary electrons in which $\Delta K = \pm 2,0$ (quadrupole transitions), and then a final dipole transition took place that populated the ionized $B^2 \sum_u^+$ state from the intermediate state. Collision cross sections for the rotational excitation of a homonuclear molecule by collisions with very slow electrons

derived by Gerjuoy and Stein (13) were used and are given below:

$$\sigma_{\Delta K = +2} \propto \frac{(K''_1 + 2)(K''_1 + 1)}{(2K''_1 + 3)(2K''_1 + 1)} \tag{59}$$

$$\sigma_{\Delta K = -2} \propto \frac{K''_1 (K''_1 - 1)}{(2K''_1 - 1)(2K''_1 + 1)} \tag{60}$$

$$\sigma_{\Delta K = 0} \propto \frac{K''_1 (K''_1 + 1)}{(2K''_1 + 3)(2K''_1 - 1)} \tag{61}$$

Using these equations and the dipole transition relative rates in the manner of the development of the intensity equations in Chapter II a $(G)_o$ analogous to that of Equation 48 for the direct excitation model is derived and given below.

$$(G)_o = \frac{K'(K'-1)(K'-2)}{(2K'-1)(2K'-3)(2K'+1)} e^{+6B_o(K'-1)hc/kT_R}$$

$$+ \frac{(K'+1)(K'+2)(K'+3)}{(2K'+1)(2K'+3)(2K'+5)} e^{-6B_o(K'+2)hc/kT_R}$$

$$+ \left[\frac{2(K')^2(K'-1)}{3(2K'+1)^2(2K'-3)} + \frac{K'(K'+1)^2}{(2K'+1)^2(2K'+3)}\right] e^{2B_oK'hc/kT_R}$$

$$+ \left[\frac{2(K'+1)^2(K'+2)}{3(2K'+1)^2(2K'+5)} + \frac{(K')^2 (K'+1)}{(2K'+1)^2(2K'-1)}\right] e^{-2B_o(K'+1)hc/kT_R} \tag{62}$$

Hickman's $(G)_o$ was used in the reduction of a set of data that had been previously reduced using the Muntz $(G)_o$. The comparison is made in Figure 31, page 65. Use of the Hickman $(G)_o$ does indeed lower the measured temperature on the average, but the variation of the measured

temperature with number of spectral lines used has greatly increased.

By trial and error it was found that a direct addition of a Muntz $(G)_o$ and a Hickman $(G)_o$, neglecting the $\Delta K = 0$ terms, resulted in lowering the measured temperature to very near the desired value, and it also decreased the variation of measured temperature with K' (see Figure 31, page 65). The modified $(G)_o$ used is given as

$$(G)_o^{mod} = \frac{(K'+1)e^{-2B_o(K'+1)hc/kT_R} + (K')e^{2B_oK'hc/kT_R}}{2K'+1}$$

$$+ \frac{(K')(K'-1)(K'-2)}{(2K'-1)(2K'-3)(2K'+1)} e^{6B_o(K'-1)hc/kT_R}$$

$$+ \frac{(K'+1)(K'+2)(K'+3)}{(2K'+1)(2K'+3)(2K'+5)} e^{-6B_o(K'+2)hc/kT_R}$$

$$+ \frac{(K')\ (K'+1)^2}{(2K'+1)^2(2K'+3)} e^{+2B_oK'hc/kT_R}$$

$$+ \frac{(K')^2(K'+1)}{(2K'+1)^2(2K'-1)} e^{-2B_o(K'+1)hc/kT_R} \qquad (63)$$

Additional results from using the $(G)_o^{mod}$ are shown in Figure 28, page 62, and Figure 36, page 71, and it is seen that the $(G)_o^{mod}$ brings about excellent agreement between the measured and wall temperature for conditions believed to be free from a beam heating influence.

The model implied from the use of the $(G)_o^{mod}$ would seem to be one in which approximately half of the molecules in the N_2 $X^1\Sigma$ state at densities on the order of 10^{-8} grams per cubic centimeter are rotationally excited by slow secondary electrons before direct excitation by primaries

to the $N_2^+ B^2\sum$ state. This model would also be expected to have a density dependence due to increasing collision effects on the ground state molecules with increasing density. At this time, however, there is no absolute justification of this model due to the fact that the collision cross sections derived by Gerjuoy and Stein (13) are for secondary electrons with energies below 0.29 ev, and little is known as to the relative number of secondaries in this range within the electron beam.

Harbour, using a plasma treatment of the electron beam, has calculated secondary electron number densities several orders of magnitude larger than those expected by neglecting electrostatic forces and assuming secondary concentration on the same order of magnitude as the primary concentration. Muntz (1) had estimated the ratio of the number of transitions caused by secondaries to those caused by primaries to be on the order of 10^{-4}. Frankenthal, Manly, and Treve (14), however, have shown that in the primary range of 10-100 KV the contribution to the total number of $N_2^+ B^2\sum$ state molecules due to first generation secondaries (energies greater than 25 ev and less than one-tenth the energy of the primaries) is of the same order of magnitude as that of the primaries. It was also shown by Frankenthal, Manly, and Treve (14) that if account is taken of $N_2^+ B^2\sum$ excitation by Auger electrons the ratio of secondary transitions to primaries is almost 1:1.

These calculations indicate that the excitation processes of the secondaries must be thoroughly investigated to determine their effect on the measured rotational temperature value. However, it is also necessary to explain the result shown in Figure 34, page 69, that no

measured temperature change was observed between the halo and the main portion of the beam. At the density and beam energy at which this measurement was made it is entirely possible that the main part of the "halo" observed was just the spreading of the electron beam primaries. This possibility also exists for the halo measurement of Ashkenas which was made at the high density of approximately 1.03×10^{-5} grams per cubic centimeter.

Finally, it has been shown in Figure 39 that the measured temperature is dependent on the band used in the case of the bands shown albeit the data were of poorer quality than usual due to the weakness of some of the bands.

B. VIBRATIONAL TEMPERATURE DATA

Vibrational bands were integrated using the electronic integrator, the circuit of which is shown in Figure 14, page 44. The spectrometer slit width was set at 200 microns. Immediately before the beginning of a scan the integrator was switched to operate, and with the light from the beam blocked from the spectrometer the photomultiplier dark current and other noise was nulled out so that the integration would not include it. The optics light path was then unblocked and the scan made. At the end of the scan, characterized by the recorded trace assuming a zero slope, the feedback loop of the integrator amplifier was short-circuited causing the recorder trace to return to the zero point. Beam current and chamber pressure were kept as steady as possible during these scans. A typical integrated trace is shown in Figure 40. The maximum

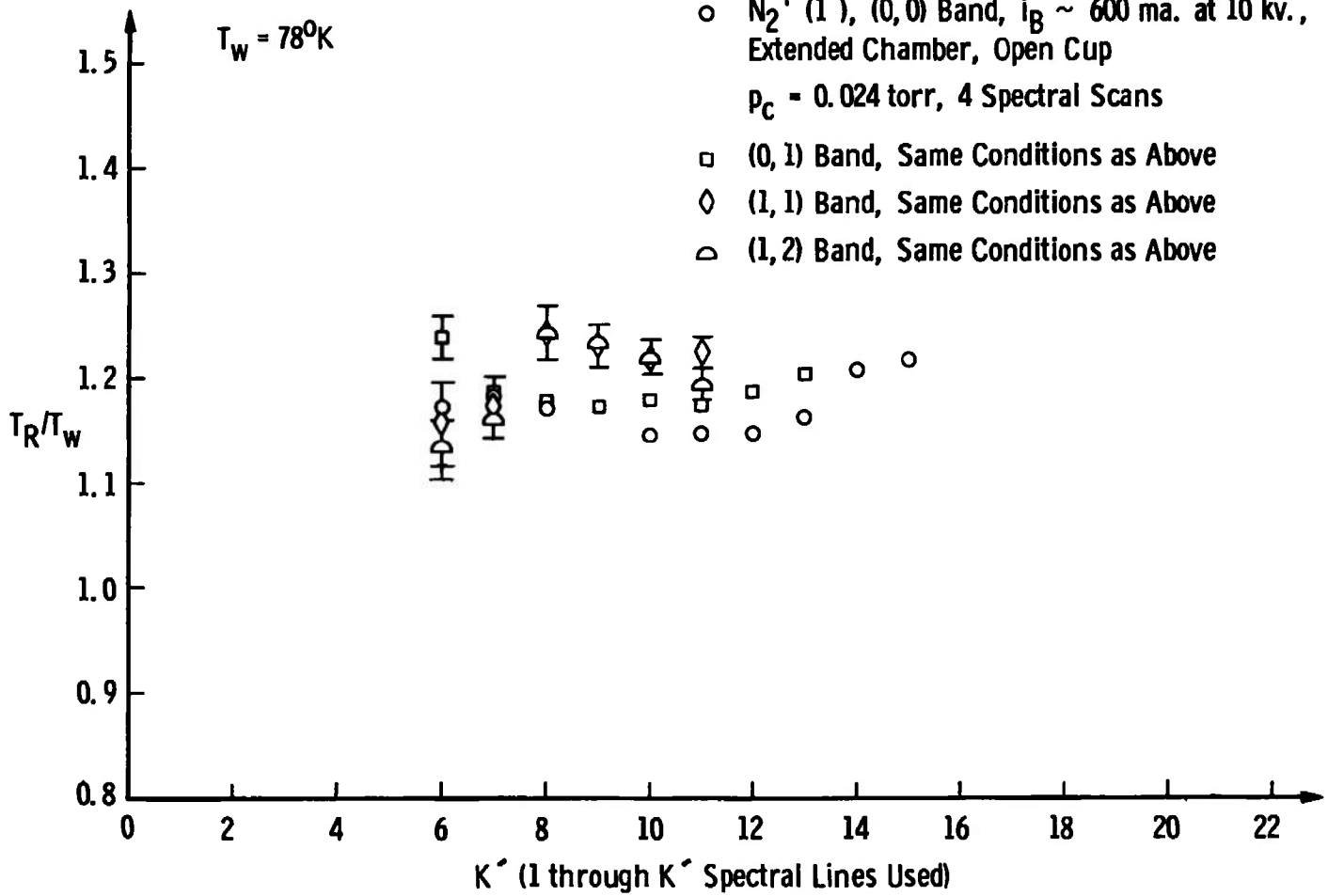

Fig. 39 Ratio of Measured Rotational Temperature to Chamber Wall Temperature versus Number of Spectral Lines Used for the Temperature Determination with Vibrational Band as a Parameter, $T_w = 78°K$

Fig. 40 Typical Band Integration Trace

of the traces are proportional to the intensity of the band.

Figure 41 is a diagram of the prominent bands observed in the spectral region of this investigation. Relative intensity results of integrated scans of several of the bands at pressures less than 0.100 Torr are given in Table 2 and compared with the theoretical values calculated from Equation 57 using $p(v',v''_2)$ and $q(v',v''_1)$ values from Tables 3 and 4, respectively. These values were calculated at AEDC using band intensity data of Nicholls (15). It was shown by Lewis that the use of $q(v',v''_1)$ values instead of $p(v',v''_1)$ values is acceptable. All experimental values were adjusted for the optics and photomultiplier sensitivity variation with wavelength shown in Figure 42.

Figures 4 and 5, pages 23 and 24, and Figure 43 show the results of band ratios determined by integration as a function of pressure compared with theoretical values determined from Equation 57 using Tables 3 and 4. In Figure 4 the data of Harbour are plotted for comparison. Absolute values differ by as much as 20 per cent; however, the pressure dependence agrees very well. Harbour corrected the data for band overlap, but the data of this investigation were for pressures less than 1 Torr, and according to Harbour's data, do not require overlap correction.

The indicated random error of the band ratio measurements was due primarily to beam generated noise, drift in beam current, and possible band overlap at the beginning and end of the scans. Systematic error was primarily due to inaccuracies in the determination of the optical

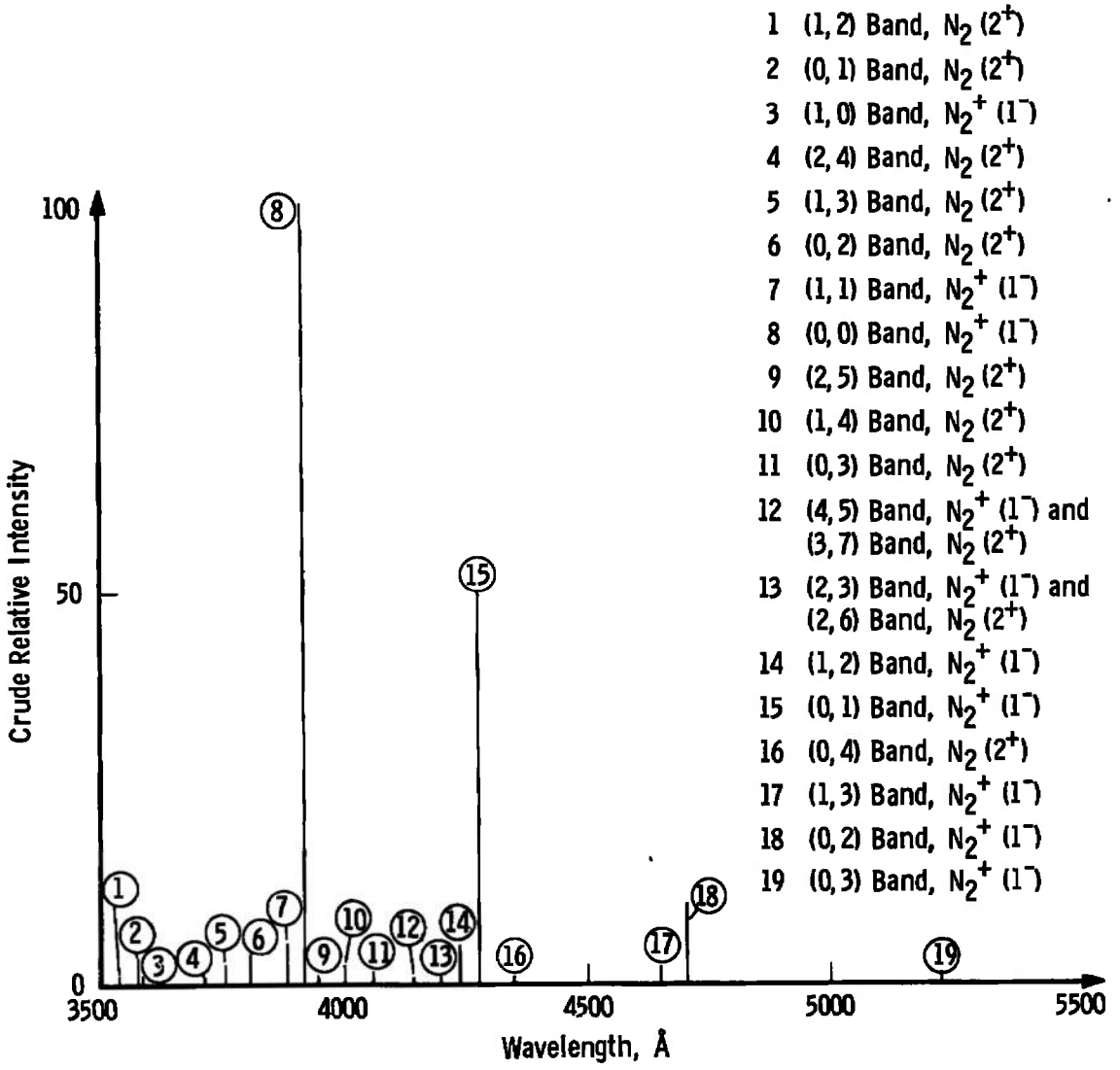

Fig. 41 Electron Beam Excited Bands Observed in the Laboratory System

TABLE 2
BAND INTENSITY RATIOS, EXPERIMENTAL AND THEORETICAL

v'/v''_2	0	1	2	3
0	1.00	0.27	0.06	
	1.00	0.32	0.063	
1		0.05	0.04	0.02
		0.05	0.04	0.017

Legend: Experimental ratio
Theoretical ratio
} normalized to I(0,0)

The band intensity ratio data precision is approximately ± 10 per cent.

TABLE 3
FRANCK-CONDON FACTORS FOR THE v''_1 TO v' TRANSITION

v'/v''_1	0
0	0.8926
1	0.1059

TABLE 4
VIBRATIONAL STRENGTH FACTORS OF THE v' TO v''_2 TRANSITION

v'/v''_2	0	1	2	3
0	0.540	0.245	0.072	0.017
1	0.169	0.204	0.275	0.134

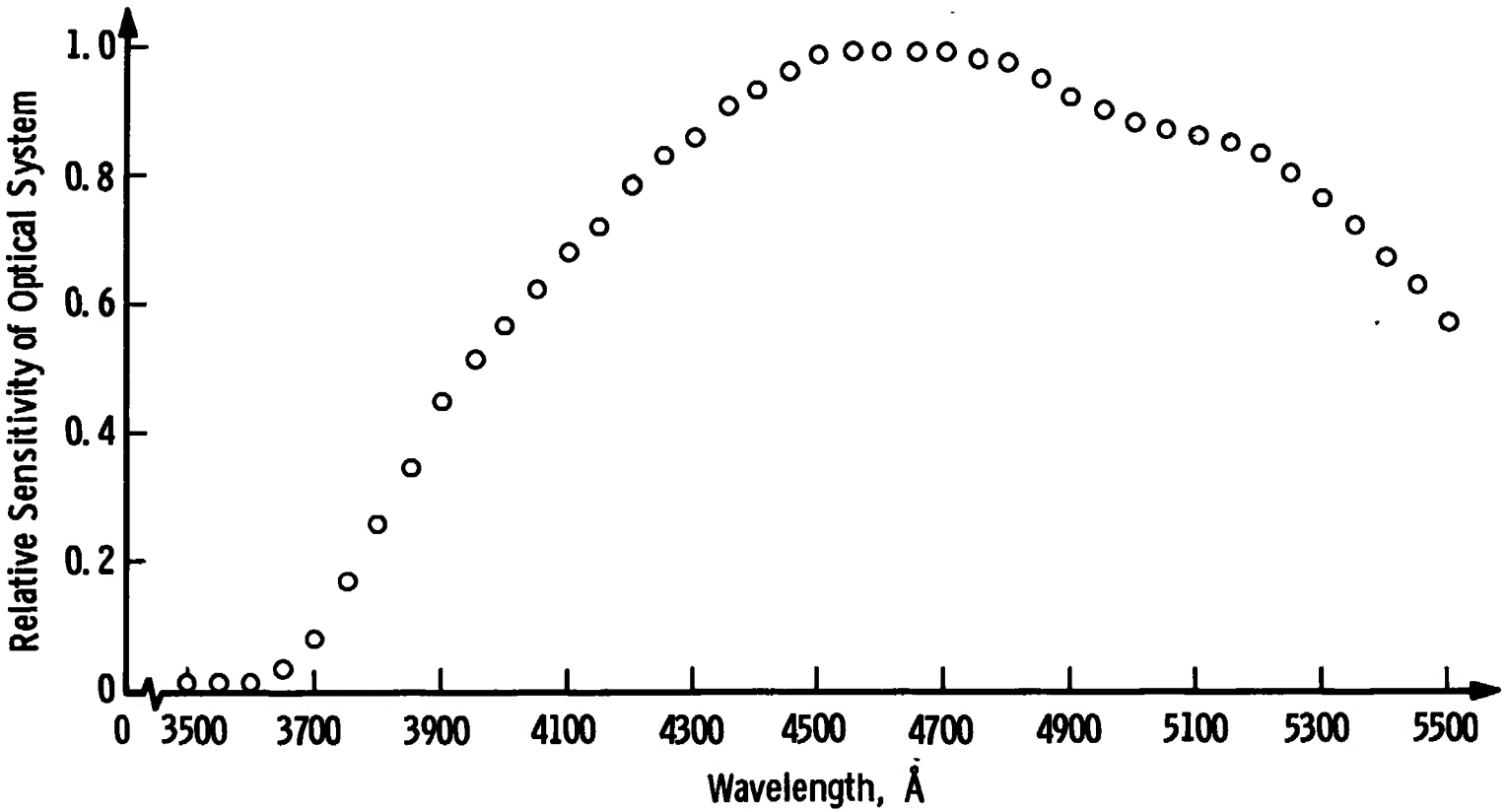

Fig. 42 Optical System Sensitivity versus Wavelength

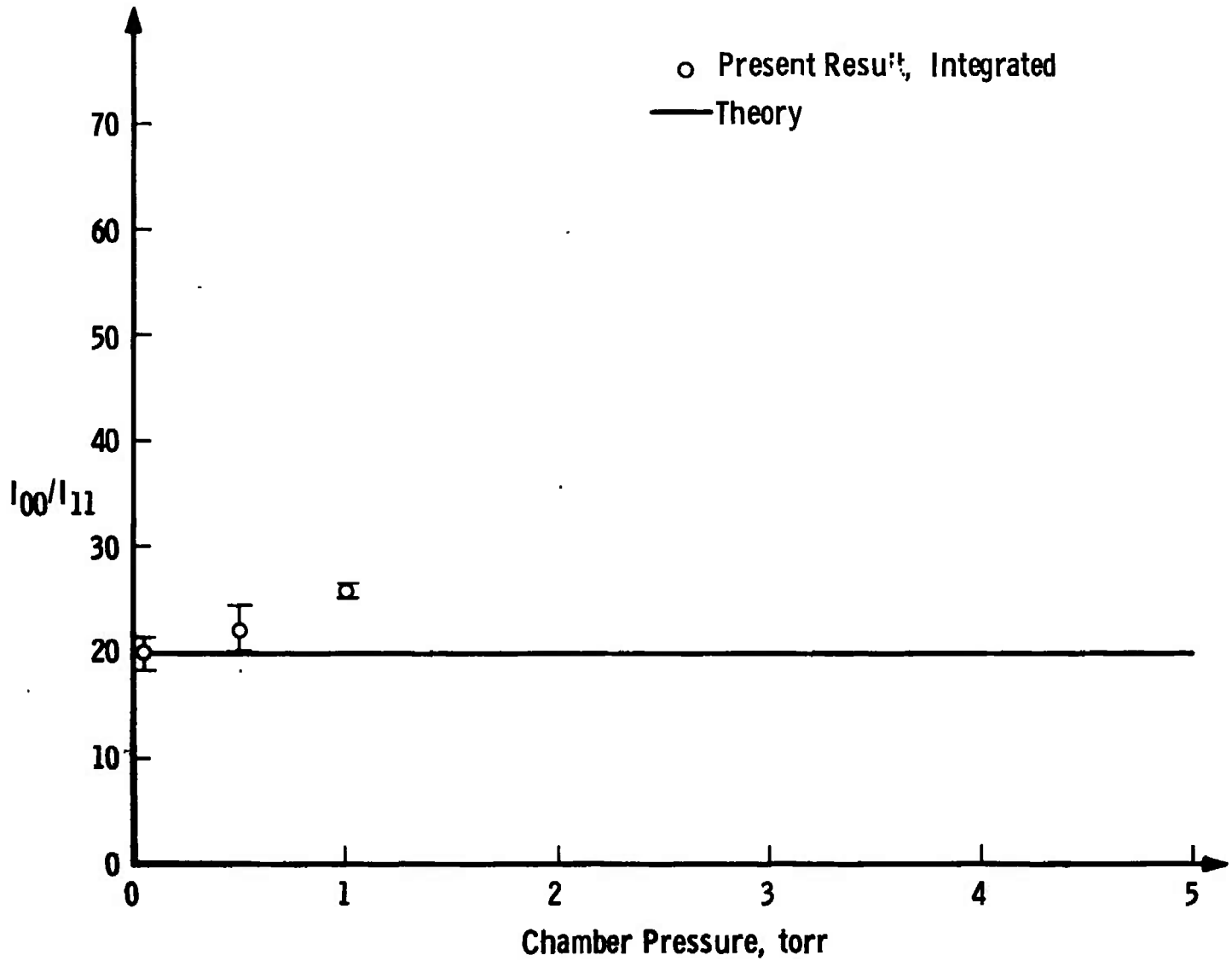

Fig. 43 I_{00}/I_{11} versus Chamber Pressure

sensitivity versus wavelength curve.

Accuracy values of the presented measurements do not, however, prohibit recognition of the pressure dependence of the (0,1)/(1,2), (0,0)/(1,1), and (0,2)/(1,3) band ratios. This pressure dependence most surely impedes development of methods for measuring vibrational temperature and must also certainly cast doubt upon some previous tunnel measurements of vibrational temperatures made using the electron beam technique.

CHAPTER VI
SUMMARY AND SUGGESTIONS FOR FUTURE WORK

An electron beam excitation system, a spectroscopic system, and a signal detection and recording system have been developed for laboratory studies of vibrational and rotational temperature measurement using the electron beam technique. Rotational temperature measurements have been made over the temperature range 78°-300°K at pressures of 0.001-1.0 Torr. Integrated vibrational band intensity measurements were made at 300°K at pressures of 0.100-1.0 Torr.

Results of this investigation are summarized as follows:

1. High quality data (low noise, excellent resolution) coupled with proper data reduction techniques are believed to have yielded the most precise measurements of rotational temperature and vibrational band intensity to date.

2. The measured rotational temperatures were observed to be in increasing disagreement with chamber wall temperature, or actual gas temperature, as the temperature decreases. The measured rotational temperature was always higher than the actual gas temperature.

3. The ratio of rotational temperature to wall and gas temperature was observed to be dependent on the number of spectral lines used in the temperature determination and the ratio increases as more high K' numbered lines are used. Further, this dependence is more pronounced

at lower temperatures.

4. At low temperature and high densities (10^{-7}-10^{-6} grams per cubic centimeter) a definite band overlap effect has been observed in the rotational lines of the R branch of the (0,0) band of the N_2^+ [i^-] system due to the presence of the (3,6) band of the N_2 [2^+] system. Therefore the number of spectral lines in the (0,0) band that may be used may be limited to no more than 14.

5. At low densities ($\sim 10^{-8}$ grams per cubic centimeter) there is little indication of a rotational temperature dependence on beam current. However, at higher densities a definite dependence on beam current has been observed and explained as a localized beam heating of the test chamber gas.

6. The ratio of measured rotational temperature to wall and gas temperature was observed to increase with increasing nitrogen density.

7. Vibrational band intensity ratios were also observed to be density dependent, and this dependence is probably due to collision quenching effects.

8. It was shown that rotational temperature measurements in the beam "halo" region did not differ from rotational temperature measurements in the main portion of the beam.

9. It was shown that measured rotational temperatures were dependent upon the vibrational band that was used.

10. For densities on the order of 10^{-8} grams per cubic centimeter an empirical modification of the rotational line intensity equation has been shown to yield good agreement between measured

rotational and actual temperatures.

Certainly investigations of the type reported herein should be continued; therefore recommendations for future work are listed as follows:

1. The sensitivity of the detection system should be upgraded to increase the precision and range of the experiments. Improvement of at least two orders of magnitude should be possible with photomultiplier tube shielding and cooling.

2. Data quality can also be improved by reduction of beam current drift and noise. This can be accomplished by use of a beam controller system developed by Froedge (16).

3. Beam energy and flow rate need to be increased in order to eliminate the problem of localized beam heating. When this is accomplished precise documentation of the dependence of the measured rotational temperature on gas temperature, gas density, number of spectral lines, and vibrational band must be completed over a wide range of gas temperature and pressure.

4. Band overlap should be further investigated in the hope that a useful band free of overlap might be found.

5. An analytic and experimental investigation of secondary electrons should be initiated. The number density, energy distribution, and behavior of the secondaries should be determined. Experimental work should be directed toward the control of secondary electron concentration in the area of the beam under observation and toward rotational and vibrational temperature measurements using low energy electrons.

6. If vibrational band integration precision can be reduced to less than ± 5 per cent, the vibrational band intensity ratio dependence on density should be determined over a wider range of density at several temperatures. Collision quenching effects on individual bands should also be investigated as the probable cause for the density dependence.

BIBLIOGRAPHY

1. Muntz, E. P. "Measurement of Rotational Temperature, Vibrational Temperature, and Molecule Concentration in Non-Radiating Flows of Low Density Nitrogen," University of Toronto Institute of Aerophysics Report 71, Toronto, Canada, April, 1961.

2. Muntz, E. P. and S. J. Abel. "The Direct Measurement of Static Temperatures in Shock Tunnel Flow," GE TIS R64SD25, Valley Forge, Pennsylvania, 1964.

3. Muntz, E. P. and D. J. Marsden. Rarefied Gas Dynamics II. Edited by J. A. Laurmann. New York: Academic Press, 1963.

4. Muntz, E. P., S. J. Abel, and B. L. Maguire. "The Electron Beam Fluorescence Probe in Experimental Gas Dynamics," Supplement to IEEE Transactions on Aerospace, Vol. AS-3, No. 2, June 1965, pp. 210-222.

5. Petrie, S. J. "Analysis of the Thermo-Chemical State of an Expanded Air Plasma," AFFDL-TR-64-191, Air Force Flight Dynamics Laboratory, Wright-Patterson Air Force Base, Ohio, August, 1965.

6. Herzberg, G. Spectra of Diatomic Molecules. Princeton, New Jersey: Van Nostrand Company, Inc., 1950.

7. Rushbrooke, G. S. Introduction to Statistical Mechanics. London: Oxford University Press, 1964.

8. Robben, F. and L. Talbot. "Some Measurements of Rotational Temperatures in a Low Density Wind Tunnel Using Electron Beam Fluorescence," University of California Report No. AS-65-5, Berkeley, California, May, 1965.

9. Marrone, P. V. "Rotational Temperature and Density Measurements in Underexpanded Jets and Shock Waves Using an Electron Beam Probe," University of Toronto Institute of Aerophysics Report 113, Toronto, Canada, January, 1966.

10. Ashkenas, H. "On Rotational Temperature Measurements in Electron-Beam Excited Nitrogen," Physics of Fluids, 10:2509, December, 1967.

11. Instruction Manual Precision Lock-In Amplifier Model HR-8. Princeton: Princeton Applied Research Corporation, 1965.

12. Hickman, R. S. "Rotational Temperature Measurements in Nitrogen Using an Electron Beam," University of Southern California Aerospace Engineering Report 104, Los Angeles, California, September, 1966.

13. Gerjuoy, E. and S. Stein. "Rotational Excitation by Slow Electrons," Physical Review, 97:1671-1679, March, 1955.

14. Frankenthal, S., O. P. Manley, and Y. M. Treve. "Fluorescent Efficiency of Energetic Electrons in the 3914 Å Band," The Journal of Chemical Physics, 44:257-264, January, 1966.

15. Nicholls, R. W. "The Interpretation of Intensity Distributions in the N_2 Second Positive and N_2^+ First Negative Band Systems," The Journal of Atmospheric and Terrestial Physics, 24:749, August, 1962.

16. Froedge, D. T. "High Energy Electron Beam Excitation of a Gas," Unpublished Masters thesis, The University of Tennessee, Knoxville, Tennessee, 1967.

17. Beers, Y. Introduction to the Theory of Error. Reading, Massachusetts: Addison-Wesley Publishing Company, Inc., 1953.

18. Kreith, F. Principles of Heat Transfer. Scranton, Pennsylvania: International Textbook Company, 1958.

19. Gadamer, E. O. "Measurement of the Density Distribution in a Rarefied Gas Flow Using the Fluorescence Induced by a Thin Electron Beam," University of Toronto Institute of Aerophysics Report 83, Toronto, Canada, March, 1962.

APPENDIXES

APPENDIX A
ROTATIONAL TEMPERATURE DATA REDUCTION

Equation 50 is solved by an iterative machine calculation. The program for the computer (CDC-1604B) is shown in Table 5, and it was written by Mr. J. O. Hornkohl of the Hypervelocity Branch, von Karman Facility, Flow Diagnostics Section, ARO, Inc. The input requires a card for the following: spectral scan number and designation, total number of spectral lines in a scan, and each line relative intensity value. The intensities of even numbered rotational lines ($K' = 2,4, \ldots$) are doubled before input to properly take account of the influence of nuclear statistics. The program essentially performs a least squares fit of the data points to a straight line from the slope of which is calculated the rotational temperature, T_R. The iteration process continues to calculate a temperature until consecutive calculated values are within 0.01 per cent.

A temperature defined by the maximum number of spectral lines is first calculated. Then a temperature value for $K'_{max} - 1$ lines is calculated. This process is repeated i times through $K'_{max} - i + 1 = 6$. However, no more than 12 iterations for each $(K'_{max} - i + 1)$ set of data is allowed.

One of the more important outputs of the program is the value of the standard deviation (SIGMAT) of the temperature that is printed (in °K) for each $(K'_{max} - i + 1)$ data set. The value is computed using

TABLE 5
COMPUTER PROGRAM LISTING, PROGRAM TROT

```
      PROGRAM TROT
      TYPE REAL NU,NUNORM,NSUMXY,NSUMXSQ
      TYPE INTEGER VU,VL
      DIMENSION I(22),G(22),Y(22),XY(22),XSQ(22),DELTAY(22),YT(22),
     *X(22),PER(22),WAVE(22)
    1 READ 200,RUN,VU,VL
      IF (EOF,50) 12,2
    2 N=0
      PRINT 100
      PRINT 101
      PRINT 102
      PRINT 103,RUN,VU,VL
      PRINT 104
      READ 201,KMAX
      DO 3 K=1,KMAX
    3 READ 202,I(K)
      TRG=200.
    4 SUMX=0.
      SUMY=0.
      SUMXY=0.
      SUMXSQ=0.
      BU=2.083-0.020*(VU+.5)
      BL=1.932-0.020*(VL+.5)
      DO 5 K=1,KMAX
      NU=2.997925E+10*(25461.5 + 2419.84*(VU+.5)-23.19*((VU+.5)**2)
     *-2207.19*(VL+.5) +16.14*((VL+.5)**2) + K*(K+1)*BU-K*(K-1)*BL)
      NUNORM=NU/(2.997925E+10*25566.0)
      WAVE(K)=2.997925E+10/NU*1.0E+08
      G(K)=(K*EXPF(5.7258*K/TRG)+(K+1)*EXPF(-5.7258*(K+1)/TRG))/(2.*K+1)
      Y(K)=LOGF(I(K)/((NUNORM**4)*G(K)*K))
      X(K)=1.*K*(K+1)
      XY(K)=X(K)*Y(K)
      XSQ(K)=X(K)*X(K)
      SUMX=SUMX+X(K)
      SUMY=SUMY+Y(K)
      SUMXY=SUMXY+XY(K)
    5 SUMXSQ=SUMXSQ+XSQ(K)
      SQSUMX=SUMX*SUMX
      PRODSUM=SUMX*SUMY
      NSUMXY=KMAX*SUMXY
      NSUMXSQ=KMAX*SUMXSQ
      SLOPE=(NSUMXY-PRODSUM)/(NSUMXSQ-SQSUMX)
      ORDCEP=(SUMXSQ*SUMY-SUMX*SUMXY)/(NSUMXSQ-SQSUMX)
      TR=-2.8629/SLOPE
      SUMDELSQ=0.
      DO 6 K=1,KMAX
      YT(K)=SLOPE*X(K)+ORDCEP
      DELTAY(K)=Y(K)-YT(K)
      PER(K)=100.*DELTAY(K)/YT(K)
    6 SUMDELSQ=SUMDELSQ+DELTAY(K)*DELTAY(K)
      SIGMAY=(SUMDELSQ/(KMAX-2.))**.5
      SIGMAT=(2.8629*SIGMAY/(SLOPE*SLOPE))*((KMAX/(NSUMXSQ-SQSUMX))**.5)
      TESTTR=ABSF(TR-TRG)/TR
      IF (TESTTR.LT.1.E-04) 8,7
    7 TRG=TR
      GO TO 4
```

TABLE 5 (Continued)

```
    8 N=N+1
      IF (N.GT.1) 11,9
    9 DO 10 K = 1, KMAX
   10 PRINT 105,K,I(K),G(K),Y(K),X(K),WAVE(K),PER(K)
      PRINT 106
      PRINT 107,PRODSUM,NSUMXY,SQSUMX,NSUMXSQ
      PRINT 108,SLOPE,ORDCEP
      PRINT 109
      PRINT 110,KMAX,TR,SIGMAT
      KMAX=KMAX-1
      GO TO 4
   11 PRINT 111,KMAX,TR,SIGMAT
      KMAX=KMAX-1
      IF (KMAX.GT.5) 4,1
   12 STOP
  100 FORMAT (1H1,/,47X,25HROTATIONAL BOLTZMANN PLOT)
  101 FORMAT (1H ,/,57X,5HUSING)
  102 FORMAT (1H ,/,52X,14HMUNTZ G-FACTOR)
  103 FORMAT (1H ,//,21X,12HRUN NUMBER =,1X,A8,5X,I1,1H,,I1,5H-BAND)
  104 FORMAT (1H ,//,6X,1HK,7X,4HI(K),11X,4HG(K),15X,4HY(K),15X,4HX(K),
     *13X,10HWAVELENGTH,9X,27H(DELTA-Y(K))/YI(K),-PERCENT)
  105 FORMAT (1H ,4X,I2,6X,I5,8X,E11.4,8X,E11.4,8X,E11.4,8X,E11.4,
     *12X,E11.4)
  106 FORMAT (1H ,//,5X,13HSUM(X)*SUM(Y),6X,9HN*SUM(XY),8X,
     *13HSUM(X)*SUM(X),6X,10HN*SUM(X*X))
  107 FORMAT (1H ,5X,E11.4,6X,E11.4,7X,E11.4,7X,E11.4)
  108 FORMAT (1H ,//,21X,7HSLOPE =,1X,E11.4,10X,11HINTERCEPT =,1X,E11.4)
  109 FORMAT (1H ,//)
  110 FORMAT (1H ,15X,I2,6H-LINES,5X,24HROTATIONAL TEMPERATURE =,
     *E11.4,5X,26HSTANDARD DEVIATION OF TR =,E11.4)
  111 FORMAT (1H ,15X,I2,6H-LINES,5X,24H                    =,
     *E11.4,5X,26H                          =,E11.4)
  200 FORMAT (A8,1X,I1,1X,I1)
  201 FORMAT (I2)
  202 FORMAT (I5)
      END TROT
```

formulae from Beers (17).

It should be noted that in the least squares fit it would have been possible to weight each line intensity value according to some measure of signal noise used as a standard deviation of the signal. In this case, however, due to the good quality of signal at most conditions it was assumed that the error in the intensity values was independent of the rotational line number.

For a given test chamber and beam condition a number of spectral scans were taken, and it was necessary to "average" these data by some process. Since it was desired to present the deviation of the measured rotational temperature (T_R) from the test chamber temperature (T_w) as a ratio T_R/T_w, a computer program was written by Dr. J.W.L. Lewis (ARO, Inc., Hypervelocity Branch, von Karman Facility, Flow Diagnostics Section) to calculate an average T_R/T_w $\left(\overline{\frac{T_R}{T_w}}\right)$ and average standard deviation, $\bar{\sigma}$, for a given value of the number of spectral lines used in calculating a T_R in a fixed set of data. The $\overline{\frac{T_R}{T_w}}$ and σ values were weighted according to their own precision

$$\left(\overline{\frac{T_R}{T_w}}\right) \equiv \bar{y} = \left(\sum_{i=1}^{s} \frac{y_i}{\sigma_i^2}\right) \Bigg/ \left[\sum_{i=1}^{s} \left(\frac{1}{\sigma_i^2}\right)\right] \tag{64}$$

by definition of a weighted average (17).

Where,

$\sigma_i \equiv$ the standard deviation of the ith spectral scan (the standard deviation given by Program TROT as SIGMAT divided by T_{w_i}),

$y_i = \left(\frac{T_R}{T_w}\right)_i \equiv$ measured temperature divided by chamber temperature for the ith spectral scan (65)

$s \equiv$ total number of data points to be used (usually the number of spectral scans for a given condition)

$$\bar{\sigma} = \left[\left(\sum_{i=1}^{s} w_i^2 \sigma_i^2\right) \Big/ \left(\sum_{i=1}^{s} w_i\right)^2\right]^{1/2} \tag{66}$$

by definition of a standard deviation of an average (17).

Where

$$w_i = (\sigma_1/\sigma_i)^2 \tag{67}$$

$\overline{T_R/T_w}$ and $\bar{\sigma}$ are easily machine calculated. The program (PROGRAM TRADV) is given in Table 6. Inputs to the program are T_{wi}, T_{Ri}, and SIGMAT (from PROGRAM TROT), a value for s, and the number of spectral lines used ($K'_{max} - I + 1$). Outputs are T_{Ri}, T_{wi}, SIGMAT, $\overline{T_R/T_w}$, $\bar{\sigma}$, s, and number of spectral lines used.

TABLE 6
COMPUTER PROGRAM LISTING, PROGRAM TRADV

```
    PROGRAM TRADV
    DIMENSION TR(100), TW(100), SIG(100), S(100), SS(100),  Y(100),
   1 YY(100), Z(100), W(100), WY(100), ID(10)
    PRINT 40
    READ 60, ID   $    PRINT 90, ID
  3 READ 10,XLINES
    IF (EOF,50) 50,51
 50 STOP
 51 CONTINUE
    READ 10,IA1
    READ 20, (TR(I), TW(I), SIG(I), I = 1,IA1)
    PRINT 70
    PRINT 80, (TR(I), TW(I), SIG(I), I = 1, IA1)
 10 FORMAT (I3)
 20 FORMAT (2F15.9, F10.5)
 30 FORMAT (1H0,15HAVERAGE TEMP = , F15.9, 5X, 16HAVERAGE SIGMA = ,
   1F10.5)
 40 FORMAT (1H1)
 60 FORMAT (10A8)
 70 FORMAT (1H , 20HMEASURED TEMPERATURE, 5X, 16HWALL TEMPERATURE,
   *10X, 18HSTANDARD DEVIATION //)
 80 FORMAT (1H , 3X, F15.9, 7X, F15.9, 13X, F10.5)
 90 FORMAT (25X, 10A8)
    DO 1 J = 1,IA1
     Y(J) = TR(J)/TW(J)
     S(J) = SIG(J)/TW(J)
    SS(J) = S(J)**2.
    YY(J) = Y(J)/SS(J)
    Z(J) = 1./SS(J)
     W(J) = SS(1)/SS(J)
   1 WY(J) = W(J) * W(J) * SS(J)
    SUM1 = 0.0 $ SUM2 = 0.0 $ SUM3 = 0.0 $SUM4 = 0.0
    DO 2 K = 1,IA1
    SUM1 = SUM1 + YY(K)
    SUM2 = SUM2 + Z(K)
    SUM3 = SUM3 + WY(K)
   2 SUM4 = SUM4 + W(K)
    TRBAR = SUM1/SUM2
    SIGBAR = (SUM3/(SUM4 * SUM4)) ** 0.5
    PRINT 30, TRBAR, SIGBAR
    PRINT 10, XLINES
    PRINT 10, IA1
    GO TO 3
    END
```

APPENDIX B
DISSIPATIVE BEAM HEATING

The geometry shown in Figure 44 was used in this analysis. The electron beam was considered as a heat source in a gaseous medium. The general heat conduction equation in cylindrical coordinates is (18):

$$\frac{\partial^2 T}{\partial r^2} + \frac{1}{r}\frac{\partial T}{\partial r} + \frac{1}{r^2}\frac{\partial^2 T}{\partial \phi^2} + \frac{\partial^2 T}{\partial z^2} + \frac{\dot{q}}{K} = \frac{1}{a}\frac{\partial T}{\partial t} \tag{68}$$

where

$T \equiv$ temperature

$r \equiv$ radial dimension

$\dot{q} \equiv$ heat source strength per unit volume and unit time

$K \equiv$ thermal conductivity

$a \equiv K/c_p\rho$

$c_p \equiv$ specific heat

$t \equiv$ time

For a steady-state condition and symmetry in z and ϕ the general equation reduces to

$$\frac{\partial^2 T}{\partial r^2} + \frac{1}{r}\frac{\partial T}{\partial r} + \frac{\dot{q}}{K} = 0 \tag{69}$$

Or, letting $H \equiv \dot{q}/K$

$$\frac{\partial}{\partial r}\left[r\frac{\partial T}{\partial r}\right] + Hr = 0 \tag{70}$$

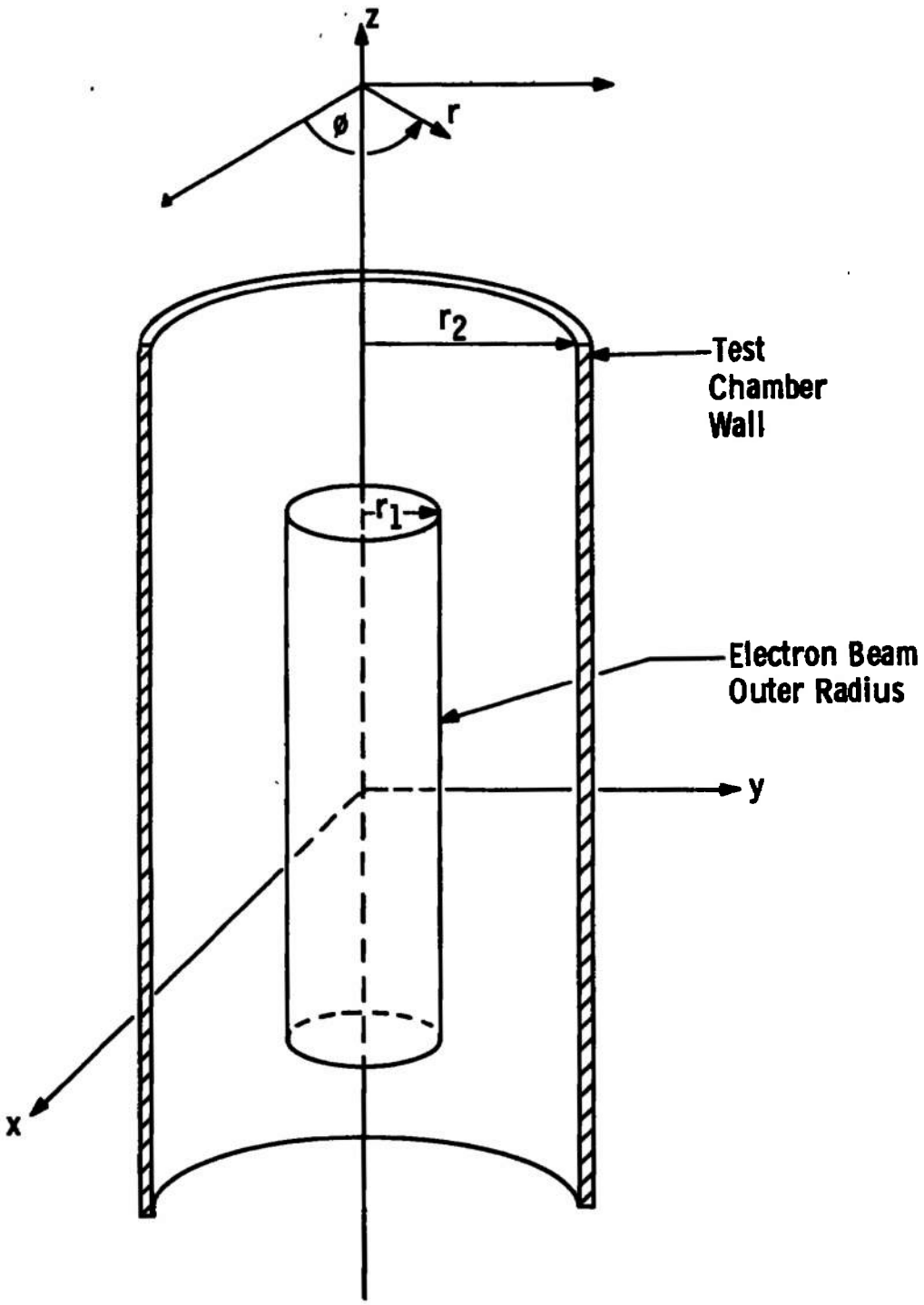

Fig. 44 Geometry for Beam Heating Calculations

Since

$$\frac{\partial T}{\partial r} = 0 \text{ at } r = 0 \tag{71}$$

and

$$r = r_1 \text{ at } T = T_1 \tag{72}$$

Therefore,

$$T = \frac{H}{4}(r_1^2 - r^2) + T_1 \tag{73}$$

for

$$0 \leq r \leq r_1$$

Now, for the range $r_1 \leq r \leq r_2$

$$\dot{q} = 0 \tag{74}$$

Therefore, the general equation reduces to

$$\frac{\partial^2 T}{\partial r^2} + \frac{1}{r}\frac{\partial T}{\partial r} = 0 \tag{75}$$

or

$$\frac{\partial}{\partial r}\left[r \frac{\partial T}{\partial r}\right] = 0 \tag{76}$$

After integration

$$T = d \ln r + f \tag{77}$$

where d and f are constants.

$$\left(\frac{\partial T}{\partial r}\right)_{\text{in the beam}} = \left(\frac{\partial T}{\partial r}\right)_{\text{in the gas}} \quad \text{at } r = r_1 \tag{78}$$

Since

$$\frac{dT}{dr} = -\frac{1}{2} \text{ Hr in the beam} \tag{79}$$

and

$$\frac{dT}{dr} = \frac{d}{r} \text{ in the gas} \tag{80}$$

then

$$d = -\frac{1}{2} H r_1^2 \text{ at } r = r_1 \tag{81}$$

Again, for the region $r_1 \leq r \leq r_2$

$$T_1 = d \ln r_1 + f \tag{82}$$

since

$$r = r_1 \text{ at } T = T_1 \tag{72}$$

$$T_w = d \ln r_2 + f \tag{83}$$

since

$$r = r_2 \text{ at } T = T_w \tag{84}$$

Therefore,

$$T_w = -\frac{1}{2} Hr_1^2 \ln r_2 + f \tag{85}$$

and

$$T_1 = -\frac{1}{2} Hr_1^2 \ln r_1 + f \tag{86}$$

Now,

$$T = -\frac{1}{2} Hr_1^2 \ln r + f \tag{87}$$

Therefore,

$$T = -\frac{1}{2} Hr_1^2 \ln r + \frac{1}{2} Hr_1^2 \ln r_1 + T_1 \tag{88}$$

But,

$$T_1 = T_w + \frac{1}{2} Hr_1^2 \left(\ln r_2 - \ln r_1\right) \tag{89}$$

Therefore,

$$T = \frac{1}{2} Hr_1^2 \left(\ln r_2 - \ln r\right) + T_w \tag{90}$$

$$\text{for } r_1 \leq r \leq r_2$$

and

$$T = \frac{H}{4}\left(r_1^2 - r^2\right) + T_w + \frac{1}{2} Hr_1^2 \left(\ln r_2 - \ln r_1\right) \tag{91}$$

$$\text{for } 0 \leq r \leq r_1$$

Now,

$$r_2 = nr_1 \tag{92}$$

where n is a constant.

Therefore, for $0 \leq r \leq r_1$

$$T = \frac{H}{4}\left(r_1^2 - r^2\right) + T_w + \frac{1}{2} Hr_1^2 \ln n \tag{93}$$

$$\frac{T}{T_w} = \frac{H}{4T_w}\left(r_1^2 - r^2\right) + 1 + \frac{H}{2T_w} r_1^2 \ln n \tag{94}$$

Therefore, for $0 \leq r \leq r_1$

$$R_T \equiv \frac{T}{T_w} = H_T \left[\frac{r_1^2 - r^2}{4} + \frac{r_1^2}{2} \ln n\right] + 1 \tag{95}$$

For $r_1 \leq r \leq nr_1$

$$T = \frac{1}{2} Hr_1^2 \left(\ln \frac{nr_1}{r}\right) + T_w \tag{96}$$

$$\frac{T}{T_w} = \frac{H}{T_w} \frac{r_1^2}{2} \left(\ell n \frac{nr_1}{r} \right) + 1 \tag{97}$$

Therefore,

$$R_T = H_T \frac{r_1^2}{2} \left(\ell n \frac{nr_1}{r} \right) + 1 \tag{98}$$

Remembering that

$$H_T = \frac{\dot{q}}{KT_w} \tag{99}$$

then

$$H_T = \frac{\left(\frac{w}{\rho J_b} \right) \rho J_b}{KT_w} \tag{100}$$

where ρ is the gas density, J_b is the beam current density, and $\frac{w}{\rho J_b}$ is Grüns experimental measure of the energy absorbed per second per cubic centimeter of air reduced to unit air density and unit beam current density (19). $\left(\frac{w}{\rho J_b} \right)$ is plotted in Figure 45.

$$J_b = \frac{i_b}{\pi r_1^2} \tag{101}$$

$$\rho = \frac{P_c}{R T_w} \tag{102}$$

Therefore,

$$H_T = \left(\frac{w}{\rho J_b} \right) \left(\frac{P_c}{KR T_w^2} \right) \left(\frac{i}{\pi r_1^2} \right) \tag{103}$$

Equations 95, 98, and 103 in conjunction with the data of Figure 48 can be used to calculate a temperature profile across a

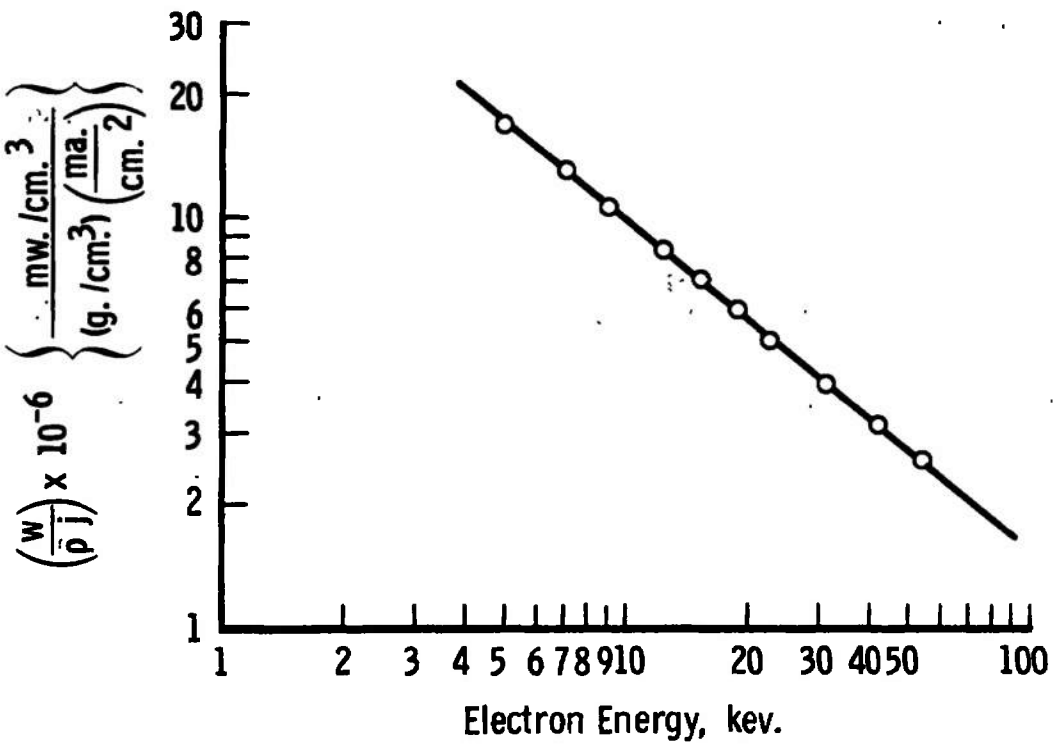

Fig. 45 Electron Beam Energy Dissipation in Air

laboratory test chamber for various conditions. A chamber centerline temperature may be easily calculated using only Equations 95 and 103.

Results of calculations at pertinent conditions are shown in Table I, page 75. The calculations do not include any effects of convection cooling, and they are not applicable under conditions for which a uniform beam radius is not clearly definable. They should, however, for the proper conditions present a maximum amount of beam heating for a result.

UNCLASSIFIED

Security Classification

DOCUMENT CONTROL DATA - R & D

(Security classification of title, body of abstract and indexing annotation must be entered when the overall report is classified)

1. ORIGINATING ACTIVITY *(Corporate author)*
Arnold Engineering Development Center
ARO, Inc., Operating Contractor
Arnold Air Force Station, Tennessee

2a. REPORT SECURITY CLASSIFICATION
UNCLASSIFIED

2b. GROUP
N/A

3. REPORT TITLE

LABORATORY VERIFICATION STUDIES OF ROTATIONAL AND VIBRATIONAL TEMPERATURE MEASUREMENTS BY THE ELECTRON BEAM TECHNIQUE

4. DESCRIPTIVE NOTES *(Type of report and inclusive dates)*
January 1 to September, 1968 - Final Report

5. AUTHOR(S) *(First name, middle initial, last name)*

William D. Williams, ARO, Inc.

6. REPORT DATE	7a. TOTAL NO. OF PAGES	7b. NO. OF REFS
February 1969	129	19

8a. CONTRACT OR GRANT NO	9a. ORIGINATOR'S REPORT NUMBER(S)
F40600-69-C-0001 b. PROJECT NO A014 c. Program Element 63101F d	AEDC-TR-68-265 9b. OTHER REPORT NO(S) *(Any other numbers that may be assigned this report)* N/A

10. DISTRIBUTION STATEMENT
This document has been approved for public release and sale; its distribution is unlimited.

11. SUPPLEMENTARY NOTES	12. SPONSORING MILITARY ACTIVITY
Available in DDC	Arnold Engineering Development Center, Air Force Systems Command, Arnold Air Force Station, Tennessee

13. ABSTRACT To verify the physical parameters and limits of the electron beam technique, precise laboratory experiments were conducted. By injecting an electron beam into an experimental chamber containing slowly flowing nitrogen and spectroscopically examining the resulting spontaneous light emission the analysis of this technique is accomplished. Measurements of the rotational and vibrational temperatures of nitrogen have been made over the temperature range 78° - 300°K and at pressures of 0.001-1.00 Torr using a 10 KV electron beam with currents of 0.06-4.5 milliamperes. The measurements were made photoelectrically, and signal amplification and averaging were accomplished with a lock-in amplifier. The results of the rotational temperature measurements display a dependence of rotational temperatures on gas density and beam current. Rotational temperature was also found to vary with the number of spectral lines used and with the vibrational band as well. Vibrational band intensities of the $N_2^+(1^-)$ system were measured by electronic integration of the rotational structure, and a pressure dependence of various band intensity ratios was observed

DD FORM 1 NOV 65 1473

UNCLASSIFIED

Security Classification

14. KEY WORDS	LINK A		LINK B		LINK C	
	ROLE	WT	ROLE	WT	ROLE	WT
electron beams						
temperature measurements						
temperature measuring instruments						
gas flow						
vibration						
nitrogen						
tests						

17-5

AFSC
Arnold AFS Tenn